UNIVERSITÄT ZU LÜBECK

From the Priority Area Infections
of the Research Center Borstel
Leibniz Lung Center
Director: Prof. Dr. Ulrich Schaible

Division of Immunobiophysics
Head: Prof. Dr. Andra Schromm

Anti-inflammatory immune regulation of anionic phospholipids on macrophages and pulmonary surfactant lipid*omics* in the context of neonatal acute respiratory distress syndrome

DISSERTATION

for Fulfillment of
Requirements
for the Doctoral Degree
of the University of Lübeck
from the Department of Natural Sciences

Submitted by
Sarah Kupsch
from Prenzlau

Lübeck 2021

First referee:	Prof. Dr. Andra Schromm
Second referee:	Prof. Dr. Peter König
Date of oral examination:	02.06.2022
Approved for printing:	02.06.2022

“Science is a way of thinking much more than it is a body of knowledge.”

~ Carl Sagan

Table of Contents

Abstract

Neonatal acute respiratory distress syndrome (nARDS) is a frequent and severe inflammatory condition of the lungs in newborns and is characterized by an intensely activated immune response of alveolar macrophages, persistent lung surfactant degradation and in consequence defective lung mechanics and gas exchange, and ultimately irreversible fibrosis of lung tissue. The replenishment of that surfactant pool with Curosurf®, a clinically approved porcine lung surfactant preparation, is an effective treatment option, but mortality from nARDS remains between 15-30%. Therefore, a study was conducted that aimed to achieve an improved inflammation control by supplementing the current Curosurf® composition with the anionic phospholipid species POPG, DOPG, PIP2 and the headgroup variant IP3, and to understand the impact of nARDS and the supplemented Curosurf® on the piglet pulmonary surfactant lipid*ome*.

The efficacy of the thus fortified Curosurf® was tested in a triple-hit piglet model of nARDS in which acute respiratory distress was induced in term-born piglets by removal of endogenous surfactant via repeated lavage, injurious artificial ventilation and simulation of bacterial infection via exposure to lipopolysaccharide (LPS).

The clinical data collected throughout the study provided ample evidence for a strong anti-inflammatory mediation by the supplemented anionic lipids and an improved clinical outcome. Cytokine measurements in the lavage fluid could not corroborate the clinical data and the lavage fluid was eventually determined to be an inadequate means to understand the detailed inflammatory state in the lung in this context. The porcine alveolar macrophages retrieved from the lavage fluid had entered a state of tolerance 24h after *in vivo* LPS challenge.

Alveolar macrophages are part of the first line of pulmonary immune defense and their activation due to i.e. bacterial infection is a main driver of the hyper-inflammatory state that defines nARDS. *In vitro* investigations employing several types of macrophages showed that POPG, DOPG and PIP2 significantly inhibited the LPS-driven macrophage activation for both the TNFα/NFκB-pathway and the canonical inflammasome, regulated by both the headgroup and the lipid acyl chain composition. Interestingly, IP3 had no such effect on human and porcine macrophages, but it showed great promise on a systemic level.

The acute phase protein LBP (LPS-binding protein) is of essential importance in LPS-recognition and transport to LPS-receptor complexes on the macrophage cell surface, and it was detected in significantly elevated concentrations in the piglet nARDS lung, indicating a pulmonary immune function. Indeed, this study highlights the potential of LBP to confer LPS-induced macrophage non-canonical signaling.

Modern mass spectrometric techniques allowed for the creation of a detailed qualitative compound analysis of the porcine pulmonary surfactant lipid*ome* – healthy, diseased and treated with the lipid-supplemented Curosurf®. It is essential to understand the molecular changes initiated by the onset of nARDS and to determine if the fortification of Curosurf® with the four anionic lipids and derivative alter the piglet pulmonary lipid*ome*. This piglet surfactant analysis revealed that, while interesting smaller changes on the single lipid species level were detected, the fundamental surfactant composition was actually not altered in sick piglets and, importantly, qualitative pulmonary surfactant homeostasis was not negatively affected by treatment with Curosurf® and the intervention lipids.

In conclusion, the study demonstrates the strong potential of anionic phospholipid supplementation of Curosurf® to exert inflammation control *in vivo*, *in vitro* and a molecular level in the context of nARDS. Furthermore, a detailed picture of the piglet surfactant composition in health and disease could be painted and it was shown that the candidate molecules, POPG, DOPG, PIP2 and IP3 support, but do not disrupt the surfactant composition, which is of paramount importance for pulmonary homeostasis.

Deutsche Zusammenfassung

Das akute Atemnotsyndrom des Neugeborenen (nARDS) ist eine durch u.a. bakterielle Infektionen hervorgerufene, postnatale Erkrankung der Lunge, die durch starke Entzündungsreaktionen charakterisiert ist. Eine drastische Immunantwort der Alveolarmakrophagen, kollabierte Alveolen, sowie pathologischer Abbau von Lungensurfactant prägen das Krankheitsbild, das schlussendlich in respiratorischer Insuffizienz mit irreversibler Fibrose des Lungengewebes mündet. Therapeutisch wird neben künstlicher Beatmung ein aus Schweinelungen gewonnenes Surfactant-Präparat (Curosurf®) eingesetzt, um dem Surfactant-Mangel entgegen zu wirken und die Atemmechanik zu normalisieren. Trotz dieser Therapieoption verbleibt eine Mortalität von 15-30%, was eine klinische Weiterentwicklung absolut erfordert. Vor diesem Hintergrund hatte die vorliegende Studie eine Verstärkung der antiinflammatorischen Wirkung von Curosurf® zum Ziel. Dahingehend wurde Curosurf® mit den anionischen Phospholipiden DOPG, POPG, PIP2 und dessen Derivat IP3 versetzt. Die potentiell erhöhte immunologische Effizienz des mit den Lipiden versetzten Curosurf® wurde in einem Tiermodel des nARDS getestet, bei dem nARDS in reif geborenen Ferkeln durch ein „Triple-Hit"-Protokoll schrittweise durch Auswaschen des endogenen Surfactants (bronchoalveoläre Lavage), künstliche Beatmung sowie LPS-Exposition als simulierte bakterielle Infektion ausgelöst wurde.

Die aus der Lavage gewonnenen porcinen Alveolarmakrophagen befanden sich 24h nach initialer LPS-Gabe *in vivo* in einem refraktären Zustand und zeigten nach erneuter LPS-Gabe *in vitro* keine proinflammatorische Zytokinausschüttung. Die Lavageflüssigkeit selbst wurde eingehend auf inflammatorische Marker untersucht, wurde schlussendlich aber als unzureichendes Mittel zur detaillierten Diagnose des Entzündungszustandes in der Ferkellunge dieses nARDS Modells definiert. Nichtsdestotrotz, zeigten die klinischen Daten der Ferkel deutlich, dass die therapeutische Verabreichung des mit den anionischen Lipiden angereicherten Curosurf® eine Verbesserung der klinischen Symptome des induzierten nARDS der Ferkel erzielte.

Eine durch Alveolarmakrophagen getragene Hyperinflammation in der Lunge ist ein Hauptmerkmal des nARDS. Untersuchungen zur antiinflammatorischen Regulierung von Makrophagen *in vitro* durch die in dieser Studie eingesetzten anionischen Lipide hat eine

signifikante Reduzierung bis zu kompletter Unterdrückung der Makrophagenantwort (TLR4/NFκB und canonical Inflammasom-Signalweg) auf LPS durch PIP2, DOPG und POPG, in absteigender Effizienz, aufgezeigt. Hier waren sowohl die Natur der Lipidkopfgruppe, als auch der Acylketten von Bedeutung. Tatsächlich zeigte IP3 *in vitro* keinen solchen Effekt, jedoch eine systemisch regulierende Wirkung *in vivo*.

Das Akut-Phase-Protein LBP ist von besonderer Wichtigkeit für die Erkennung und den Transport von LPS. In der erkrankten Ferkellunge wurden erhöhte LBP-Konzentrationen nachgewiesen, was diesem Akutphaseprotein eine pulmonal-immunologische Rolle in der LPS-Erkennung zuordnet. Dahingehend konnte in dieser Studie erstmals gezeigt werden, dass LBP potentiell die LPS-induzierte Aktivierung des non-canonical Inflammasoms vermittelt.

Durch massenspektrometrische Untersuchungen des porcinen pulmonalen Surfactant-*Lipidoms* wurde der Fragestellung nachgegangen, ob sowohl nARDS als auch die therapeutische Gabe von angereichertem Curosurf® kompositionelle Änderungen dieses *Lipidoms* bedingen. Es konnte ein detailliertes Bild des porcinen Lipidoms der gesunden und erkrankten Ferkellunge erstellt werden, welches verdeutlicht, dass die grundlegende qualitative Zusammensetzung des pulmonalen Surfactants zwar kleinere Änderungen einzelner Lipidspezies erfahren hat, aber das Gleichgewicht der Lipidgruppen des Surfactants weder durch nARDS, noch durch die Gabe von mit anionischen Lipiden angereichertem Curosurf® qualitativ verändert wurde.

Zusammenfassend belegt diese Studie das große therapeutische Potenzial der Anreicherung des Curosurf® mit den anionischen Lipiden DOPG, POPG, PIP2 und dessen Derivat IP3 im Zusammenhang mit der Curosurf®-Applikation bei nARDS. Hierbei ist das in dieser Studie gezeigte antiinflammatorische Wirkprofil der eingesetzten Moleküle von äußerster Relevanz. Weiterhin wurde belegt, dass eine solche Anreicherung des Curosurf® neben der deutlichen Verbesserung der Lungenfunktion die für die Homöostase in den Alveolen zwingend notwendige endogene Zusammensetzung des Lungensurfactants nicht unphysiologisch verändert, was für eine potenzielle, vor allem sichere Anwendung in der klinischen Behandlung von nARDS grundlegend wichtig ist.

List of Figures

List of Tables

List of Abbreviations

α	alpha
β	beta
K	Kappa
A. bidest	Aqua bidest
A. Braun	Aqua braun
AECI	Alveolar epithelial cell type I
AECII	Alveolar epithelial cell type II
ANOVA	Analysis of variance
ASC	apoptosis-associated speck like protein
aSMase	Acid sphingomyelinase
ATP	Adenosine triphosphate
a.u.	Arbitrary unit
BAL	Broncho-alveolar lavage
BALF	Broncho-alveolar lavage fluid
BI	Before injury
BSA	Bovine serum albumin
C_{res}	Compliance of the respiratory system
CB	Composite bodies
CD	Cluster of differentiation
CH_3COCl	Acetyl chloride
CH_3COOH	Acetic acid
$CHCl_3$	Chloroform
CO_2	Carbon dioxide
DAG	Diacylglycerol
DAMP	Danger-associated molecular pattern
DOPC	1,2-dioleoyl-sn-glycero-3-phosphocholine

DOPG	1,2-dioleoyl-sn-glycero-3-phosphoglycerol
DPPC	1,2-dipalmitoyl-sn-glycero-3-phosphocholine
DTT	Dithiothreitol
ELISA	Enzyme-linked immunosorbent assay
ER	Endoplasmic reticulum
EU	Endotoxin unit
EVLWI	Extravascular lung water index
FCS	Fetal calf serum
FRC	Functional residual capacity
h	Hour(s)
HBSS	Hank's balanced salt solution
HC	Hierachical clustering
HRP	Horseradish peroxidase
Ig	Immunoglobulin
IL	Interleukin
IP3	D-myo-inositol-1,2,6-trisphosphate
i-PrOH	Isopropanol
IRDS	Respiratory distress in premature infants
LAL	Limulus amebocyte lysate
LBP	Lipopolysaccharide-binding protein
LDH	Lactate dehydrogenase
LPC	Lyso-Phosphatidylcholine
LPS	Lipopolysaccharide
MØ	Macrophage
MD-2	Myeloid Differentiation factor 2
MeOH	Methanol

NaCl	Sodium chloride
NAD^+	Nicotinamide adenine dinucleotide, oxidized
NADH	Nicotinamide adenine dinucleotide, reduced
$NaHCO_3$	Sodium bicarbonate
nARDS	Neonatal respiratory distress syndrome
NFκB	Nuclear factor kappa B
NLRP3	Nucleotide-binding oligomerization domain-like receptor family, pyrin domain-containing 3 (NACHT, LRR and PYD domains-containing protein 3)
OI	Oxygenation index
PAMP	Pathogen-associated molecular pattern
PBMC	Peripheral blood mononuclear cell
PBS	Phosphate-buffered saline
PCA	Principle component analysis
PI	Phosphatidylinositol
PIP_2	Phosphatidylinositol-4,5-bisphosphate
PIP_3	Phosphatidylinositol-3,4,5-trisphosphate
PKC	Phosphokinase C
POPC	1-palmitoyl-2-oleoyl-glycero-3-phosphocholine
POPG	1-palmitoyl-2-oleoyl-glycero-3-phosphoglycerol
PRR	Pattern recognition receptor
R_{rs}	Resistance of the respiratory system
rhM-CSF	Recombinant human monocyte colony stimulating factor
rpm	Rounds per minute
RPMI	Roswell Park Memorial Institute 1640 cell culture medium
S50	50 mg/kg Curosurf®
S200	200 mg/kg Curosurf®
S+IP3	50 mg/kg Curosurf® + IP3

S+PIP2	50 mg/kg Curosurf® + PIP2
S+POPG	50 mg/kg Curosurf® + POPG
S+DOPG	50 mg/kg Curosurf® + DOPG
SDS-PAGE	Sodium dodecyl sulphate–polyacrylamide gel electrophoresis
SP-A/D	Surfactant protein A/D
$sPLA_2$	Secreted phospholipase A2
TLR	Toll-like receptor
TM	Tubular myelin
TMB	3,3',5,5'-Tetramethylbenzidin
TNFα	Tumor necrosis factor alpha
VEGF	Vascular endothelial growth factor
VEI	Ventilation efficiency index

1. Introduction

1.1. The lung and the pulmonary immune defense

In humans and in all vertebrates, the lung is the organ responsible for the uptake of oxygen into and the release of carbon dioxide from the blood. It is situated within the thoracic cavity (Cavitas thoracis) along with the heart, the thymus and the esophagus. Technically, humans have two lungs consisting of two (left lung) and three (right lung) lobes. As both lungs are functionally homologous and for simplicity reasons, “the lung” will further be used to refer to both units. As the lung itself does not have any muscles, the inspiration movement is enabled mainly by downward contraction of the diaphragm (and helped by contraction of the intercostal muscles between the ribs). Expiration is a passive process as the muscles relax and

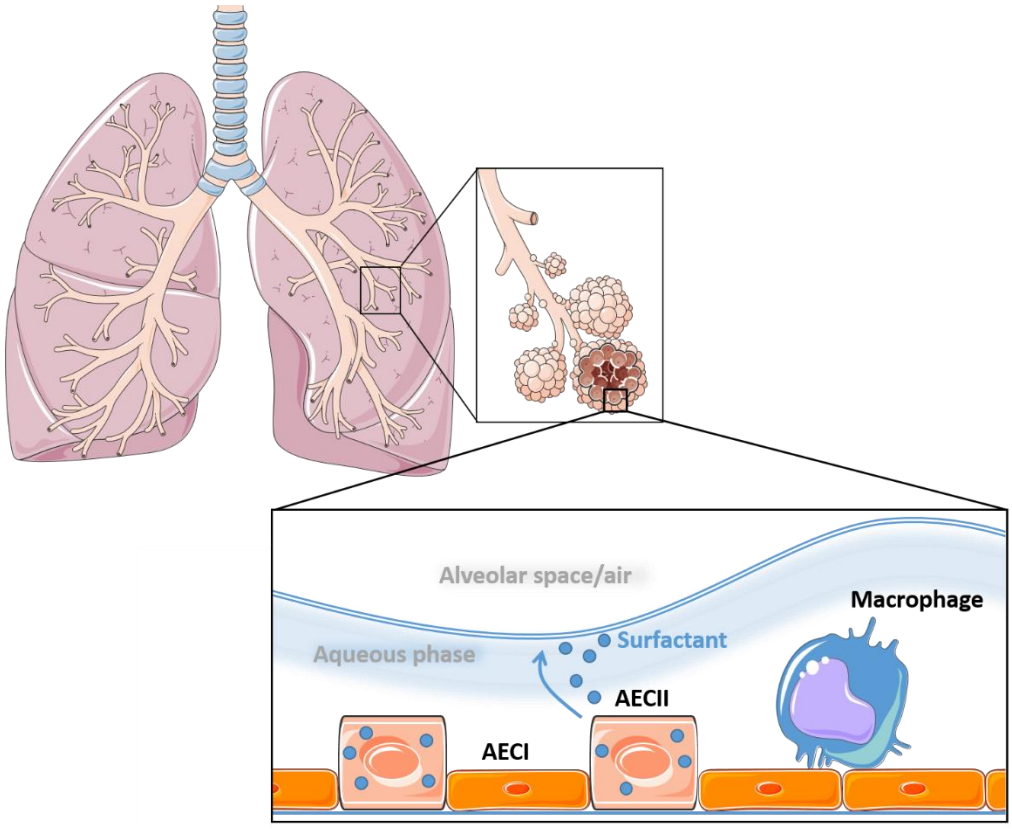

Figure 1.1: *Schematic of the respiratory system and morphology of the alveoli.* Created and adapted using smart servier medical art under https://creativecommons.org/licenses/by/3.0/.

the lung compresses due to its elastic recoil which forces the air to leave the lungs. A residual volume (functional residual capacity, FRC) of air remains in the lung after expiration. The lung of an adult human has an approximate end-expiration volume of 2-3 liters (FRC), upon

expansion up to 8 liters, and weighs about 800 g (500 g without blood). It is connected to the outside by the upper airways (nasal cavity, pharynx, larynx) and the lower airways (trachea and two primary bronchi). Each primary bronchus enters the lung and divides into lobar bronchi (one for each lobe) which in turn divide into segmental bronchi and further down merge into the bronchioles (cartilage-free from here on). These conductive airways end with the terminal bronchioles (approx. 0.2 mm in diameter). Here, the respiratory airways start with the respiratory bronchioles which lead to the alveolar ducts and finally into the alveoli (approx. 300-400 in adult humans) [1]. Due to that extensive branching of the airways, the lung has a surface area of 70 m^2 on average but can double at maximum inspiration.
At 20 weeks of gestation complete branching of the lung in the human fetus has occurred, though sufficient development of alveoli and the underlying capillary system to allow for reasonable gas exchange commences around week 24 [2].

The alveolar epithelium is essentially built up of two different cell types: the big squamous lining alveolar epithelial cell type I (type I pneumocytes, AECI) and the secretory alveolar epithelial cell type II (type II pneumocytes, AECII) in a numerical ratio of 2:1, respectively [1], (see Figure 1.1). Type I pneumocytes cover up to 97 % of the alveolar space and are responsible for the air-blood barrier and thus for oxygen exchange. In fact, efficient gas exchange has to be guaranteed while ensuring an intact barrier that can resist the multiple forces exerted on it, such as capillary blood pressure, surface tension in the alveoli, as well as tissue tension during inspiration and expiration. AECII are metabolically very active, cuboidal cells that produce, secrete and recycle pulmonary surfactant and, at least in adult mice, have a role in alveolar epithelial renewal [3,4].

With every breath, the lung has to cope with inhaled microorganisms as well as other particulate matter. Therefore several pulmonary defense mechanisms along the respiratory tract, specific as well as non-specific, have evolved in the lung. The complex branching of the airways forces a deceleration of the airstream while the contained particles and microorganisms are caught within the mucus layer lining the airways. The mucociliary escalator and coughing eventually transport the particles out of the airways. Furthermore, the airway mucosa (lining epithelium made up of different, often secretory cell types) produces several antimicrobial mediators, such as immunoglobulin A (IgA), lysozyme (hydrolysis of mostly Gram-positive bacterial cell wall), defensins (permeabilization of bacterial and fungal membranes and prevention of viral replication), reactive oxygen and nitrogen species.

Microorganisms and other particles that do travel as far as the alveolar space are efficiently taken up and digested by the alveolar macrophages via phagocytosis. If a stronger, orchestrated immune reaction is necessary to clear the intruding microorganisms, the alveolar macrophages induce an inflammatory response to attract neutrophils and other immune cells. Finally, pulmonary surfactant, a surface-active substance lining the inside of the alveoli (see chapter 1.3), has immunological (and structural) functions and contributes strongly to the immune defense of the lung.

The disruption of that important and sensitive homeostasis in the lung can lead to various respiratory issues. Secondary surfactant deficiency in term-born infants as a result of surfactant inactivation by factors such as injurious (over)ventilation, bacterial or viral infection, or aspiration of meconium and/or maternal blood during birth, or other unusual substances, can lead to the neonatal acute respiratory distress syndrome (nARDS). This disease is characterized by excessively high alveolar surface tension, disruption of the alveolar epithelium integrity, impaired gas exchange and pulmonary edema [5]. This work is a part of a research cooperation between several collaborating groups that investigated different aspects of the enrichment of the clinically approved, exogenous surfactant preparation (Curosurf®) with anionic phospholipids as a new approach to improve the therapy of nARDS.

This chapter will present the relevant background information on:

- Immune-activation of macrophages by the bacterial compound lipopolysaccharide (LPS), as an example of bacterial infection, and the underlying signaling pathways
- Pulmonary surfactant structure and immune-regulatory function
- Pathology of nARDS and the current therapeutic approach
- Scientific rationale behind the present study.

1.2. Macrophages and the interaction with LPS

The term *macrophage* was first introduced by the Russian scientist Elie Metchnikoff (1845–1916). He described large mononuclear phagocytic cells [6] which are the first immune cells in the tissue to encounter invading pathogens: "*These cells accumulate at the point of inflammation and devour the particles available to them" (1866)* [7]. Macrophages are cells of the innate immune system and are key players in tissue homeostasis, coordination of adaptive

immune responses, inflammation, and tissue repair. Their job is to engulf and take up pathogens and damaged or infected cells and destroy them by a variety of means, including enzymes (i.e. elastase, metalloproteases) as well as reactive oxygen (ROS) and nitrogen species (RNOS) (i.e. superoxide anion, hydrogen peroxide, hydroxyl radical). Macrophages also take up indigestible particulate matter (i.e. carbon black particles) [8].

Macrophages originate from pluripotent hematopoietic stem cells in the bone marrow which differentiate into granulocyte/macrophage progenitor cells. These cells give rise to monocytes (and granulocytes) which circulate in the blood until they enter tissues and differentiate into tissue-specific macrophages. They belong to the cells of the innate immune system but are able to induce the adaptive immune response if necessary.

In the last two decades a pattern has emerged that sorts macrophages into two categories based on their phenotype: The macrophage paradigm describes whether a macrophage is of inflammatory M1 (classically activated) or repair M2 type (alternatively activated). M1 macrophages are primed by pro-inflammatory cytokines, such as TNFα and IFNγ, or microbial PAMPs, such as LPS, and are characterized by the production of ROS/RNOS, pro-inflammatory cytokines, such as TNFα, IL-1β, IL-6, that drive the inflammatory process to respond to pathogens, which unfortunately can also lead to surrounding tissue destruction. In contrast, M2 macrophages are primed by anti-inflammatory cytokines such as IL-4, IL-13 and transforming growth factor beta (TGF-β) and produce pro-fibrotic cytokines, such as IL-1β, TGF-β, vascular endothelial growth factor (VEGF) and arginase-1 that aid in the wound-healing process and attract fibrocytes [7], [8]. However, macrophages are amazingly adaptable to their surrounding milieu and may readily change phenotype to accommodate new environmental challenges. It has therefore been proposed that a stiff categorization into M1 or M2 macrophages may be outdated and should be based on the inducing cytokine, rather than the temporarily induced phenotype [9,10].

A special subtype of macrophages is found in the mammalian lung: the alveolar macrophages, which arrive in the lung within the first few days of life. They are patrolling the alveoli, with their main task being the clearance of inhaled, exogenous organisms and particles, endogenous cellular debris, as well as the uptake and degradation of pulmonary surfactant (see chapter 1.3). Direct relatives are the less differentiated macrophages in the lung interstitial tissue, which is the connective tissue around the airways, arteries and veins. They present an intermediate state of monocytes entering the interstitial tissue to become mature

alveolar macrophages. In a state of acute inflammation, tissue residency is cut short to increase the number of alveolar macrophages at the expense of complete differentiation. In mice, the macrophage pool within the alveoli can also be boosted by proliferation and division of resident, fully differentiated macrophages, independently of hematopoietic progenitor cells [11,12]. To which extend the latter mechanism also applies to human macrophages remains to be determined.

After patrolling the alveoli lumen (guided on their route by the epithelial lining that expresses chemotactic factors) for around 7 up to 28 days the alveolar macrophages usually exit the lung via the mucociliary escalator and are thereby transported to the pharynx to be either swallowed or coughed out. It has also been proposed that alveolar macrophages may enter back into the interstitium, thereby crossing the alveolar epithelium, in order to travel to the regional lymph nodes [13–15].

In summary, the macrophage's most important mechanisms to uphold immune homeostasis and combat microorganisms are antigen presentation and activation of other immune cells, secretion of antimicrobial and signaling effector molecules, phagocytosis and clearance of dead cells and other debris. In the present study, macrophages were analysed for their response to the chosen intervention strategy. Which such a central importance, in the following the interaction of macrophages with bacterial LPS and the subsequent activation of their signaling pathways is described in more detail.

1.2.1. Lipopolysaccharide and its recognition by LBP

One of the major constituents of the outer membrane of Gram-negative bacteria that induce an inflammatory response in the human host is the glycolipid lipopolysaccharide (LPS). Bacterial lipopolysaccharides are macromolecules of 10-20 kDa and are vitally important for the integrity of the bacterial cell. They are composed of three major parts (see Figure 1.2): The hydrophobic lipid section, called *lipid A*, anchors the molecule to the outer leaflet of the bacterial membrane. It is followed by a hydrophilic core polysaccharide chain, which in turn is bound to the *O-antigen*, which is composed of repeating units of oligosaccharide chains that define the bacterial serotype and colony phenotype. These oligosaccharide chains protect bacteria against e.g. complement lysis and antibiotic treatment.

The word *endotoxin* is commonly used in the scientific community as a synonym for LPS. Originally, the term was coined by Richard Pfeiffer, a student of Robert Koch in Berlin,

Germany, in the late 1890s, while researching on *Vibrio cholerae*. He discovered that the pathogenicity of the bacteria does not depend on their viability and therefore soluble toxins must be released from the inside (therefore *endo*) of dead bacteria which cause the infection [16]. Today we know that LPS, the endotoxin Pfeiffer had postulated, is readily released by viable bacteria without prior destruction of the cell wall, e.g. during bacterial growth as outer membrane vesicles (OMVs) or after antibiotic exposure [17–19].

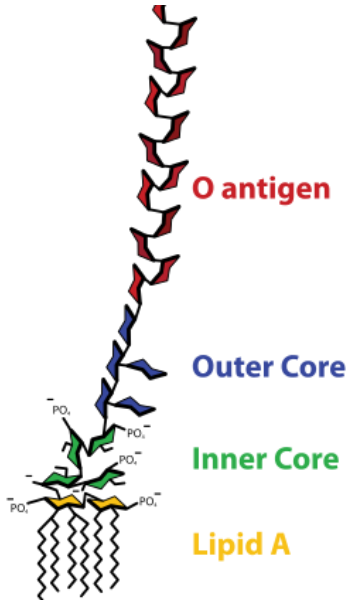

Figure 1.2: Schematic structure of lipopolysaccharide (LPS). LPS is a component of the outer membrane of Gram-negative bacteria and elicits a strong immune response in the host. The immunogenic, hydrophobic lipid A anchor is connected to a core region of hydrophilic polysaccharide chains which can end in the O-antigen oligosaccharide repeats that define the bacterial serotype. Adapted from: Mike Jones, CC BY-SA 3.0 <https://creativecommons.org/licenses

LPS elicits a powerful immunological reaction in the host, but only in the presence of lipid A moiety of LPS [16,18], which therefore represents the *endotoxic principle* of LPS [20]. It is recognized by the Toll-like receptor 4 (TLR4) on monocytes and macrophages (see chapter 1.2.2). That recognition of LPS by immune cell receptors is facilitated by the lipopolysaccharide-binding protein (LBP) [21]. LBP is a 60kDa acute-phase-protein mainly produced in hepatocytes in response to increased plasma levels of TNFα, IL-1β, and IL-6. However, it is also constitutively found in low plasma levels (5 – 10 µg/mL) under resting conditions. In addition to production by hepatocytes, LBP mRNA was detected in human lung tissue and the human lung epithelial cell line A549 secretes LBP spontaneously as well as in increased amounts in response to IL-1β and IL-6 [22–26]. LBP binds to the amphipathic lipid A moiety of LPS and transfers it to the soluble, membrane-bound cluster of differentiation 14 (CD14) and finally to the TLR4-receptor complex anchored to the plasma membrane of monocytic cells [27,28]. The resulting intracellular signaling cascade leads to the secretion of pro- and anti-inflammatory cytokines that regulate the inflammation induced by LPS.

Furthermore, our lab group and others have shown that LBP can intercalate into the plasma

membrane of human monocytic cells in the absence and in the presence of LPS (independent of the TLR4 receptor complex) – a mechanism that could potentially deliver LPS to intracellular receptors such as human caspase-4 [29–31] (see chapter 1.2.6).
Besides increasing immune-recognition of LPS, LBP at high plasma concentrations also protects from severe systemic inflammatory response, such as septic shock, via neutralization of LPS by scavenging it from CD14 and transporting it to high density lipoproteins (HDL) [32–36].

1.2.2. Key mediators released from activated macrophages: TNFα and IL-1β

Macrophages can be activated by pathogen associated molecular patterns (PAMPs) via different pathways resulting in the release of several cytokines (i.e. TNFα, IL-1β). LPS, described above, is a central microbiological structure that initiates inflammation upon pulmonary exposure in newborns and was therefore used in this study as the prominent example of a macrophage-activating PAMP.

Over three decades ago, Carswell et al. identified a "factor released from host cells […] which is effective in causing necrosis of sarcoma and other transplanted tumors" [37] in the serum of bacteria-infected mice. Ten years later, that human *tumor necrosis factor* α (TNFα) was first cloned and expressed in *E.coli* and today we know that it is only one of the members of the TNF/TNFR superfamily (40+ proteins). This work will strongly focus on the inflammatory role of TNFα. It is a 27 kDa (233 amino acid) protein and is encoded as a single copy gene on the human chromosome 6 (and murine chromosome 17) [38]. The membrane-bound precursor protein (mTNFα) is cleaved by the TNFα-converting enzyme (TACE) which results in the soluble 17 kDa form (157 amino acids; TNFα or less common sTNFα) [39,40]. TNFα signals with high affinity through both its two transmembrane receptors: TNFR1 (expressed on most mammalian tissues) and TNFR2 (exclusively expressed in immune cells) [41].
TNFα has been given the nickname "master regulator" of pro-inflammatory cytokines, as it is upon the first mediators to be secreted after inflammatory events and it regulates production of other cytokines and lipid mediators (such as prostaglandin and platelet activating factor), it can induce macrophage activation (after IFNγ-priming), differentiation and apoptosis, it is a prime player in the pathology of septic shock, bone remodeling, several autoimmune and neurological diseases (such as rheumatoid arthritis and multiple sclerosis), and it is an early mediator in acute lung injury, such as nARDS [42–50].

Also in the early 1970's, another macrophage-secreted protein was identified, initially known as lymphocyte-activating factor (LAF) [51] and today known as interleukin 1 (IL-1). Its most remarkable known feature back then was the fact that it could induce fever when injected into rabbits in the absence of endotoxin [52]. Though there are 11 proteins in the IL-1-family, this work will focus on IL-1β. It affects most cell types, usually works in concert with TNFα and has pro-inflammatory, but also anti-inflammatory effects.

The microbial recognition that leads to the release of the cytokines TNFα and IL-1β involves, among others, the toll-like receptors (TLRs), which are a family of membrane surface receptors that are highly conserved from Drosophila flies all the way to humans. Until now, there are 11 known TLRs in humans which are expressed especially on immune cells such as macrophages, monocytes, granulocytes, and neutrophils, but e.g. also on epithelial and glial cells. They can either be expressed on cell plasma membrane surfaces (TLR1, 2, 4, 5, 6, 10 and 11) to recognize extracellular bacterial cell wall components (such as LPS or flagellin) and protozoan proteins, or on the inner side of endosomal, lysosomal and endoplasmic reticulum (ER) membranes (TLR3, 7, 8 and 9) where they recognize viral and bacterial nucleic acid. TLRs are all characterized by a horse-shoe shape, including a leucine-rich repeat (LRR) domain, and a Toll/IL-1 receptor (TIR) domain. The TLRs dimerize upon ligand binding (heterodimers or homodimers, depending on the type of TLR), induced by a conformational change in their c-terminal and trans-membrane region, and recruit intracellular effector molecules to propagate the signaling cascade which leads to activation of pro- and anti-inflammatory genes. The recruitment of co-receptors on the membrane surface is required for some TLR's, such as TLR4 and possibly also 3, 7 and 9 (co-receptor CD14) [53–55].

The TLR4-dependant signaling pathway for LPS-induced production of TNFα and IL-1β by macrophages are of central interest in this work and will be described in the following chapters. As these pathways vary between species (e.g. human and mice) the focus will be put on human macrophage pathways.

1.2.3. TLR4/NFκB-pathway activation by extracellular LPS: TNFα production

The first TLR4-dependant pathway discovered was the TLR4/NFκB pathway leading to TNFα secretion. As mentioned above, macrophages can be activated by LPS, whereby aggregates of LPS are captured by LBP, delivered to the hydrophobic pocket of the co-receptor CD14

(located within lipid rafts of the macrophage membrane) which then splits it into LPS monomers. CD14 subsequently presents the LPS monomer to the TLR4-MD-2 complex [56–58]. The ligand binding pocket of MD-2 confers the signaling on the TLR4 receptor: MD-2 and TLR4 form a stable heterodimer in which five of the six lipid A acyl chains of LPS are located inside the MD-2 pocket and the sixth acyl chain induces dimerization with another TLR4-MD-2 complex [57,59,60]. The receptor complex dimerization results in spatial proximity of the intracellular Toll/IL-1R homology (TIR)-domains of TLR4 and their adaptor proteins. The TLR4-TIR domains subsequently recruit the TIR domains of several myeloid differentiation factor 88 (MyD88) molecules, which is a process shared by all TLR's except TLR3 [61,62]. MyD88 initiates a series of downstream kinase phosphorylations ("Myddosome"-assembly) which lead to the release and translocation of the transcription factor nuclear factor κB (NFκB) to the nucleus for target gene transcription, such as TNFα and pro-IL-1β [63], see Figure 1.3.

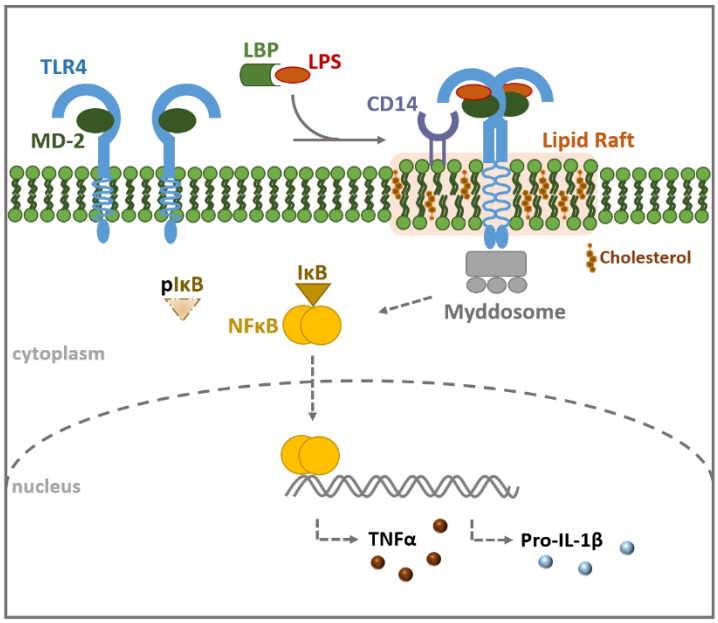

Figure 1.3: TLR4/NFκB-pathway schematic. LPS is captured by LBP and delivered to the co-receptor CD14 which is located within lipid rafts of the macrophage membrane. CD14 presents the LPS monomer to the TLR4-MD-2 complex. MD-2 and TLR4 form a stable heterodimer which dimerizes with another TLR4-MD-2 complex. The receptor complex dimerization results in spatial proximity of the intracellular TIR-domains of TLR4 which recruit the TIR domains of several MyD88 molecules. MyD88 initiates a series of downstream kinase phosphorylations ("Myddosome"-assembly) which lead to the phosphorylation of IκB and subsequent release and translocation of the transcription factor NFκB to the nucleus for target gene transcription, such as TNFα and pro-IL-1β.

In summary, this TLR4/NFκB-pathway of macrophage activation requires *one* stimulus to initiate the secretion of mature TNFα: a PAMP - extracellular LPS in this study. In contrast, the secretion of mature IL-1β requires another signal besides the recognition of PAMPs, as described below.

1.2.4. Inflammasome activation by extracellular LPS: The canonical pathway and IL-1β production

The secretion of active IL-1β as a result of *two* stimuli, including the sensing of extracellular LPS or other PAMPs, has been named the *canonical inflammasome activation pathway*.

The first signal for IL-1β induction in macrophages is provided by the recognition of LPS or other microbial PAMPs, or by the activation of cytokine receptors on the cell membrane. This *priming step* leads to the gene transcription of pro-IL-1β. That pro-IL-1β is lacking a leader sequence and thus requires an additional signaling step in order to be processed into its active form by caspase-1. A cytoplasmic multiprotein complex termed *inflammasome* [64] is, in turn, responsible for the activation of caspase-1. The priming step also leads to the transcription of genes coding for nod-like receptor proteins (NLRP) of the NLR-family, which are needed for the assembly of the inflammasome complex. NLRP3 is expressed upon macrophage activation by LPS and initiates the fibrillary assembly of the adaptor apoptosis-associated speck like protein (ASC). These ASC fibrils form clusters called *ASC speck* and recruit pro-caspase-1 which is consequently activated via autocatalytic processing [65,66]. Active caspase-1 can then cleave pro-IL-1β into its active, mature form IL-1β.

This formation of the inflammasome complex is initiated via a second stimulus which can be provided by multiple substances, such as microbial components, aggregated substances (e.g. asbestos, uric acid crystals), toxins, as well as extracellular ATP (which was used in this work as the 2nd stimulus) [67]. Extracellular ATP leads to the activation of the membrane ion channel $P2X_7$ which triggers the efflux of K^+ which in turn initiates the NLRP3 inflammasome formation. Processing of pro-IL-1β is indeed quite inefficient without the occurrence of that second signal (less than 5%) [68–70].

Another effector function of caspase-1 is the cleaving of gasdermin D (GSDMD) into an N-terminal and a C-terminal part. The GSDMD-N initiates the induction of a special kind of cell death termed *pyroptosis* [72]. To that end, GSDMD-N locates phosphatidylinositol phosphates, phosphatidylserine and cardiolipin on the inner leaflet of the cytoplasmic membrane and forms membrane pores of 10-20 nm in diameter by oligomerization [73]. That cell membrane disruption leads to swelling and release of cytoplasmic content (lysis), such as inflammatory mediators which can in turn activate and recruit other immune cells to the place of inflammation [71,72].

In summary, in order for IL-1β to be activated and secreted along the canonical pathway, a gene transcription activation priming step (signal 1, LPS in this work) and an inflammasome-assembly activation step (signal 2, ATP in this work) are required (see Figure 1.4B). The reason for this high level of regulation of inflammasome activation is commonly seen in the prevention of accidental and potentially destructive NLRP3 and inflammasome activation, as it is the case in some auto-inflammatory diseases [73].

1.2.5. Inflammasome activation by intracellular LPS: The non-canonical pathway

An increased understanding of a new LPS-induced signaling pathway in macrophages has emerged within the last decade. The two pathways described above are initiated by LPS which is detected outside of the immune cell. In contrast, the *non*-canonical pathway of inflammasome activation revolves around the sensing of *intracellular* LPS directly by caspases [74]. The delivery of LPS into the cytosol is therefore the central step in this pathway. This can be achieved either by uptake via the TLR4/MD2/CD14 receptor complex [75], uptake of bacterial OMVs [76], or it can reach the cytosol via vacuole-living bacteria [77]. LBP could act as an alternative LPS-carrier, see chapter 1.2.6. Once intracellular, the Lipid A moiety of LPS can be

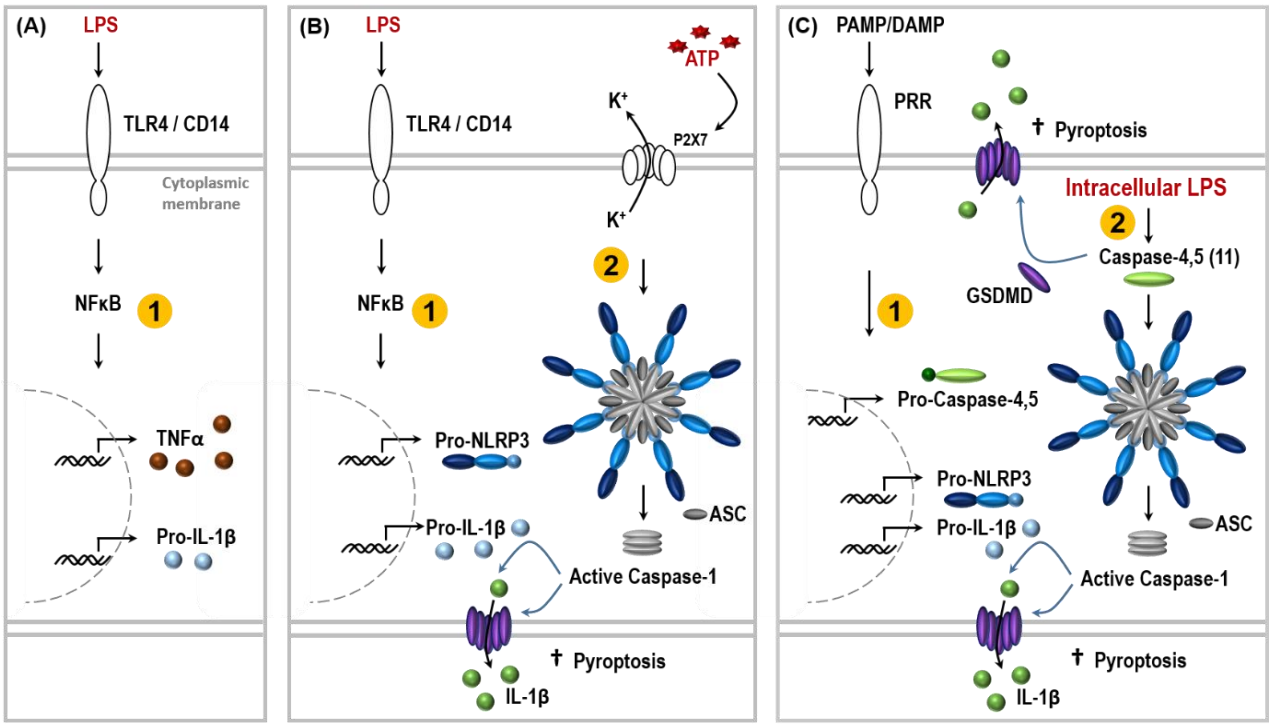

Figure 1.4: Activation pathways in human macrophages induced by extracellular or intracellular LPS. (A) TLR4/NFκB-pathway senses extracellular LPS (1st signal) and induces TNFα-production. (B) Canonical inflammasome pathway senses extracellular LPS (1st signal) via TLR4/CD14 and leads to inflammasome complex formation, IL-1β production and ATP-dependent K^+ release (2nd signal), and pyroptosis. (C) Non-canonical inflammasome pathway senses intracellular LPS via caspases-4 & -5 (caspase-11 in mice) and leads to inflammasome complex formation, IL-1β production, ATP-independent release and pyroptosis. 1 = priming step. 2 = inflammasome activation.

sensed and bound directly by the N-terminal caspase-activation and recruitment domain (CARD) of human caspase-4 & -5 (murine caspase-11) [78]. The binding (signal 2) activates the effector functions of caspase-4 & -5 which leads again to the assembly and activation of the NLRP3-inflammasome complex, with the subsequent release of mature IL-1β, and to the induction of pyroptosis via cleaving of GSDMD [79] (see Figure 1.4C).

In summary, human caspase-4 & -5 act as *intracellular* pattern recognition receptor by binding directly to intracellular LPS which leads to the activation of the downstream NLRP3-ASC-inflammasome complex, resulting in the maturation of IL-1β (and IL-18) as well as to Caspase-1- dependant and -independent pyroptosis.

1.2.6. LBP and its potential role in macrophage non-canonical inflammasome activation

The role of LBP in the immune recognition of LPS in concert with TLR4/CD14 has been described above. However, our lab group [29] showed that LBP not only transports LPS to membrane-bound receptors, but that it binds to the membrane on human monocytes and macrophages under resting conditions and even more so in the presence of LPS. It also mediates LPS intercalation into reconstituted membrane bilayers [31]. It is furthermore internalized in a TLR4 independent pathway and is intracellularly co-localized with LPS. Under conditions of inflammasome activation, intracellular LBP also co-localized with activated caspases associated with canonical and non-canonical inflammasome pathways. These observations allowed for the hypothesis, that LBP not only mediates LPS-recognition by the TLR4 receptor complex, but that it acts as a TLR4-independent LPS-transporter into the cytoplasm possibly to initiate intracellular inflammasome activation. Therefore this study investigated whether LBP conveys activation of non-canonical inflammasome activation in macrophages in the absence of danger signals as they are needed for the canonical inflammasome pathway.

1.2.7. Immune functions of surfactant proteins A and D and interaction with alveolar macrophages

The surfactant proteins SP-A and SP-D are soluble pulmonary collectins of the C-type lectin superfamily and have a collagen-like domain (CD) which is coupled to a COOH-terminal carbohydrate recognition domain (CRD). By disulfide-linkage, homotrimers of SP-A assemble into an octadecamer flower bouquet-like superstructure and homotrimers of SP-D into

dodecamers.

Both SP-A and SP-D have a strong immunological defense function in the lung via several pathways. SP-A and SP-D interact with the rough-form of LPS (lipid A and inner core, respectively) of Gram-negative bacteria, which marks them for phagocytosis by macrophages and thereby prevents recognition of LPS via the LBP/TLR4-pathway [80–82]. But they also extract LPS from the bacterial cell wall and are thereby directly bactericidal. While SP-A and SP-D enable microbial recognition, they can confer an anti-inflammatory state by downregulating the secretion of inflammatory cytokines in macrophages and upregulating the anti-inflammatory IL-10, aiding inflammation resolution [83,84]. In rat alveolar macrophages, SP-A mediates constitutive down-regulation of NFκB pathway by upreglation of IκB-α, the negative-regulator of NFκB [85]. It has also been shown that SP-A decreases the expression of TLR4 on the surface of rodent alveolar macrophages in the presence of LPS [86]. The manifold pathways of anti-inflammatory regulation of SP-A are central to maintain immune-homeostasis in the lung. SP-A is able to bind phospholipids, especially DPPC and is to a great extent localized in the corners of the tubular myelin lattice of pulmonary surfactant. SP-D specifically binds to phosphatidylinositol and aids the breakdown of pulmonary surfactant into smaller complexes which are then recycled or degraded by AECII [84,87]. The characteristics and importance of pulmonary surfactant are described in the following part.

1.3. Pulmonary surfactant and phospholipids

The inner surface of the alveoli at the air-water interface is covered by a lipoprotein layer which is called *pulmonary surfactant*. It is composed of about 90 % lipids, mostly phospholipids, and about 10 % surfactant proteins. 60 – 80 % of the phospholipids are phosphatidylcholine (PC), predominantly dipalmitoylphosphatidylcholine (DPPC) which constitutes about 50 % of the total surfactant lipids. In healthy humans adults, up to 15 % of the surfactant lipids are phosphatidylglycerols (PG). Other lipids in smaller abundance are phosphatidylethanolamine, phosphatidylserine and phosphatidylinositol. Interestingly, PG lipid species are found in only one other tissue in humans: in mitochondrial membranes.

At end-expiration, the alveoli of the lung have the tendency to collapse due to the high surface tension between the water layer and the air. The pulmonary surfactant adsorbs at exactly that

interface and displaces water molecules to lower the surface tension from ~23 mN/m down to ~0mN/m. The tighter the surfactant layer is packed, the more it lowers the surface tension. A surface tension above 2 mN/m may lead to alveolar collapse (atelectasis) [88].

The proteins contained in the surfactant consist of the hydrophilic SP-A (about 50% of the surfactant proteins) and SP-D, and of the hydrophobic proteins SP-B and SP-C. SP-A and SP-D exert mostly immunological functions, as described before, while SP-B and SP-C contribute directly to the structural stability and flexibility of the surfactant layer.
Lack of or pathological compositional changes in pulmonary surfactant can lead to impacted respiration, as in the respiratory distress syndrome.

In the following chapters, the basics of phospholipids and the life cycle of pulmonary surfactant are explained.

1.3.1. Phospholipids and pulmonary surfactant membrane

Phospholipids have a glycerol backbone with two hydrophobic fatty acid chains attached to its first and second carbon. A hydrophilic headgroup (see Table 1.1) is bound to the sn3-carbon via a phosphate group that is negatively charged. A wide variety of fatty acyl chains (differing in length and saturation) can be bound to the glycerol backbone, giving rise to a multitude of different molecular phospholipid species. The distribution of lipid species differs between mammal species, tissue and cell types.

One of the major enzyme families to degrade phospholipids is the secretory phospholipases type A2 ($sPLA_2$) family. Pulmonary macrophages secrete several forms of $sPLA_2$ from cytoplasmic granules upon stimulation, such as $sPLA_2$ type V and type X [89]. $sPLA_2$ hydrolyzes phospholipids at the sn-2 position and thereby creates free polyunsaturated fatty acids such as arachidonic acid (AA), a precursor for lipid mediators called eicosanoids, and pro-inflammatory lysophospholipids.

In lipid bilayers, the hydrophilic headgroups are directed towards the aqueous surrounding outside of the bilayer and the hydrophobic acyl chains point towards each other on the inside of the bilayer. Proteins are anchored in the membrane by mostly hydrophobic interactions with the acyl chains. They can be located on only one side of the bilayer or can span the bilayer as trans-membrane proteins, and they can be located in lipid rafts, cholesterol-enriched domains with a diameter of ~10-200 nm (liquid-ordered phase, L_O) [90]. The surrounding

membrane with low cholesterol but high amount of unsaturated phospholipids is in the liquid disordered state, L_D. Sterols, such as cholesterol, therefore have an important function in keeping membrane fluidity stable: At conditions below the transition temperature they increase the membrane fluidity by hindering tight packing of the lipid acyl chains. Above the transition temperature, they reduce the movement of the acyl chains and thus decrease fluidity.

The pulmonary surfactant in mammal lungs is essentially an oriented lipid monolayer where the lipid headgroups are directed towards the aqueous phase covering the alveolar epithelium and the hydrophobic acid chains are pointing into the air-filled alveolar lumen (see Figure 1.6). The pulmonary surfactant layer therefore forms at the liquid-air-interface. Destruction of 10 to 20% of the pulmonary surfactant, mainly by sPLA2 group V and group X, can cause acute respiratory distress [89,91]. Pulmonary Surfactant also contains cholesterol-rich lipid rafts, as cholesterol makes up about 8-10% by weight of mammalian alveolar surfactant [92], compared to approx. 30% of plasma membranes [93]. An excess in cholesterol, e.g. through leakage of blood plasma lipoproteins as a result of alveolar tissue damage, leads to a less flexible surfactant monolayer and with that to impaired surfactant function [94].

Table 1.1: Common phospholipid headgroups.

Phospholipid Species	**Abbreviation**	**Headgroup name (Charge)**	**Net charge (pH 7)**
Phosphatidylethanolamine	PE	Ethanolamine (+1)	0
Phosphatidylcholine	PC	Choline (+1)	0
Phosphatidylserine	PS	Serine (0)	-1
Phosphatidylglycerol	PG	Glycerol (0)	-1
Phosphatidylinositol	PI	Inositol	-1
Phosphatidylinositol-3,5-bisphosphate	PIP_2	Inositol-3,5-bisphosphate (-4)	-5

1.3.2. Secretion, recycling and degradation of surfactant

Pulmonary surfactant is produced by alveolar type II cells and is secreted into the alveoli where it spreads and fulfills its functions in surface tension reduction and immune defense. It is then metabolized and recycled by type II cells and by alveolar macrophages.

The production of surfactant in preterm infants, based on the synthesis of its major lipid component phosphatidylcholine (PC) from glucose, was estimated to take at least around

19 hours, with a peak at 70 hours and a half-life of 4 to 5 days [95]. There are several mechanisms that induce its increased production after birth: Surfactant synthesis is enhanced by physical stretching of the lung, but also by ATP, β-adrenergic agonists and lipid mediators like arachidonic acid and PGE_2 [96–103]. After final lung development, surfactant is going through a complex life cycle. The biosynthesis of the surfactant phospholipids starts within the Golgi bodies and the endoplasmic reticulum of type II epithelial cells. The hydrophobic surfactant proteins SP-B and SP-C are synthesized within the same compartments [104]. The lipids and proteins are stored as granular material within the cytoplasm in structures called lamellar bodies (LB). LBs have a diameter of 0.1 – 2.4 µm and there may be up to 180 LBs in any given type II cell. LBs are the product of several reorganization steps: initial phospholipid membrane accumulation within late endosomes, formation of multivesicular bodies (MVB), composite bodies (CB), and eventually lamellar bodies [105,106]. SP-B seems to promote these formation steps by facilitating the fusion of internal vesicles into these typical membrane structures. When needed, the limiting phospholipid bilayer of LBs will fuse with the cell membrane to release the content into the subphase of the alveolar space [107].

In the alveolar space the hydrophilic surfactant protein SP-A will merge with the secreted LBs and mediate the formation of a structure called tubular myelin (TM). It is a lattice-like structure that is characteristic for pulmonary surfactant. It is directly bound to, and acts as a reservoir for the surfactant monolayer at the air-water interface [108–110]. Thus, the pulmonary surfactant film is made of an apical monolayer with one or several lipid bilayers bound (via SP-B) below.

The surfactant monolayer is highly compressed during expiration, leading to low surface tension. DPPC, which is selectively integrated into the monolayer, can be tightly packed due to its saturated acyl chains and high transition temperature and gives rise to a gel-like, tilted condensed (TC) phase. Upon inspiration, other lipids from the TM, which were squeezed out during expiration, are reincorporated into the monolayer. Further liquid ordered and liquid disordered phases can be observed in the associated multilayers, which are rich in unsaturated phospholipids, aiding the squeeze-out and absorption process. These absorption mechanisms are supported by SP-B and SP-C, which reside in the fluid-phase patches. However, even at end-expiration, the monolayer does not exclusively contain DPPC, but non-DPPC patches along with surfactant proteins remain. In general, absorption of new lipid material into the surfactant structure only occurs in response to a surface tension that is above

equilibrium (20-25 mN/m). In the healthy lung, the new material is then absorbed in a matter of milliseconds in a process that is usually initiated simply by a deep breath. In contrast, desorption of lipid material from the surfactant film can take hours and occurs in response to a surface tension that is below equilibrium [111–116].

During the course of expansion and compression cycles of the pulmonary surfactant, small surfactant aggregates/vesicles are detached from the interfacial layer. They have low surface activity and contain low amounts of SP-A. These vesicles are taken up by type II cells and alveolar macrophages into early endosomes for degradation. The bulk of SP-A is redirected to the cell surface where it can re-localize with secreted lamellar bodies to form TM. Most of the phospholipids are redirected to the forming MVBs to enter the surfactant cycle anew. The remaining surfactant components undergo degradation in lysosomes [111,115,117,118].

The hydrophilic surfactant proteins SP-A and SP-D can inhibit surfactant secretion and also promote its recycling. SP-D is reported to bind the anionic phospholipid phosphatidylinositol (PI) and increase the recycling of surfactant via AECII in mice [119–121]. So far, no evidence was found that SP-D has a similar role to SP-A in assembly of tubular myelin or lipid supply for the surfactant layer.

In the previous chapters, it was established that pulmonary surfactant is of vital importance for lung homeostasis. It adjusts surface tension during inspiration and expiration to enable proper and constant gas exchange and has immunological function as it lines the biggest internal surface in contact with the outside air. It is therefore not surprising that changes in surfactant composition and quantity lead to several pathological conditions, such as the respiratory distress syndrome in newborn infants, as described in the next chapter.

1.4. Neonatal respiratory distress syndrome and the scientific rationale

Generally, the respiratory distress syndrome is a disorder in newborns characterized by impaired lung mechanics and gas exchange, surfactant deficiency and degradation, alveolar collapse, pulmonary edema and fibrosis. Different disease entities have been designated by the Montreux definition a few months after the practical work for this present study was finalized (see Table 1.2).

Table 1.2: Disease entities of the respiratory distress syndrome (RDS) as defined by the Montreux definition from 2017 [122]***.***

Abbreviation	Name	Primary cause
IRDS	respiratory distress syndrome of the premature infant	Endogeneous surfactant deficiency
nARDS	Neonatal acute respiratory distress syndrome	pneumonia, sepsis, trauma, and aspiration
PARDS	pediatric acute respiratory distress syndrome (infants between 2 and 10 months of age)	pneumonia, sepsis, trauma, and aspiration

1.4.1. Hallmarks of the respiratory distress syndrome

Primary surfactant deficiency due to immaturity of the lungs is the prominent cause of the acute respiratory distress syndrome in prematurely born babies (IRDS) and it affects almost all babies born before gestational week 28. These babies have a smaller respiratory surface with lower mechanical stability, fewer lymphatic vessels, insufficient vascular development and epithelial cell differentiation, and insufficient production of endogenous surfactant. Furthermore, the surfactant composition differs from that of term-born babies: Only at around gestational week 36 the so-called "PI/PG-switch" marks the start of pulmonary phosphatidylglycerol (PG) production and the consequent decrease in phosphatidylinositol (PI) concentration in the surfactant [4], [122], [123].

In term-born infants, respiratory distress (nARDS) can be caused by aspiration of surfactant-inactivating substances such as meconium or blood during birth, or by bacterial or viral pneumonia or sepsis. Surfactant inactivation and deficiency is not the primary cause but a direct result of the inflammatory response [122], [124].

Recognition of PAMPS, such as LPS of Gram-negative bacteria that enter the alveoli, by the local alveolar tissue macrophages leads to their activation and the secretion of inflammatory cytokines and chemokines (see chapter 1.2), and in turn to the homing of other lymphocytes, such as neutrophils, to the site of inflammation, as well as to plasma influx. The production of new surfactant is impaired due to epithelial damage, and existent surfactant is degraded by secreted phospholipase A2, which is upregulated during inflammation, and inactivated by an influx of plasma proteins such as albumin or other proteases/lipases. Lack of functional pulmonary surfactant leads to high surface tension at the air-water interface and to alveolar

collapse at end-expiration (atelectasis). The impaired gas exchange leads to decreasing blood oxygenation and the need for artificial ventilation, which in turn further damages the alveoli and terminal bronchi epithelium mechanically and finally generates pulmonary edema. An ongoing accumulation of extracellular matrix and collagen within the interstitial space by mobilized fibroblasts leads to irreversible pulmonary fibrosis [124–129] (see Figure 1.5).

The clinically established therapy and the only effective therapy option for respiratory distress to date is the application of an animal-derived pulmonary surfactant preparation (such as Curosurf®) to compensate for the insufficient amount of the endogenous surfactant and its destruction during the course of nARDS. However, the high mortality rate in babies with nARDS and the danger of permanent damage of the respiratory tissue demands further research on and improvement in clinical therapies.

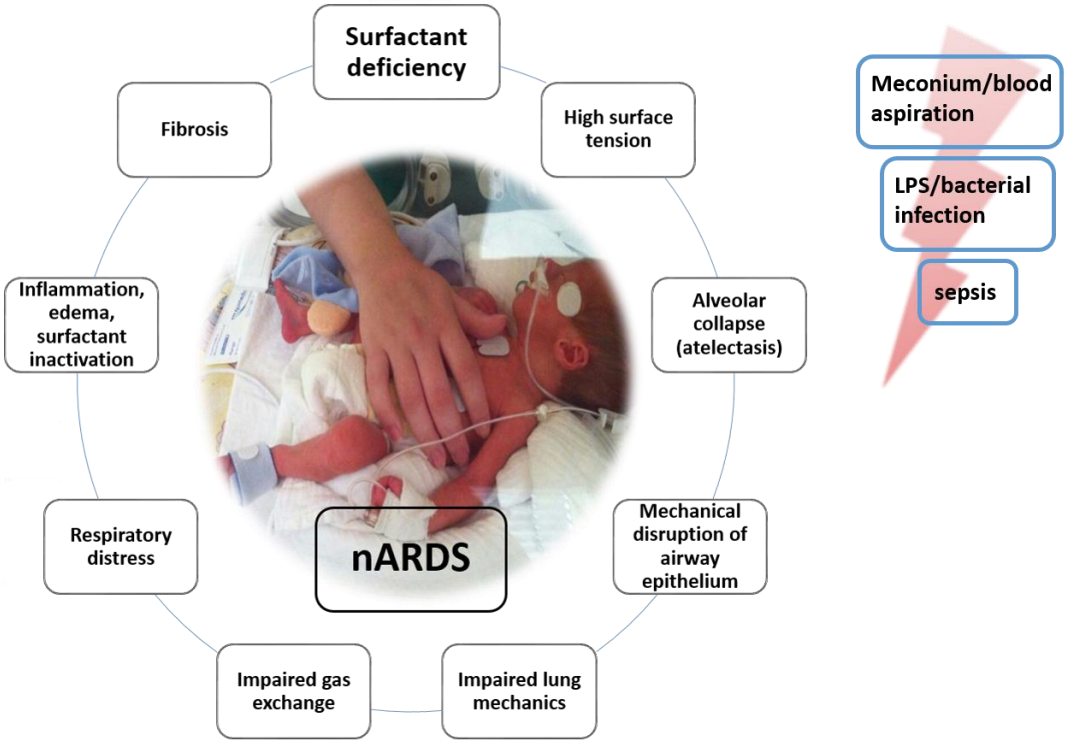

Figure 1.5: Hallmarks of neonatal respiratory distress syndrome (nARDS) caused by aspiration of meconium or blood, bacterial infection, or sepsis. Photo taken by the author in July 2013.

1.4.2. Surfactant replacement therapy of neonatal respiratory distress

Description of respiratory failure (especially in neonates) as a result of low amounts of pulmonary surfactant dates back to 1959 [130] (Avery and Meads then called it hyaline

membrane disease [HMD]), though research on neonatal respiratory care started in the late 18th century. A French physiologist called Francois Chaussier constructed a machine capable of artificially ventilating newborns with varying pressure and oxygen concentrations [131]. Further development of infant ventilation was halted until a century later when Alexander Graham Bell constructed a new ventilator jacket in 1889 [132]. Finally, in 1953 artificial ventilation became a standard treatment in neonatal care.

The first description of pulmonary surfactant was published in 1854 by the German pathologist Rudolf Virchow. He discovered a neuro myelin-like substance in alveoli [133]. Research on this "hyaline membrane" was continued in 1931 by Farber and Sweet, though it was still believed to be a remnant of aspirated amniotic fluid [134]. Two years previously, Kurt van Neergaard had described the surface tension at the air-tissue-interface inside the alveoli [135]. Brought on by research on treating gas injuries after World War II, Charles Macklin wrote that 'many hints […] point to the existence of an aqueous mucoid film clinging to the alveolar wall, and to the granular pneumocytes as its source' in 1954 [136]. It was only one year later that Richard Pattle suspected that the lack of the aforementioned substance is a frequent complication with prematurely born babies [137]. Finally in 1959, Mary Ellen Avery and Jere Mead traced HMD back to surfactant deficiency, as mentioned above. Yet, the successful implementation of artificial surfactant therapy only started in 1980, when Tetsuro Fujiwara successfully treated eight out of ten infants with artificial surfactant [138]. The use of (mostly natural) surfactant has been a common and safe treatment for infants with ARDS ever since [139].

This work undertook a new therapeutic approach by fortifying the commercially available surfactant preparation Curosurf® with the anionic phospholipids POPG, DOPG, PIP2, which are already a natural component of pulmonary surfactant, and the headgroup variant IP3. In the following, the reasoning for choosing these anionic phospholipids and derivative as a therapeutic supplement will be explained in more detail.

1.4.3. Curosurf® supplementation with anionic phospholipids as a new therapeutic approach

Phosphatidylinositol and -glycerol species belong to the group of anionic phospholipids and are natural components of (mature) pulmonary surfactant. A list of experimental and clinical

data has been published that give indications that PI and PG species would be ideal candidates to be tested in a clinical model as putative surfactant supplement.

Taken together all mammalian membrane lipids, phosphatidylglycerols present a very low percentage (about 1%). In fact, in mammals it is mostly found as a surfactant component in the lung and in mitochondrial membranes. In general, it is most commonly found as a major lipid species in bacterial and plant membranes. That makes it even more surprising, that the human adult lung can have a PG content of up to 15%, which assigns a very specific, pulmonary role to this anionic phospholipid [140].

Many immune functions of phosphatidylglycerol and phosphatidylinositol (in conjunction with surfactant) had been described prior to the start of this study. Apart from the fact that phosphatidylglycerols have a role in facilitating monolayer spreading at the air-water-interface [141], it has been shown that POPG has antiviral activity against respiratory syncytial virus and influenza A [142–144]. It also steps into agonistic interaction with TLRs (1, 2, 4 and 6) to inhibit inflammatory response by competing for binding with LPS to MD-2 and CD14 [145–147]. Berger et al. showed that DOPG is a potent inhibitor of secreted type II phospholipase A2 (sPLA2-II) synthesis by macrophages [148]. Furthermore, the PI species inositol-1,4,5-trisphosphate (IP3) initiates calcium flux from the endoplasmic reticulum by binding to IP3 receptors and thus function as second messenger. Calcium influx is especially important in the context of immune cell activation [149–151]. In this work, the non-natural occurring isomer inositol-1,2,6-trisphosphate was used. Originally produced and patented as a pharmaceutical compound by Perstorp Pharma (PP56, α-Trinositol™), it does not initiate calcium influx but it has been shown to have several anti-inflammatory effects such as pulmonary edema reduction and reduction of vascular permeability [152]. In a previous piglet model of neonatal acute lung injury it has been shown that the application of IP3 in conjunction with surfactant led to reduced influx of macrophages into the airspace and reduced pulmonary edema [153]. Phosphatidylinositol-3,5-bisphosphate (PIP2) inhibits the acid sphingomyelinase, which is upregulated during lung injury and leads to increased synthesis of ceramide, which in turn blocks DPPC synthesis and thereby increases surface tension at the air-water-interface [154–156]. Hydrolysis of PIP2 releases IP3 and DAG and IP3 is as such a derivative of the anionic phospholipid PIP2.

Ultimately in this work, for the reasons just described, these four anionic PG and PI species (DOPG, POPG, PIP2 and IP3) were chosen as additives to the commonly used Curosurf®

preparation in order to assess the potential of phospholipid supplementation as a novel therapy strategy towards nARDS in a piglet model on a clinical, tissue and cellular level. It is noteworthy that no adverse reactions towards the supplemented phospholipid species or derivative were expected from the piglets, as they occur naturally in lower amounts in the physiological pulmonary surfactant, making them ideal therapeutic candidate molecules.

1.4.4. Objective

In this work, the effect of Curosurf® supplemented with the anionic phospholipids DOPG, POPG and PIP2 as well as the headgroup variant IP3 on the regulation of inflammatory processes in nARDS was evaluated as a strategy for therapy improvement. A piglet model for nARDS was employed to mimic the inflammatory processes of the disease in term-born piglets and to analyze the novel therapy strategy. nARDS was induced in the piglets over the course of three days by a **triple hit model**:

(I) removal of endogenous pulmonary surfactant and macrophages by repeated lavages on day 1
(II) injurious mechanical ventilation on day 2 and
(III) LPS-instillation on day 3

The piglets received a defined dose of Curosurf® with or without supplemented intervention lipids 2h subsequent to each hit.

From these piglets the broncho-alveolar lavage fluid, alveolar macrophages as well as the pulmonary surfactant were experimentally assessed in the present work to answer the following questions:

- Do the clinical parameters of the piglets indicate a therapy improvement in correlation with the surfactant supplementation?
- Are the piglet alveolar macrophages in an active inflammatory state after 72h of the disease model and still responsive to LPS?
- Do the broncho-alveolar lavage fluid cytokine and surfactant protein concentrations mirror the clinical assessments?
- Does the onset of nARDS result in compositional changes of the piglet pulmonary surfactant?

- Does the fortification of Curosurf with the four anionic lipids and derivative change the piglet pulmonary lipid*ome*?

Inflammatory regulation of human peripheral blood macrophages and lung tissue macrophages was addressed experimentally to bridge animal model and human immunology:

- To what extent do the intervention lipids modify the activation of the macrophage TLR4/NFκB and canonical inflammasome pathways?
- Is the anti-inflammatory potential of the intervention lipids mirrored in the human system *in vitro*?
- Does LBP confer non-canonical inflammasome activation in human macrophages?

The key players of this study are shown in Figure1.6.

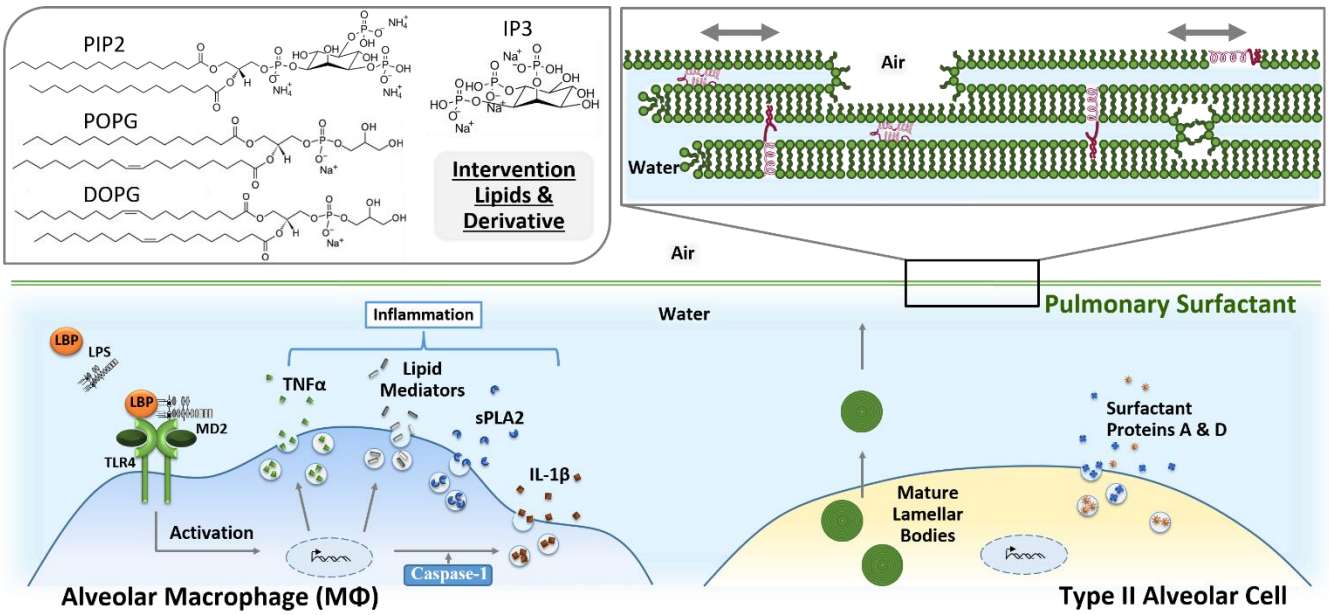

Figure 1.6.: Scientific rationale of this work.

2. Materials

2.1. Cells

Cell Type	Source
Primary human peripheral blood monocytes	Healthy adult volunteers
Primary human alveolar macrophages	Bronchoalveolar lavage from human volunteers from healthy study cohort; provided by Clinical Trial Center, Biobank Nord, Research Center Borstel
Primary human interstitial alveolar macrophages	From lung cancer patients undergoing surgery; provided by Clinical & Experimental Pathology, DZL Laboratory
Primary porcine peripheral blood monocytes	Healthy piglets
Primary porcine alveolar macrophages	Piglets undergoing triple-hit lung injury model

2.2. Primary and secondary antibodies and surfactant proteins

Donkey anti-goat IgG-HRP, polyclonal, sc-2020	Santa Cruz, Dallas, TX, USA
Goat anti-human SP-A (N19), polyclonal, sc-7700	Santa Cruz, Dallas, TX, USA
Goat anti-human SP-D (N14), polyclonal, sc-7709	Santa Cruz, Dallas, TX, USA
Goat anti-rabbit IgG-HRP, polyclonal, 7074	Cell Signaling, Danvers, MA, USA
Human SP-A	In-house preparation from human BALF
Human SP-D	In-house preparation from human BALF
Rabbit anti-human IL-1β, polyclonal, sc-7884	Santa Cruz, Dallas, TX, USA

2.3. Surfactant and intervention lipids

Curosurf® (poractant alpha), ATC-Code: R07AA02	Chiesi, Parma, Italy
DOPC (1,2-dioleoyl-sn-glycero-3-phosphocholine), 18:1 (Δ9-Cis) PC, 850375	Avanti Polar Lipids, Alabaster, AL, USA
DOPG (1,2-dioleoyl-sn-glycero-3-phospho-(1'rac-glycerol)), 18:1/18:1 (Δ9-cis) Phosphatidylglycerol, ID 840475	Avanti Polar Lipids, Alabaster, USA
Egg-PC (L-α-phosphatidylcholine (Egg, Chicken)), ID 840051	Avanti Polar Lipids, Alabaster, USA
IP3 (D-myo-Inositol-1,2,6-triphosphate), ID 10007780	Cayman, Tallinn, Estonia

PIP2 (1-(1,2R-dipalmitoyl) Phosphatidylinositol-3,5-bisphosphate), ID 10008398	Cayman, Tallinn, Estonia
POPC (1-palmitoyl-2-oleoyl-glycero-3-phosphocholine), 16:0-18:1 PC, 850457	Avanti Polar Lipids, Alabaster, AL, USA
POPG (1-palmitoyl-2-oleoyl-sn-glycero-3-phospho-(1'rac-glycerol)), 16:0/18:1 Phosphatidylglycerol, ID 840457	Avanti Polar Lipids, Alabaster, AL, USA

2.4. MS standard mix reference lipids

Cholesterol-D7, ID 700041	Avanti Polar Lipids, Alabaster, AL, USA
Cholesteryl ester 17:0 (cholest-5-en-3ß-yl heptadecanoate), ID 110864	Avanti Polar Lipids, Alabaster, AL, USA
LPC 17:0 (1-heptadecanoyl-2-hydroxy-sn-glycero-3-phosphocholine), ID 855676	Avanti Polar Lipids, Alabaster, AL, USA
PA 12:0/12:0/12:0 (1,2-dilauroyl-sn-glycero-3-phosphate (sodium salt)), ID 840635	Avanti Polar Lipids, Alabaster, AL, USA
PC OO- 4Me 16:0/4Me 16:0 (1,2-di-O-phytanyl-sn-glycero-3-phosphocholine), ID 999984	Avanti Polar Lipids, Alabaster, AL, USA
PE OO- 4Me 16:0/4Me 16:0 (1,2-di-O-phytanyl-sn-glycero-3-phosphoethanolamine), ID 999985	Avanti Polar Lipids, Alabaster, AL, USA
PG 12:0/12:0/12:0 (1,2-dilauroyl-sn-glycero-3-phospho-(1'-rac-glycerol)), ID 840435	Avanti Polar Lipids, Alabaster, AL, USA
PS 12:0/12:0/12:0 (1,2-dilauroyl-sn-glycero-3-phospho-L-serine), ID 840038	Avanti Polar Lipids, Alabaster, AL, USA
SM d18:1/17:0 (N-heptadecanoyl-D-erythro-sphingosylphosphorylcholine), ID 860585	Avanti Polar Lipids, Alabaster, AL, USA
TAG 17:0/17:0/17:0 (1,2,3-Triheptadecanoylglycerol,), ID T2151	Sigma-Aldrich, St. Louis, MO, USA

2.5. Culture media and reagents

Adenosine 5'-triphosphate disodium salt (ATP)	InvivoGen, San Diego, CA, USA
Biocoll	Biochrom GmbH, Berlin, Germany
ChillProtec	Merck Chemicals GmbH, Darmstadt, Germany
Dulbecco's MEM	Biochrom GmbH, Berlin, Germany
LPS from *E. coli* serotype O127:B8, L5668	Sigma Aldrich, St. Louis, MO, USA
FBS, fetal bovine serum	LINARIS Biologische Produkte GmbH, Dossenheim, Germany
HBSS, Hank's balanced salt solution (10x), w/ $MgCL_2$ and $CaCl_2$	Sigma-Aldrich, St. Louis, MO, USA
HEPES	Merck Chemicals GmbH, Darmstadt, Germany
L-Glutamine	Biochrom AG, Hamburg, Germany

OptiMEM®, w/ L-glutamine and HEPES, w/o phenol red	Gibco™, ThermoFisher Scientific, Rochester, NY, USA
PBS Dulbecco (10x) w/o Mg^{2+} and Ca^{2+}	Biochrom GmbH, Berlin, Germany
PBS Dulbecco (1x) w/o Mg^{2+} and Ca^{2+}	Biochrom GmbH, Berlin, Germany
Penicillin/Streptomycin	Biochrom AG, Hamburg, Germany
rhM-CSF, recombinant human M-CSF	R&D Systems, Minneapolis, MN, USA
Trypan Blue	Merck Chemicals GmbH, Darmstadt, Germany
Trypsin-EDTA 0.25%, w/o Ca^{2+} and Mg^{2+}	Biochrom GmbH, Berlin, Germany
VLE RPMI 1640 w/ 20 g/L $NaHCO_3$, w/o L- glutamine	Biochrom GmbH, Berlin, Germany

2.6. Kits

BD OptEIA human TNFα ELISA Set	BD Biosciences, San Jose, CA, USA
Human IL-1b/IL-1F2 Duoset ELISA	R&D Systems, Minneapolis, MN, USA
Pierce LDH Cytotoxicity Assay Kit	Pierce Biotechnology, Rockford, IL, USA
Porcine IL-1β DuoSet ELISA	R&D Systems, Minneapolis, MN, USA
Porcine LBP ELISA Kit	MyBioSource, San Diego, CA, USA
Porcine $sPLA_2$ ELISA kit	BlueGene, Shanghai, China
Porcine TNF-alpha DuoSet ELISA	R&D Systems, Minneapolis, MN, USA

2.7. Reagents

Acetic Acid 100% or LC-MS LiChropur™	Merck Chemicals GmbH, Darmstadt, Germany
Acryl-Bisacrylamid 40%	Merck Chemicals GmbH, Darmstadt, Germany
APS, ammonium persulfate	SERVA Electrophoresis GmbH, Heidelberg, Germany
BHT, butylhydroxytoluol	Sigma-Aldrich, St. Louis, MO, USA
Chloroform, p.a, EMSURE®	Merck Chemicals GmbH, Darmstadt, Germany
Chloroform CHROMASOL plus for HPLC	Sigma-Aldrich, St. Louis, MO, USA
Dithiothreitol (DTT)	Roche Diagnostics, Mannheim, Germany
DMSO, dimethyl sulfoxide, anhydrous	Sigma-Aldrich, St. Louis, MO, USA
EtOH, ethanol, p.a., EMSURE®	Merck Chemicals GmbH, Darmstadt, Germany
Glycine	Serva Electrophoresis GmbH, Heidelberg, Germany
H_2SO_4, sulfuric acid, p.a.	Sigma-Aldrich, St. Louis, MO, USA
HCL, 1N, Titrinorm®	VWR International, Darmstadt, Germany
Isopropanol	Sigma-Aldrich, St. Louis, MO, USA
KCL, potassium chloride	Sigma-Aldrich, St. Louis, MO, USA
MeOH, methanol, p.a.	Merck Chemicals GmbH, Darmstadt, Germany
Methanol LC-MS CHROMASOL	Sigma-Aldrich, St. Louis, MO, USA
Milk, dried	Carl Roth GmbH & CO. KG, Karlsruhe, Germany

MTT, Thiazolyl blue tetrazolium bromide, BioReagent, ≥97.5% (HPLC)	Sigma-Aldrich, St. Louis, MO, USA
Sodium chloride (NaCl)	Merck Chemicals GmbH, Darmstadt, Germany
Sodium desoxycholate	Sigma-Aldrich, St. Louis, MO, USA
Sodium orthovanadate	Sigma-Aldrich, St. Louis, MO, USA
NaOH, 1N, Titrinorm®	VWR International, Darmstadt, Germany
PageRuler™ Plus Prestained Protein Ladder, 10 to 250 kDa	ThermoFisher Scientific, Waltham, MA, USA
Pierce ECL Western Blotting-Substrate	Pierce Biotechnology, Rockford, IL, USA
Protease inhibitor (cOmplete mini EDTA-free)	Roche Diagnostics, Mannheim, Germany
SDS 10 % (w/v) solution	Bio-Rad Laboratories GmbH, Munich, Germany
TEMED	AppliChem GmbH, Darmstadt, Germany
TMB, 3,3',5,5'-Tetramethylbenzidine	Sigma-Aldrich, St. Louis, MO, USA
Tris	neoLab Migge GmbH, Heidelberg, Germany
Triton X-100	Roche Deutschland Holding GmbH, Grenzach-Wyhlen, Germany
Tween 20	Merck KGaA, Darmstadt, Germany
Tween 80	Carl Roth GmbH & CO. KG, Karlsruhe, Germany

2.8. Laboratory instruments and supplies

C-Chip disposable hemocytometer	NanoEnTek Inc., Seoul, South Korea
Centrifuge Eppendorf 5415 R	Eppendorf AG, Hamburg, Germany
Centrifuge Eppendorf 5810 R	Eppendorf AG, Hamburg, Germany
Centrifuge Labofuge	Heraeus-Christ, Osterode, Germany
CO_2 incubator *HERAcell150*	Heraeus Instruments GmbH, Osterode, Germany
EVE Automated Cell Counter	NanoEnTek Inc., Seoul, South Korea
Hotplate Stirrer, Stuart heat-stir CB162	Bibby Scientific Ltd., Staffordshire, UK
Hybond ECL Nitrocellulose	GE Healthcare Europe GmbH, Freiburg, Germany
Laminar flow hood Lamin Air HB2472	Heraeus Instruments GmbH, Osterode, Germany
Magnetic stirrer MR Hei-Mix L	Heidolph Instruments GmbH, Schwabach, Germany
Nano Drop 1000 Spectrophotometer	Thermo Fisher Scientific, Wilmington, DE, USA
Orbital shaker DOS-20S	neoLab Migge Laborbedarf-Vertriebs GmbH, Heidelberg Germany
pH electrode InLab Semi-Micro	Mettler-Toledo GmbH, Gießen, Germany
pH meter pH537	WTW GmbH, Weilheim, Germany
Q Exactive™ Plus Hybrid Quadrupole-Orbitrap™ Mass Spectrometer	Thermo Scientific, Bremen, Germany
Scale ED623S-CW	Sartorius AG, Göttingen, Germany
Scale R200D	Sartorius AG, Göttingen, Germany
Scanner CanoScan LiDE 210	Canon Deutschland GmbH, Krefeld, Germany
SDS-PAGE equipment Mini-PROTEAN® 3 System	Bio-Rad Laboratories GmbH, Munich,

Sonorex RK100 ultrasonic bath	Bandelin electronic GmbH & Co. KG, Berlin, Germany
Tecan Infinite 200P microplate reader	Tecan, Crailsheim, Germany
Teflon bags	American Fluoroseal Corp., Gaithersburg, USA
Vacuum concentrator Savant SpeedVac	Thermo Fisher Scientific, Asheville, NC, USA
Vortex mixer Vortex-Genie2	Scientific Industries, Inc., Bohemia, NY, USA
Water Bath	GFL, Burgwedel, Germany
Water purification system Milli-Q Advantage	Merck Millipore KGaA, Darmstadt, Germany
X-ray processor Kodak X-OMAT M35	Eastman Kodak Company, Rochester, UK

2.9. Software

Data Analysis 4.0	Bruker Daltonics, Bremen, Germany
FactoMineR	The R Project, version 3.2.042
Gene Cluster 3.0	Open source clustering software
GraphPad Prism 5.04	GraphPad Software, Inc., la Jolla, CA, USA
Image J 1.48v	National Institute of Health, Bethesday, MD, USA
Java Treeview-1.1.6r4	Java TreeView
LipidXplorer 1.2.7	Lipidomics Informatics for Life Sciences (LIFS)
Magellan 7.1	Tecan, Crailsheim, Germany
Microsoft Office 2010	Version 2007 SP3, Microsoft Corporation, Redmond, USA

2.10. Buffer solution recipes

Cell lysis buffer	50 mM Tris 150 mM NaCl 1 mM EDTA 0,25% sodium desoxycholate 1 mM sodium orthovanadate 1% Nonidet P40 1% Triton X–100 1 mM PMSF ddH_2O Storage at -20°C
APS 10%	1 g APS 10 mL ddH_2O 0.2 µm sterile filtration Storage at -20°C

Running buffer 10x	30.3 g Tris 144,1 g Glycin 10 g SDS 5 L ddH_2O Storage at room temperature
Sample Buffer 5x	1.5 g SDS 8.6 mL 87% Glycin 2.5 mL TBS 10x 0.9 mL ddH_2O Bromphenol blue Add 10 µL 2,5 M DTT per each 40 µL Buffer 5x before use
TBS 10x	60.57 g Tris 87.66 g NaCl 1 L ddH_2O 0.2 µm sterile filtration Storage at room temperature
TBST 1x	100 mL 10x TBS 900 mL ddH_2O 1 mL Tween20 Storage at room temperature
Transfer Buffer 1x	200 mL Ethanol 700 mL ddH_2O 100 mL Running Buffer 10x Storage at room temperature

3. Methods

3.1. Animal model

The piglet model study protocol

The entire execution of the piglet treatment regime was done by Prof. Dr. Martin F. Krause and Dr. Dietmar Spengler from the Department of General Pediatrics, University Hospital Kiel, Germany, and is comprehensively described in [157]. The following description is a summary of the procedures, including the BALF processing, that preceded the experimental analysis of the BALF, pulmonary surfactant, and piglet alveolar macrophages in this study.

75 newborn piglets (mixed country breed piglets, male and female, 2 to 3 days old, mean weight 2.5 kg) were taken directly from their sows, sedated and artificially ventilated for 72h (the full length of the animal model). An initial diagnostic lavage with 30 mL/kg warmed saline preceded the following regime within these 72h that induced acute respiratory failure in these piglets by a triple-hit lung injury model:

- **1st hit at 0h: repeated broncho-alveolar lavage** with 30 mL/kg warm physiological saline per lavage injected into the lung via a syringe hooked up to the endotracheal tube (mean 16 lavages) to achieve endogenous pulmonary surfactant deficiency
- **2nd hit at 24h: injurious ventilation** (120 min duration) by doubling the tidal volume to achieve stretch-induced injury in the alveolar epithelial cells
- **3rd hit at 48h: endotracheal instillation of 2.5 mg LPS** in 1 mL physiological saline to mimic bacterial infection

At 72h, a final lavage was performed and the piglets were killed by injection of 5 mL KCL 7.45% (for overview see Figure 3.1).

All piglets were randomized into 7 intervention groups after finalization of the initial repeated airway lavages at time point 0h. Depending on their group, each piglet received the surfactant preparation Curosurf® (poractant alpha), kindly gifted by Chiesi (Parma, Italy) with or without the addition of intervention lipids at 2, 26 and 50h of the study protocol (2h post-hit,

respectively). The untreated control group only received an air bolus at the same time points (Table 3.1). See supplementary information for detailed calculations on Curosurf® and the supplemented lipid concentrations. Curosurf® (poractant alpha) was diluted in NaCl 0.9% to a concentration of 20 mg/mL. In the S200 group Curosurf® was applied undiluted (80 mg/mL).

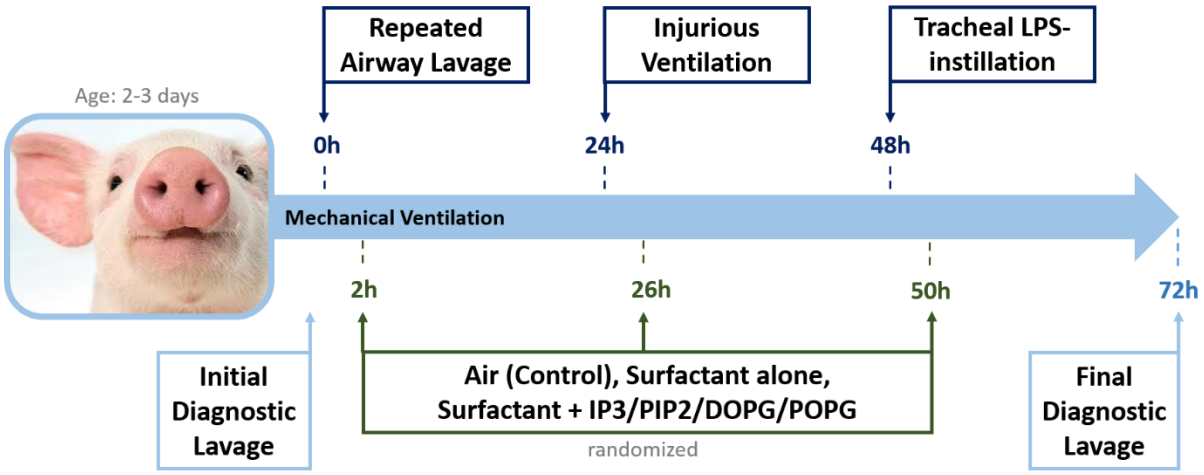

Figure 3.1: nARDS piglet triple-hit study protocol. All piglets were sedated and artificially ventilated for the duration of the study (72h). An initial diagnostic lavage with 30 mL/kg warmed saline was followed by group randomization and the following regime: Repeated airway lavages with 30 ml/kg warm normal saline per lavage to remove endogenous surfactant (at 0h). 2h of injurious ventilation to initiate mechanical stress (at 24h). Tracheal LPS instillation to mimic bacterial infection (at 48h). Application of air bolus or Curosurf® with or without intervention lipids 2h post-hit (at 2h, 26h and 50h). Final diagnostic lavage with 30 ml/kg warm normal saline per lavage before killing of the piglets with 5 mL KCL 7.45% (at 72h).

Due to its poor clinical outcome and enormous consumption of Curosurf® (1500 mg/piglet in total), the S200 group was discontinued after three piglets. Furthermore, 16 piglets in total were excluded from any data analysis due to various reasons: premature decease, severe medical conditions, and study protocol violations. Detailed data on piglet age, gender, weight, and aforementioned dropouts can be reviewed in the original publication [157].

Table 3.1: nARDS piglet study intervention groups. The study piglets were randomized into 7 treatment groups.

GROUP	CUROSURF®	ADDITIONAL INTERVENTION LIPID
CONTROL	None, only air bolus	None
S50	50 mg/kg	None
S200	200 mg/kg	None
S+IP3	50 mg/kg	+ 2.5 mg D-myo-Inositol-1,2,6-triphosphate (Cayman, Tallinn, Estonia) in 1 mL PBS

S+PIP2	50 mg/kg	+ 2.5 mg 1-(1,2R-dipalmitoyl) Phosphatidylinsositol-3,5-bisphosphate, Cayman, Tallinn, Estonia) in 1 mL PBS
S+POPG	50 mg/kg	+ 7.5 mg 1-palmitoyl-2-oleoyl-sn-glycero-3-phospho-(1'rac-glycerol) (16:0/18:1 Phosphatidylglycerol) (Avanti Polar Lipids, Alabaster, USA) in 1 mL PBS
S+DOPG	50 mg/kg	+ 7.5 mg 1,2-dioleoyl-sn-glycero-3-phospho-(1'rac-glycerol) (18:1/18:1 (Δ9-cis) Phosphatidylglycerol) (Avanti Polar Lipids, Alabaster, USA) in 1 mL PBS

3.1.1. Broncho-alveolar lavage processing

Broncho-alveolar lavage (BAL) was performed by the instillation of saline into and consequent extraction from the distal airways to recover parts of the epithelial lining fluid to receive information about the inflammatory status on an alveolar level.

For all lavages, 30 mL/kg of warm saline was instilled and extracted via an endotracheal tube. In the present animal model, the very first (at 0h) and final lavage (at 72h) were processed for diagnostic analysis. The initial lavage yielded a mean of 50 mL broncho-alveolar lavage fluid (BALF) per piglet. 0.02 mL protease inhibitor cocktail/mL BALF was added and the BALF was centrifuged at 1500 rpm for 10 min. The surfactant lipid phase, which thereby gathered as the supernatant, was collected and stored at -80°C. The cell-free lavage fluid was stored at -20°C. Single cell suspensions were created by filtering the remaining cell pellet through a 70 µM cell strainer and dissolving in 3x 10 mL PBS. One 10 mL aliquot was centrifuged at 1500 rpm for 10 min and the cell pellet was dispensed in 3 mL ChillProtec for analysis of the alveolar macrophages. The sample was maintained at 4°C while being shipped from the UKSH Kiel to the Research Center Borstel and was analyzed within 4h after harvest.

3.2. Cell culture

Primary cells from piglets and human volunteers/patients (Table 3.2) were employed.

Table 3.2: Primary cell types employed in this study.

	CELL TYPE	SOURCE
PIGLET	PBMCs	Peripheral blood from healthy control piglets
	Alveolar macrophages	BALF from piglets, triple hit study
HUMAN	PBMCs	Peripheral blood from healthy volunteers
	Alveolar macrophages	BALF from healthy volunteers (healthy study cohort)
	Interstitial macrophages	Cancer patient pneumonectomy or lobectomy

3.2.1. Preparation of human AB-Serum

Human AB-type blood from healthy donors was drawn into glass vials without heparin. Initially, the blood was incubated at room temperature for 4h to allow for complete coagulation. The blood was then centrifuged at 2500 rpm for 30 min at 4°C. The serum supernatant was withdrawn and heat inactivated at 56°C for 10 min to inactivate complement components. The serum stock was stored at -20°C and the working aliquot at 4°C.

3.2.2. Human and porcine blood mononuclear cell isolation and differentiation into macrophages

Human donor and porcine blood was drawn into heparinized glass vials to block coagulation. The blood was diluted 1:2 with Hank's balanced salt solution (HBSS) supplemented with 7.5% $NaHCO_3$. The diluted blood was then layered on top of Biocoll separating solution (3.3:1; respectively) and centrifuged at 1800 rpm for 30 min at 4°C without breaks. The top 20 mL of the supernatant (mainly plasma) was discarded and the PBMCs were harvested (Figure 3.2) and washed by dilution in HBSS, followed by centrifugation for 10 min at 1400 rpm at 4°C with breaks. All cell pellets were combined and washed again as described above.

The supernatant was discarded and the cell pellet was dissolved in RPMI 1640 supplemented with 100 U/mL penicillin, 100 µg/mL streptomycin and 2 mM L-glutamine, termed $RPMI_{PSG}$ in this work, and centrifuged at 394xg for 10 min at 4°C. The supernatant was discarded, cells were dissolved in $RPMI_{PSG}$ and counted with trypan blue staining in a hemocytometer. To

differentiate the harvested PBMNCs into macrophages, the PBMNCs were cultivated in $RPMI_{PSG}$ supplemented with 4% human AB-serum and 2 ng/mL human monocyte colony stimulating factor (rhM-CSF) in teflon bags for 6 to 8 days. Prior to use, the teflon bags were washed twice with 70% ethanol and once with the respective cell culture medium. The loaded teflon bags were incubated for 7 days at 37°C with 5% CO_2.

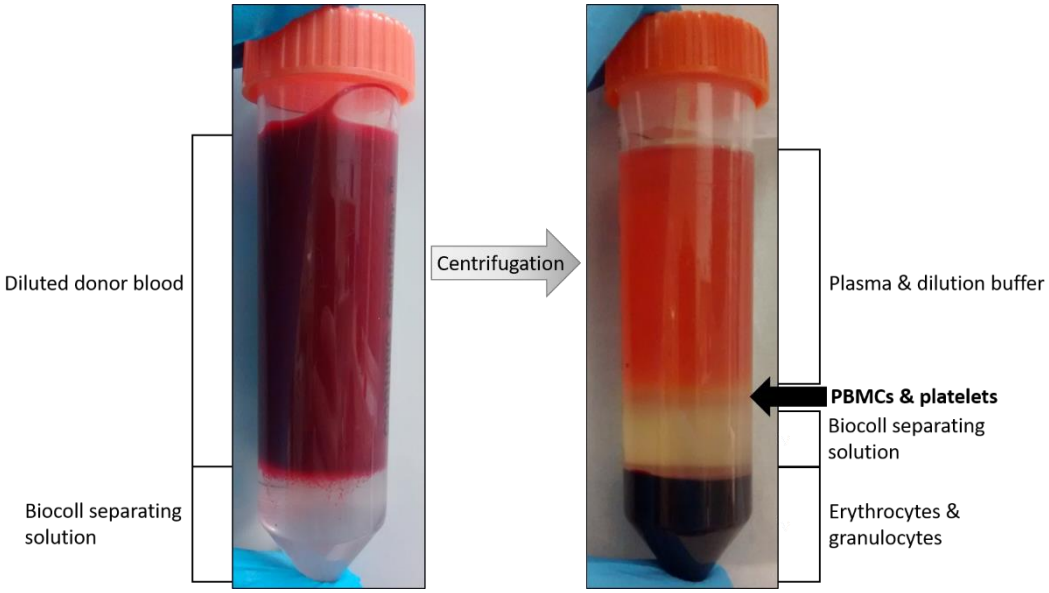

Figure 3.2: Separation of blood components by density gradient centrifugation. Blood components migrate during centrifugation dependent on their density. Black arrow = Interphase with PBMCs.

For extraction of the macrophages, the teflon bags were incubated on ice for 30 min and subsequently tilted gently several times to allow detachment of the cells from the bag. The cell solution was collected and centrifuged at 394xg for 10 min at 4°C and the cell pellet was suspended in the appropriate cell culture medium, again centrifuged and suspended, counted as described above and seeded for the experiment.

3.2.3. Isolation of primary human interstitial and alveolar macrophages

Human primary lung interstitial macrophages were isolated from surgical material of patients who underwent pneumonectomy or lobectomy due to cancer at the LungenClinic Grosshansdorf, Germany. The study was performed with permission of the local ethical committee at the University of Lübeck, (Approval number: 15-163A). Cells were isolated from non-cancer tissue areas of the specimen in the Clinical and Experimental Pathology, DZL Laboratory, and kindly provided for experiments.

Human primary alveolar macrophages from BALF of healthy human volunteers were isolated

and kindly provided by the BioMaterialBank Nord, Germany. The BAL procedure was performed at the Center for Clinical Studies Borstel, Germany.

These primary human macrophages were incubated in cell culture flasks in Opti-MEM® reduced serum media (Thermo Scientific) for 24h at 37°C, 5% CO_2, before the experiments.

3.2.4. Preparation of LPS

LPS from *E. coli* serotype O127:B8 was obtained as an aqueous ready-to-use solution of 1 mg/mL.

3.2.5. Stimulation of the macrophage TLR4/NFκB pathway and the canonical IL-1β pathway

This procedure is relevant for all macrophages with the exception of piglet BALF alveolar macrophages (described in chapter 3.2.5). The cells were harvested, counted with trypan blue staining in a hemocytometer and seeded at $1x10^5$ per well in a 96-well plate in Opti-MEM™ reduced serum media and incubated for 1h at 37°C with 5% CO_2 to allow for adherence. Afterwards, the supernatant was discarded to remove unbound cells and 180 µL fresh medium was added. Cells were incubated with the indicated concentrations of Curosurf® and/or intervention lipids IP3, PIP2, POPG or DOPG for 30 min (Curosurf® was premixed with intervention substances, where applicable) followed by stimulation with indicated concentrations of LPS for 4h at 37°C with 5% CO_2. After centrifugation for 5 min at 394xg, cell-free supernatant was collected and TNFα concentrations were determined by ELISA.
For analysis of canonical IL-1β production, the cells were instead incubated with LPS for 23h at 37°C with 5% CO_2. 5 mM ATP was subsequently added for 1h at 37°C and 5% CO_2 to induce conversion of pro-IL-1β into mature IL-1β and subsequent release into the medium. Cell-free supernatant was harvested after a total of 24h and IL-1β was determined by ELISA. Supernatants were stored at -20°C.
After collection of the supernatant, human PBMC-derived macrophages treated with the intervention lipids were lysed with 50 µL cell lysis buffer per well and lysates were subsequently stored at -20°C for Western blot analysis.

3.2.6. Stimulation of porcine alveolar macrophages retrieved from BALF

Macrophages from BALF stored at 4°C in ChillProtec were washed in $RPMI_{PSG}$ and centrifuged at 394xg for 5 min at 4°C. The cell pellet was dissolved in $RPMI_{PSG}$ + 2% FBS. The cells were subsequently counted with trypan blue staining in a hemocytometer and seeded at $5*10^4$ cells in 200 µL per well in a 96 well plate. After 1h of incubation at 37°C with 5% CO_2 the cells were directly stimulated with 10 ng/mL LPS, where applicable. After incubation for 4h at 37°C with 5% CO_2 the cells were centrifuged and the cell-free supernatant was stored at -20°C until assayed by porcine TNFα ELISA.

3.2.7. Stimulation of the macrophage non-canonical IL-1β pathway

Human PBMCs were differentiated as described above and seeded at $1x10^5$ cells per well in a 96-well plate in Opti-MEM™ reduced serum media and incubated for 1h at 37°C with 5% CO_2 to allow for adherence. Afterwards, the supernatant was discarded to remove unbound cells and fresh medium was added. As the priming step, the cells were incubated with 10 ng/mL LPS for 16h. Subsequently, the well plates were centrifuged at 394xg for 5 min at 4°C and the supernatant was discarded. The cells were then incubated with either ATP as inflammasome activation control, LPS alone, LBP alone or as a LBP/LPS mixture at indicated concentrations. The cells were again centrifuged at 394xg for 5 min. Where applicable, LBP was added to the wells prior to LPS, to avoid premature complex formation. After 4h of incubation ATP control supernatants were harvested. All other wells were then further incubated for 16 hours. The plates were centrifuged and cell-free supernatants were harvested and stored at -20°C for analysis of mature IL-1β concentrations by ELISA.

3.3. Preparation of intervention lipids

3.3.1. IP2 and PIP2

IP3 and PIP2 were used in the cell culture experiments as provided by Prof. Dr. Martin Krause, UKSH Kiel: IP3 dissolved in ddH_2O, PIP2 in PBS, each at 2.5 mg/mL. Prior to the cell culture experiments, IP3 and PIP2 were diluted to the appropriate concentrations in PBS.

3.3.2. POPG, POPC, DOPG, DOPC and Egg-PC

POPG, POPC, DOPG, DOPC and Egg-PC were obtained as powder, stored at -20°C and were formed into liposomes prior to use in the cell culture with a stock concentration of 5 mM in PBS. Therefore, appropriate amounts of DOPG and POPG were weighed into a glass vial and dissolved in chloroform. The chloroform was then evaporated under a stream of nitrogen to form a uniform lipid layer on the wall of the glass vial (a visible, colorless smear). This step is needed to pre-align the lipid headgroups along the glass wall with the acyl chains sticking out into the air. Next, PBS was added and the solution was vortexed vigorously. During agitation, the lipid sheaths detach from the glass walls to self-form large multilamellar vesicles (LMVs) to prevent contact of the hydrophobic acyl chains with the aqueous surrounding. The vial was put into an ultrasound bath for 30 min followed by a temperature cycle: 30 min incubation at 4°C and 30 min incubation at 60°C. The temperature cycle was performed three times in total. The ultrasound leads to oscillation of the gas bubbles within the solution which causes microstreaming along the LMVs causing the outer membrane leaflets to come off. Due to the aqueous surrounding, the detached bilayer leaflets automatically close up to form small unilamellar vesicles (SUVs). The liposomes were kept at 4°C over night.

3.4. Endotoxin and cytotoxicity tests

3.4.1. Limulus amoebocyte lysate (LAL) test

In this test, the lysate of granulated cells called amebocytes from the horseshoe crab (Limulus polyphemus) is used. These amebocytes contain a variety of pro-enzyme factors and proteolytic enzymes that work in unison to detect (and neutralize) pico to nano gram ranges of bacterial LPS (endotoxin). The assay was kindly performed by Dr. Nicolas Gisch, Bioanalytical Chemistry lab group, Research Center Borstel, as described in [158]. The endotoxin level in the samples measured by the LAL-test is given in endotoxin units per mL sample (EU/mL).

3.4.2. LDH-Assay

To measure cytotoxicity as a side effect of non-canonical inflammasome activation the LDH Cytotoxicity Assay Kit (Thermo Scientific™) was employed. The kit uses a colorimetric method

to evaluate the amount of lactate dehydrogenase (LDH) in the sample. LDH is a cytosolic enzyme and is only released from the cells if the plasma membrane has been damaged and/or the cell is dying. Lactate serves as the substrate that is oxidized to pyruvate by LDH (see Figure 3.3). The reaction is coupled to the reduction of NAD^+ to NADH. The kit further uses a tetrazolium salt called INT (2-(4-Iodophenyl)-3-(4-nitrophenyl)-5-phenyl-2H-tetrazolium chloride) which is reduced to a formazan product of cherry red color while NADH is oxidized back to NAD^+. The amount of LDH released is directly proportional to the amount of formazan produced which is in turn proportional to the degree of cell cytotoxicity.

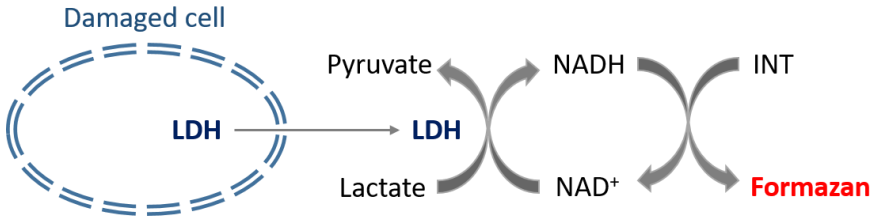

Figure 3.3: Reaction principle of the LDH cytotoxicity assay.

Macrophages differentiated from human peripheral blood monocytes were seeded and stimulated as described in section above. 45 minutes prior to end of the final 16h incubation period, the LDH Assay was performed according to the manufacturer's instructions. Three controls were run, in duplicate each: positive control as included in the kit, lysis buffer to determine maximum LDH-activity and ddH_2O to determine spontaneous LDH-activity. Absorption was read at 490 nm, as well as at 680 nm which was subtracted from all intensities as background signal.

%-Cytotoxicity was determined by the following formula:

$$\%Cytotoxicity = \frac{(LDH\ intensity\ of\ sample - spontaneous\ LDH\ intensity)}{(maximum\ LDH\ intensity - spontaneous\ LDH\ intensity)} * 100$$

3.4.3. MTT Assay

This is an assay for the metabolic activity of cells and was used as an indicator of cell cytotoxicity of Curosurf®, IP3 and PIP2 preparations. In principle, a yellow tetrazolium salt (3-(4,5-dimethylthiazol-2-yl)-2,5-diphenyltetrazolium bromide, MTT) is reduced to purple formazan crystals by NAD(P)H-dependent oxidoreductase if the cells are metabolically active (see Figure 3.4). The intensity of formazan in the sample is proportional to the cell activity.

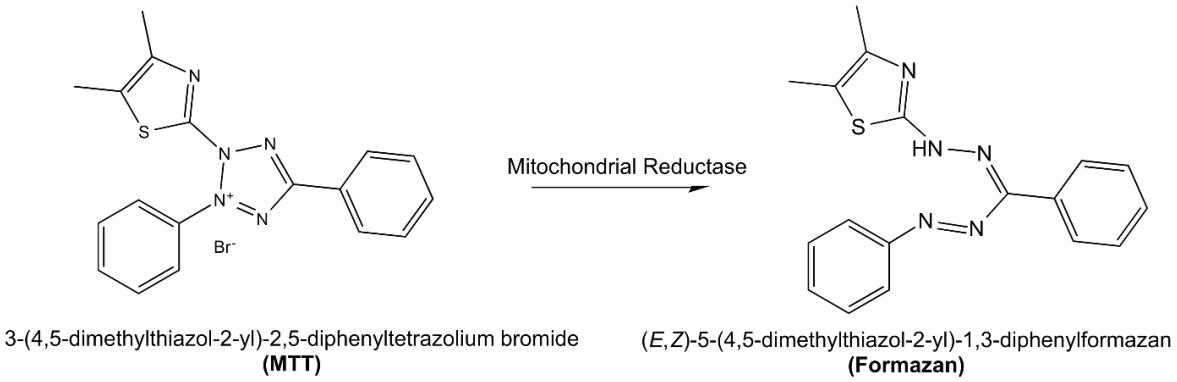

Figure 3.4: Principle of the MTT test. MTT is reduced to formazan by oxidoreductase if the cell is metabolically active. Reprinted from: Rogan Grant, CC BY-SA 4.0 <https://creativecommons.org/licenses/by-sa/4.0>, via Wikimedia Commons.

The human PBMC-derived macrophages were harvested, counted with trypan blue staining in a hemocytometer and seeded at $5x10^5$ per well in a 96-well plate in Opti-MEM™ reduced serum media and incubated for 1h at 37°C with 5% CO_2 to allow for adherence. Afterwards, the supernatant was discarded to remove unbound cells and cells were washed twice with 90 µL PBS + 10 µL Opti-MEM™. Cells were incubated in duplicates with 100 µL of Opti-MEM™ reduced serum media with the respective concentrations of Curosurf®, IP3, PIP2 or Triton X-100 (as negative control) for 4h at 37°C with 5% CO_2. Subsequently, 10 µL of MTT solution was added into each well. The solution of 12 mM MTT was freshly prepared with 5 mg MTT in 1 mL PBS. After incubation for 2h at 37°C with 5% CO_2, 100 µL stop solution (54 mL isopropanol, 6 mL Triton X-100, 480 µL HCL 37%) was added to each well. Formazan formation was immediately measured at 570 nm with a reference wavelength of 690 nm. The intensity of the medium control well was set as 100% cell activity.

3.5. Protein analysis

3.5.1. Sandwich ELISA

All TNFα, IL-1β and LBP ELISAs in this work were Sandwich ELISAs. In a sandwich ELISA, antibodies with the specificity for the target molecule are coated onto the bottom of the reaction well. Unspecific binding sites in the well are blocked with a blocking buffer. Next, the sample is added and the target molecule can bind to the capture antibodies. A biotinylated detection antibody with specificity for the target molecule is added (the epitope must differ

from the epitope recognized by the capture antibody). Streptavidin coupled horseradish peroxidase is used as reporter enzyme, which couples to biotin, and it oxidizes the chromogenic substrate 3,3'5,5'-Tetramethylbenzidine (TMB) into a diamine with a blue color, which is read at 450 nm.

Macrophage supernatants were analysed via ELISA according to the manufacturer's instructions.

3.5.2. Competitive ELISA

In a competitive ELISA the target molecule competes for binding to the detection antibody with a reference molecule bound to the plate. After washing only detection antibody bound to the reference molecule remains. The more target molecule present in the sample, the lower the output signal from the detection antibody is, and the target molecule concentration is therefore inverse proportional to assay intensity.
Porcine $sPLA_2$ ELISA was measured in BALF according to manufacturer's instructions.

3.5.3. Measurement of protein concentration in piglet BALF

To measure the total protein concentration in the piglet BALF samples, the Nano Drop 1000 Spectrophotometer (Thermo) was used. Therefore, 2 µL of the undiluted sample was pipetted onto the lower measurement pedestal (fiber optic). It is held in place by the droplets surface tension. The sampling arm is closed to bring the upper fiber optic in contact with the sample droplet. The absorbance of each samples was measured at 280 nm, where proteins typically have a strong absorbance, and is directly proportional to the total protein concentration. NaCl 0.9% was used as a blank control.

3.5.4. SDS-PAGE

Another way to detect proteins in a biological sample is by sodium dodecyl sulfate polyacrylamide gel electrophoreses (SDS-PAGE). This method was developed by Ulrich Lämmli and was first published in 1970. Proteins are separated according to their molecular weight which is based on their migration through a gel matrix (with a defined pore size) under the influence of an electric field. Theoretically, proteins of the same molecular weight would migrate differently due to distinct 3D structures and net charges. Therefore, proteins are

denatured (tertiary and secondary structures are broken down) by dithiothreitol (DTT) in the sample buffer and by short boiling. The detergent sodium dodecyl sulfate (SDS) masks the net charge and coats the protein with a negative charge that is solely dependent on the length of the protein and is thus approximate to the molecular weight.

SDS-page was run according to standard protocols with 12% acrylamide separation gels. In short, the resolving gel was prepared and poured between two ethanol-cleaned glass slides in the gel chamber. It was immediately topped with isopropyl alcohol to remove air bubbles. After 45 min incubation at room temperature the gel was completely polymerized and the isopropyl alcohol was removed. The stacking gel (5%) was poured onto the separation gel and an ethanol-cleaned vertical comb was immediately inserted into the stacking gel. After 30 min incubation at room temperature the stacking gel had polymerized as well and the gel chambers were used immediately or stored at 4°C in a humidity chamber for several days.

The samples were diluted 1:4 with Lämmli buffer (5x) which was diluted 4:1 with 2.5 M DTT. The samples were boiled for 5 min at 95°C in a thermocycler. The gel chambers were assembled in the electrophoresis chamber which was then filled with 1x running buffer. 10 µL of the samples or 2.5 µL pre-stained protein ladder were loaded into the gel pockets. The gel was run at constant 20 mA per gel per electrophoresis chamber. In the separation gel, proteins with higher molecular weight migrate slower than the proteins with lower molecular weight. The run was finished when the blue bromophenol blue tracking dye had reached the bottom of the gel after 45 - 60 min.

3.5.5. Western Blot

Following SDS-PAGE, the separated proteins were transferred to a membrane in a wet-wet system in order to stain the protein bands. Therefore the separation gel was taken out of the gel chamber (the stacking gel is discarded) and placed on top of a nitrocellulose membrane. Gel and membrane were sandwiched between filter paper and foam pads. The sandwich was then placed inside a blotting chamber cassette with the nitrocellulose membrane facing the anode in order for the negatively charged proteins to transfer onto the membrane. The blotting chamber was filled with 1x blotting buffer and electrophoresis was run at constant 400 mA for 60 min.

3.5.6. Immunostaining of Western Blot membranes

Following the protein transfer to the nitrocellulose membrane, the protein bands were stained. The membrane was removed from the electrophoresis cassette and washed in TBST for 10 min at room temperature. The membrane was blocked in 20 mL TBST + 5% dried milk for 1h at room temperature under slow, but constant shaking by a microplate orbital shaker. The membrane was washed in TBST and incubated with the protein-specific primary antibody diluted in the respective blocking buffer over night at 4°C under constant shaking at 70 rpm. After another washing step, the HRP-coupled secondary antibody was added and incubated for 2h at room temperature under constant shaking.

Table 3.3: Western Blotting and immunostaining reagents.

Analyte	TBSTT additive	Primary antibody	Secondary antibody
IL-1b	5% dried milk	Polyclonal rabbit anti-IL-1β, 1:500	goat anti-rabbit IgG-HRP, 1:5000
SP-A	5% dried milk	Polyclonal goat anti-SP-A (N19), 1:2000	donkey anti-goat IgG-HRP, 1:2000
SP-D	5% dried milk	polyclonal goat anti-SP-D (N14), 1:2000	donkey anti-goat IgG-HRP, 1:2000

After another washing step, the membrane was placed in a clear plastic wrap inside an autoradiography cassette and 3 mL of the Pierce™ ECL Western Blotting substrate was applied as instructed by the manufacturer (premixing of equal amounts of detection reagents 1 and 2). After 5 min of incubation the solution was removed from the blot with an absorbent tissue. The blot was covered with a layer of clear plastic wrap and any bubbles were carefully pressed out. An X-ray film was developed in a dark room. The horse radish peroxidase that is bound to the secondary antibody oxidizes luminol in the blotting substrate and the resulting product emits light when it decays. That way, the position of the emitted light and the intensity indicates the position and concentration of the blotted proteins. Developed X-ray films were scanned for band quantification.

3.5.7. Quantification of band intensities with ImageJ

ImageJ is an analysis software which can be used to quantify protein bands from scanned Western Blot films. The bands are selected and the software creates profile plots for each band depicting the relative intensity by plot area. For SP-A and SP-D, the intensities were normalized to the respective human SP-A or SP-D protein control in the same blot.

3.6. Mass spectrometry

3.6.1. Lipid extraction by Bligh and Dyer

Lipids from the porcine pulmonary surfactant samples (0h and 72h) obtained from BALF and three technical replicates of Curosurf® were extracted by a method described by Bligh and Dyer in 1959 [159]. NaCl was employed as blank control. For the extraction process, all glassware was pre-rinsed 3 times each with ultrapure water, methanol and chloroform. All the solvents used were LC-MS grade or of the highest purity available.

10 µL of the samples (single sample extraction) were kept on ice. 0.5 µL antioxidant (1 mg/mL BHT in MeOH) was added to each sample, as well as 5 µL internal lipid standard mix (see table 3.4), 320 µL $CHCl_3$ and 640 µL acidified MeOH (3% CH_3COOH solution). The vials were wrapped in aluminum foil to avoid light exposure. The samples were vortexed for 10 sec and mixed for 30 min at 300 rpm in a MixMate, yielding one single phase. 320 µL ultrapure water and 320 µL chloforom were added and the samples were vortexed and mixed again. The samples were then centrifuged at 3700 rcf for 15 min at 15°C to produce a biphasic system. The bottom, lipid-containing organic (chloroformic) phase was carefully collected with the use of self-sealing barrier pipet tips by slowly tilting the vial, and thereby separated from the upper, non-lipid-containing aqueous phase, and was stored on ice. To the remaining aqueous phase 320 µL $CHCl_3$ was added and the samples were again vortexed, mixed for 30 min at 300 rpm and centrifuged. The lower organic phase was again collected and the combined organic phases were centrifuged at 3700 rcf for 15 min at 15°C to separate any remaining aqueous phase. The purified organic phase was collected one last time and the solvents were evaporated with the vacuum concentrator SpeedVac. The lipid residues were resolved in

100 µL storage solution containing $CHCl_3$:MeOH:H_2O (60:30:4.5; v:v:v) and stored at -80°C until analysis.

Table 3.4: Composition of the internal lipid standard mix.

Lipid Component	Supplier	ID	Conc. in pmol/µL
SM d18:1/17:0	Avanti	860585	209
LPC 17:0	Avanti	855676	294
TAG 17:0/17:0/17:0	Sigma	T2151	176
PC OO- 4Me 16:0/4Me 16:0	Avanti	999985	193
PE OO- 4Me 16:0/4Me 16:0	Avanti	999984	183
Cholesterol-D7	Avanti	700041	1270
PA 12:0/12:0/12:0	Avanti	840635	269
PG 12:0/12:0/12:0	Avanti	840435	237
PS 12:0/12:0/12:0	Avanti	840038	232
Cholesteryl ester 17:0	Avanti	110864	234

3.6.2. Acetylation of lipid extracts for cholesterol measurement

In order to detect cholesterol by mass spectrometry it was derivatized with acetyl chloride to cholesteryl acetate, following a protocol by Liebisch et al [160]. 10 µL of the lipid extracts resolved in storage solution (see above) were mixed 1:5 (v:v) with CH_3COCl:$CHCl_3$ (1:5; v:v). The mixture was incubated at room temperature for 1h and the solvents were subsequently evaporated in a vacuum concentrator. The dried samples were stored at -20°C until analysis. Only prior to measurement were the samples resolved in 100 µL storage solution containing $CHCl_3$:MeOH:H_2O (60:30:4.5; v:v:v).

3.6.3. Mass spectrometric analysis of porcine surfactant lipids

The lipid extracts resolved in storage solution were diluted 1:50 (v:v) in spray-solution ($CHCl_3$:MeOH:i-PrOH [1:2:4; v:v:v]) supplemented with 0.05 mM tetraethyl ammonium chloride) and analyzed for lipid composition with a QExactive Plus Mass Spectrometer coupled to an automated flow-injection system and a 1100 series HPLC system. The samples were injected at a rate of 10 µL/min into an MS-Mix flow and MS scans were obtained over the course of 5 min in a mass range from m/z 350 to 1200. In total, all measurements were run

twice in positive and twice in negative ion mode. LipidXplorer was used for lipid identification and quantification.

3.7. Ethical approval

The animal study was approved by the committee on animal protection for the federal state of Schleswig-Holstein (Germany) and was carried out in accordance with the current European directive on the protection of animals used for scientific purposes.

Procedures with peripheral blood monocytes and bronchoalveolar lavage from healthy human volunteers were approved by the Ethical Commission of the University of Lübeck (Approval number AZ 15-194).

Human primary alveolar macrophages were isolated from surgical material of patients, who underwent pneumonectomy or lobectomy due to cancer at the LungenClinic Grosshansdorf, Germany. The study was performed with permission of the local ethical committee at the University of Lübeck (Approval number AZ 12-220) in collaboration with the department of Clinical & Experimental Pathology and the German Center for Lung Research (DZL) Laboratory.

The BioMaterialBank (BMB) North is funded in part by the Airway Research Center North (ARCN), Member of the German Center for Lung Research (DZL) and is member of popgen 2.0 network (P2N) which is supported by a grant from the German Ministry for Education and Research (01EY1103).

All volunteers have given informed consent.

3.8. Statistics

For statistics test the software GraphPad PRISM Version 5.04 was used. The applied test is mentioned in each diagram’s description.

3.8.1. Student's t-test

A t-test is a statistical test to compare the means of two independent, normally-distributed data sets. It offers the possibility to address the directionality of a difference between means, defining if a mean is smaller or bigger. The t-test is not to be used for more than two groups as it would underestimate the true variance and could lead to a higher chance of a type-1 error (falsely denying the null hypothesis which states that there are no differences between the mean). In such cases an ANOVA was employed.

3.8.2. Analysis of variance (ANOVA)

An ANOVA compares the means of more than two independent groups of variables to determine if there are statistically significant differences between these means. This test assumes a normal distribution in each test group. It controls the error rate of the experiment which would arise when multiple t-test were run on the same data set instead of one ANOVA. ANOVA detects these differences but does not indicate between which groups these differences exists. In order to do that a post-hoc test was used.

3.8.3. Dunnett's post test

This is a *post-hoc* test that determines which exact groups differ from one another and is usually run after an ANOVA to specify the results. Dunnet's *post-hoc* test compares several groups against one control group. The control group is always indicated in the figure details.

3.8.4. Mass spectrometric lipid*ome* data analysis and curation

Mass spectrometric measurement, spectra analysis and lipid identification was performed by Dr. Lars Eggers from the Division of Bioanalytical Chemistry, Research Center Borstel. Data output was in pmol/sample (10 µL piglet surfactant). Without cutoff, the data was expressed as absolute abundance (pmol/µL). The data was then normalized to the total lipid abundance per sample, denoted as relative abundance (mol%). To increase data quality cutoffs were set:

1a) 4 High/4 Low: Exclusion of the 4 piglet surfactant samples with the lowest total amount of lipid species and exclusion of the 4 piglet surfactant samples with the highest total amount of lipid species.

1b) 80%-Threshold: Exclusion of lipid species that were not detected in at least 80% of the piglet surfactant samples.

Table 3.5: **Overview of the piglet surfactant samples analyzed in LC-MS/MS approach and the applied data cut-off strategy.**

Total amount of surfactant samples analyzed (piglet + Curosurf®)			**84**
	0h	40	
	Control	7	
	S50	8	
	S200	3	
	IP3	5	
	PIP2	6	
	POPG	6	
	DOPG	6	
	Curosurf®	3	
Total amount of lipid species detected*			**181**
Cutoff 1a: 4 High/4 Low			-8 samples
	Control	-1	Low
	S50	-1	Low
	DOPG	-1	Low
	POPG	-1	Low
	0h	-2	High
	PIP2	-2	high
Cutoff 1b: 80%-Threshold			-101 lipid species
Final number of samples for statistical analysis			**76**
Final number of lipid species for statistical analysis			**80**
*Triglycerides not considered			

For hierarchical clustering analysis, including the intervention lipids, a higher consistency in the raw data was needed. For that reason the raw data was curated with another cutoff:

2a) 100 lipid species: Piglet surfactant samples with less than 100 identified lipid species were excluded (yielding n=60 samples).

2b) 60% Threshold: Lipid species that were not detected in at least 60% of these 60 samples were excluded (yielding n=100 lipid species).

Surfactant samples from the S200 piglet group were not included in the hierarchical clustering because initial analysis showed a wide scattering of the S200 lipid*ome*.

For hierarchical clustering without the intervention lipids, a third cutoff was implemented based on the data from the first clustering, in order to detect the strongest similarities:

2c) 10% Variance threshold: Individual lipid species that showed a variance between the samples of less than 10% were excluded.

Hierarchical clustering was calculated from the normalized abundances with Gene Cluster 3.0 and the results were visualized with Java Treeview-1.1.6r4. HC was performed for individual piglet surfactant samples and lipids using Euclidean Distance metric and Complete Linkage clustering method. The same data set (cutoff 2a and 2b) were used for PCA analysis with the software FactoMineR.

4. Results

This present study, as part of a bigger cooperation project, considers the potential of the anionic phospholipid species POPG, DOPG, PIP2 and the headgroup variant IP3 as an anti-inflammatory therapeutic supplement in the routinely used treatment of nARDS in newborns by application of Curosurf®, a porcine pulmonary surfactant extract. To that end, a triple-hit piglet nARDS model was employed to mimic the pathological conditions of nARDS in piglet lungs by repeated lavage (endogenous surfactant removal; 1st hit), injurious artificial ventilation (mechanical insult; 2nd hit) and LPS installation (Gram-negative mock infection; 3rd hit), and application of Curosurf® with or without the supplements at time point 2h post-hit, respectively.

In this chapter the results obtained from three aspects investigated in this study will be presented: The piglet clinical data and lavage analysis, anti-inflammatory mediator function of Curosurf® and anionic phospholipids on human and piglet macrophages, and a comprehensive overview of the piglet surfactant lipid*ome* in healthy, diseased and treated piglets.

4.1. Clinical parameters indicate improved therapy outcome

All piglets were thoroughly monitored throughout the entire 72h of the animal model protocol. Along with the clinical chemistry measurements, data was recorded for the following clinical parameters: Oxygenation index (OI), ventilation efficiency index (VEI), compliance of the respiratory system (C_{rs}), resistance of the respiratory system (R_{rs}) and the extravascular lung water index (EVLWI). Figure 4.1a shows exemplarily the oxygenation Index development over the course of the entire 72h, which indicates the amount of inspired oxygen needed to establish a proper partial oxygen pressure in arterial blood and is therefore a measure of the lungs gas exchange efficiency. A decreasing OI indicates improved pulmonary oxygen uptake. The healthy piglets showed a mean OI of 2.3 which increased about 5-fold with the first hit (first black arrow, see Figure 4.1a). At 2h, up to which point all piglets had received the same treatment, the mean OI decreased to 6.6. At that point the piglets received the treatment (air bolus, Curosurf® alone, Curosurf® plus intervention lipid) according to their designated group.

The OI decreased further (OI of 4.9) even in the untreated piglet control group. The second supplementation, at 26h, also decreased the OI, though to a different degree for each treatment group. The third supplementation with Curosurf® did not further decrease the OI

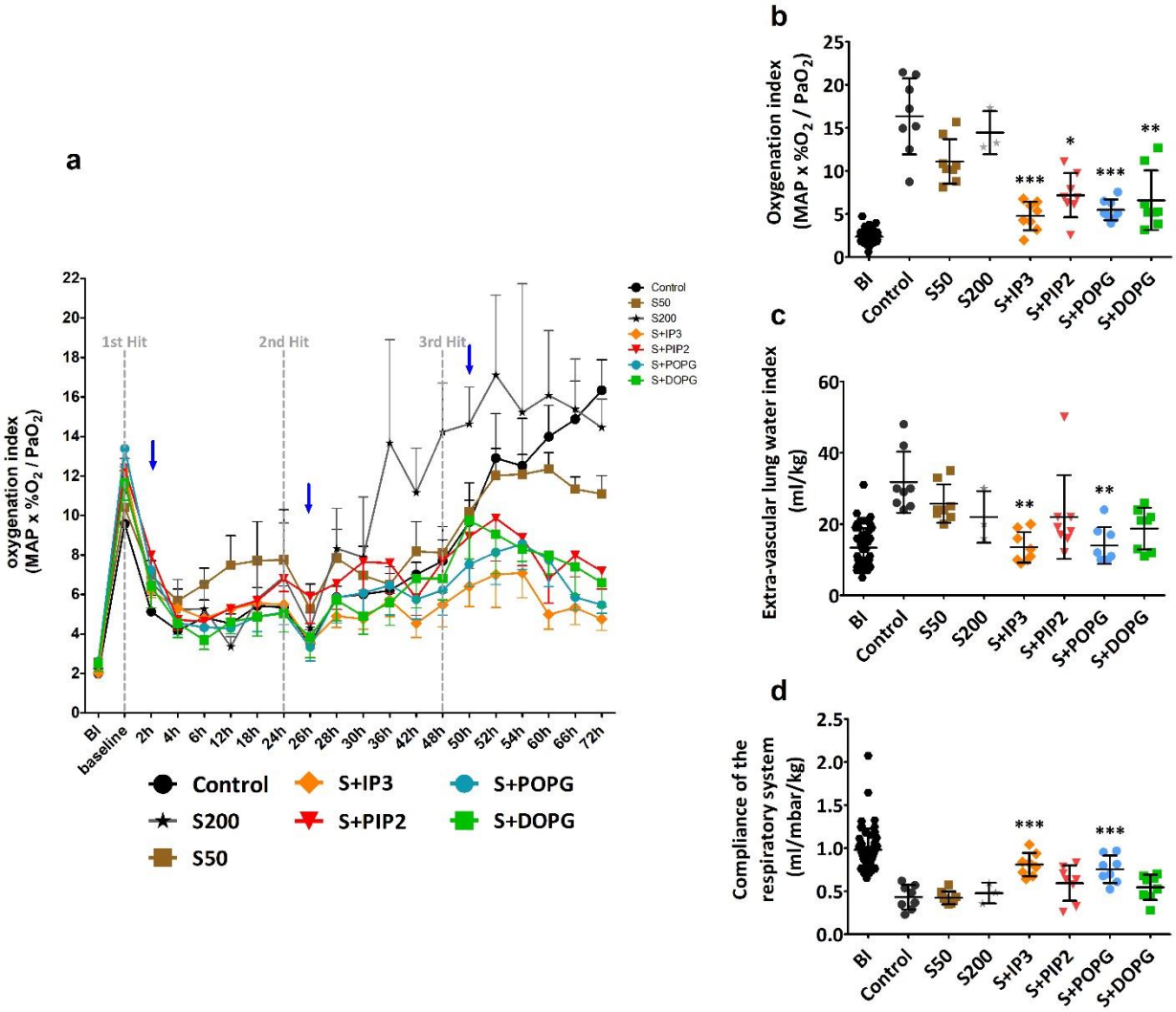

Figure 4.1: Treatment of piglets undergoing the nARDS model with anionic phospholipid supplemented Curosurf® results in improvement of clinical parameters. All piglets were artificially ventilated for 72hrs and clinical parameters were measured repeatedly. Bl = Before Injury. Repeated lavage at 0h (1st Hit), injurious ventilation (overventilation) at 24-26h (2nd Hit) and LPS instillation at 48h (3rd Hit). The respective time points are indicated by grey dashed lines. Blue arrows indicate time points of Curosurf® supplementation ± intervention lipids. a) The Oxygenation Index was measured over the course of the entire observation time (0h - 72h). b-d) Clinical parameters at the observation endpoint at 72h. Data are expressed as mean ±SD. One-way ANOVA with Dunnett's Multiple Comparison Test: *p≤0.05, **p≤0.01, ***p≤0.001. N=8 (S200 n=3). Significances shown are in comparison to the S50 control group. Data kindly provided by Prof. Martin Krause.

for any of the piglet groups beyond the OI of the 2nd supplementation. However, differences in OI between treatment groups started to emerge. By the time point 54h, the OI of all four intervention treatment groups had started to decrease whereas the OI of all three control groups (control, S50, S200) behaved contrarily. The piglets of the S200 group continuously

showed the highest OI starting at time point 28h. The endpoint measurements at 72h of the OI, EVLWI (extra vascular lung water index) and C_{rs} (compliance of the respiratory system) are shown in Figures 4.1b,c and d. While the piglets in all intervention groups displayed an improvement compared to the untreated S50 control group (Curosurf® only), piglets treated with Curosurf®+IP3 and Curosurf®+POPG had the most significant OI improvements. Additionally, supplementation with IP3 and DOPG reduced the EVLWI to the level before injury (BI).

The S200 treatment group was discontinued after treatment of three piglets due to the fact that several clinical parameters indicated a negative clinical outcome, especially the OI and the ventilation efficiency (see data in [157]). One partial exception was the lung compliance where the application of 200 mg/kg Curosurf® initially led to the highest compliance of all groups. However, it dropped after time point 12 h to reach values lower than all other piglet groups after time point 48h.

In general it can be summarized, that when all clinical parameters are considered, the treatment groups started to diverge and treatment effects became pronounced between the second and third application of Curosurf® ± supplementation. The triple hit animal model duration of 72h made it possible to monitor the animals for a prolonged time which seems to be the minimum timespan considering that the clinical parameters of the treatment groups started diverging mostly on day 2 and 3.

4.2. Analysis of broncho-alveolar lavage fluid as an indicator for disease stage

To analyze the pulmonary inflammatory status at the beginning (0h) and at the end (72h) of the nARDS animal model, several proteins that are of vital importance to the inflammatory response and surfactant homeostasis (porcine TNFα, porcine IL-1β, SP-A and SP-D, LBP, total protein) were measured in the broncho-alveolar lavage fluid (BALF) recovered from the piglets at both time points. While lavaging is a relatively invasive method (used as the first hit in this model), it nevertheless enables the removal of proteins, lipids and cells from the alveolar space of animals and can give a snapshot of the pulmonary/alveolar environment *in vivo*. As the very first lavage yielded the highest amount of cells, lipids and proteins from within the alveolar space, it was this initial BALF that was employed for the evaluation of a potential anti-

inflammatory influence of the anionic lipid species on diagnostic parameters, such as BALF content of immune-regulatory proteins (TNFα, IL-1β, surfactant proteins SP-A and SP-D) and alveolar macrophage capacity to be activated by LPS *ex vivo*. Furthermore, the LPS-binding protein (LBP), which conveys LPS recognition by macrophages, was also measured in BALF but is discussed in chapter 4.4.

4.2.1. Porcine alveolar macrophages are refractory after 72h

Broncho-alveolar lavage (BAL) with physiological saline is the most common method to sample the epithelial lining fluid and macrophages and other cells from the pulmonary space. It was consequently analyzed if piglet alveolar macrophages from BALF remain capable to respond to bacterial LPS after 72h of nARDS disease progression.

Therefore, alveolar macrophages from the piglets were harvested by BAL at 0h (initial diagnostic lavage) and at 72h (final diagnostic lavage) and stimulated with LPS *ex vivo*. The response to LPS was determined by measuring the porcine TNFα concentration in the cell culture supernatant. The results are shown in Figure 4.2**.** As all piglets were unchallenged and untreated at the time of the initial diagnostic lavage at 0h, the results from these samples were pooled.

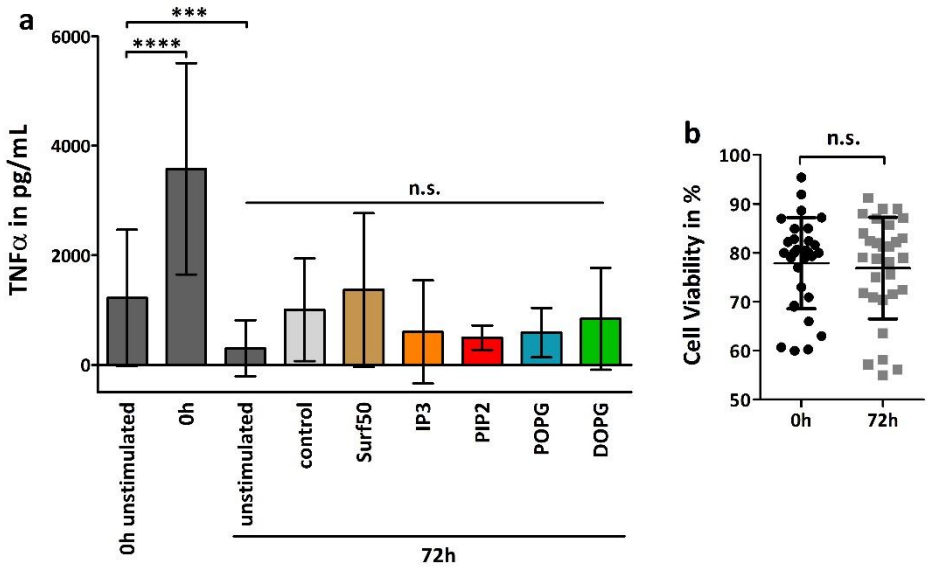

Figure 4.2: Alveolar macrophages are refractory after 72h of disease progression. Alveolar macrophages were extracted from piglet lungs by lavage at 0h and 72h, separated from BALF by centrifugation and seeded at $5x10^4$ per well. Macrophages were stimulated with 10 ng/mL LPS. a) Porcine TNFα was measured by ELISA in cell-free culture supernatant. Data from stimulated and unstimulated alveolar macrophages harvested from 0h BALF were each pooled because there is no group distinction at time point 0h (n=34). Data from all 72h alveolar macrophages that were not LPS-stimulated were pooled (n=31). 72h alveolar macrophages that were stimulated with LPS were grouped into their respective piglet group (n=4-7). b) Macrophage viability as determined by Trypan Blue. Data are expressed as mean±SD. Two-tailed t-test: ***p≤0.001, ****p≤0.0001 (n.s. = no statistical significance).

The porcine alveolar macrophages isolated at timepoint 0h showed an average baseline activation of 1195 ±209.1 pg/mL porcine TNFα ($Q_{0,25}$ = 173,3 pg/mL) even though they were not stimulated with LPS *in vitro*. That pre-stimulation might be a result of stress exerted on the macrophages by the lavage procedure, as also commonly observed in human BALF samples, transport to the analyzing laboratory or general handling. The baseline activation did not seem to significantly interfere with the LPS response since the alveolar macrophages that were harvested at time point 0h and stimulated *in vitro* with LPS did show a mean increase of TNFα secretion of ~200% compared to unstimulated macrophages. Unstimulated alveolar macrophages extracted from the piglet lung at time point 72h of disease progression showed a significantly reduced baseline level of TNFα secretion (302 ±513 pg/mL; p=0.0004), compared to 0h unstimulated samples. Upon LPS-stimulation of piglet alveolar macrophages isolated at time point 72h, no significant increase in LPS-induced TNFα secretion was observed for any of the treatment groups compared to the unstimulated 72h macrophages. That is in strong contrast to the response of the macrophages to LPS at time point 0h. The observed inactivity was not due to reduced cell viability, as can be seen in Figure 4.2b.

As a side note, the recovered cell number from each piglet varied and for some piglets too few macrophages were recovered to allow for the above mentioned experimental setup. Also, very high biological variances were apparent between the piglet samples at 72h.

4.2.2. Inflammatory protein levels in BALF indicate strong inflammatory state

Complementary to the activation status of the porcine macrophages recovered from BALF, measured by TNFα secretion after alveolar macrophage stimulation *in vitro*, the concentration of TNFα in the cell-free BALF was measured by ELISA. Figure 4.3a depicts the pooled data from the BALF analysis for TNFα concentration. Again, as all piglets were unchallenged and untreated before the initial diagnostic lavage at 0h, the data of these samples were pooled. TNFα was almost undetectable in the 0h BALF samples (with 84% of the 0h samples under the detection limit of the ELISA), indicating no initial inflammation in the piglet lung. The 0h data set showed very little variance. Mean TNFα-levels increased after 72h of disease progression and 24h after LPS-challenge in the 72h untreated control piglet BALF samples (117.5 ±119.5 pg/mL). Curosurf® application with or without intervention lipid supplementation provoked no significant difference in TNFα-levels at 72h compared to the control samples, though high biological variances were obvious for all 72h piglet groups.

IL-1β secretion into the alveolar space is an indication of inflammasome activation in alveolar macrophages. Therefore, IL-1β was measured in cell-free piglet BALF by ELSIA. Figure 4.3b depicts the pooled data from the piglet BALF analysis. Again, as all piglets were unchallenged

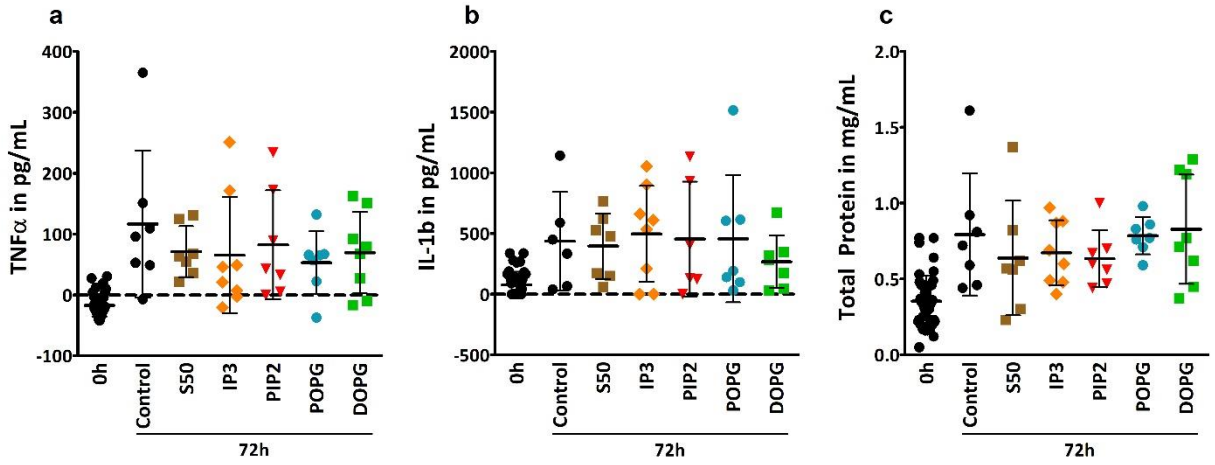

Figure 4.3: Cytokine and total protein concentration in piglet BALF before injury at 0h and at 72h. a) TNFα and b) IL-1β concentrations in cell-free porcine BALF were measured by ELISA in duplicates. c) Total protein concentration in cell-free BALF was measured by nano drop spectrophotometer. Data of all 0h BALF-samples were pooled. Data are expressed as mean±SD. No significances were detected between S50 and IP3/PIP2/POPG/DOPG. N = 7-8.

and untreated before the initial diagnostic lavage at time point 0h, the data of these samples were pooled. A low basic level of porcine IL-1β was detected in the 0h BALF samples (77.8 ±106.7 pg/mL). Mean IL-1β-levels increased 5-fold after 72h of disease progression (24h after LPS-challenge) in 72h control BALF samples (436.4 ±406.8 pg/mL). Neither did Curosurf® intervention alone (S50 group) lead to a significant difference in cytokine levels compared to the untreated control group at time point 72h, nor did a significant decrease in IL-1β level emerge between the different treatment groups and the S50 control group. Again, high biological variances were apparent. The IL-1β levels in BALF of the DOPG piglet group at 72h showed a slightly lower mean than in the other treatment groups, as well as the lowest variance (266.7 ±217.5 pg/mL). Yet no statistically significant difference to the untreated control group and S50 control group was detected.

During inflammation in the lung, numerous mediator proteins are increasingly secreted by alveolar macrophages and alveolar type II cells. Additional proteins may also enter the alveoli by plasma infiltration as a result of tissue injury. The total protein concentration in the porcine BALF samples was therefore another parameter analysed in this model of lung inflammation. The total protein concentration was measured by nano drop spectrophotometer. Figure 4.3c

depicts the data from the analysis of the initial diagnostic BALF at time point 0h and of the BALF at time point 72h. As all piglets were unchallenged and untreated before the initial diagnostic lavage at 0h, the data from these samples were pooled. A mean total protein concentration of 0.35 ±0,16 mg/mL was detected in the BALF samples at time point 0h. After 72h without intervention (control group), the mean total protein concentration doubled to 0.79 ±0.4 mg/mL. Intervention with Curosurf® (Surf50 group) did not lead to a significant decrease in protein concentration at 72h, neither did supplementation with the intervention lipids. Again, high standard deviations were observed with the highest SD in the 72h control group and the lowest in the 72h POPG group.

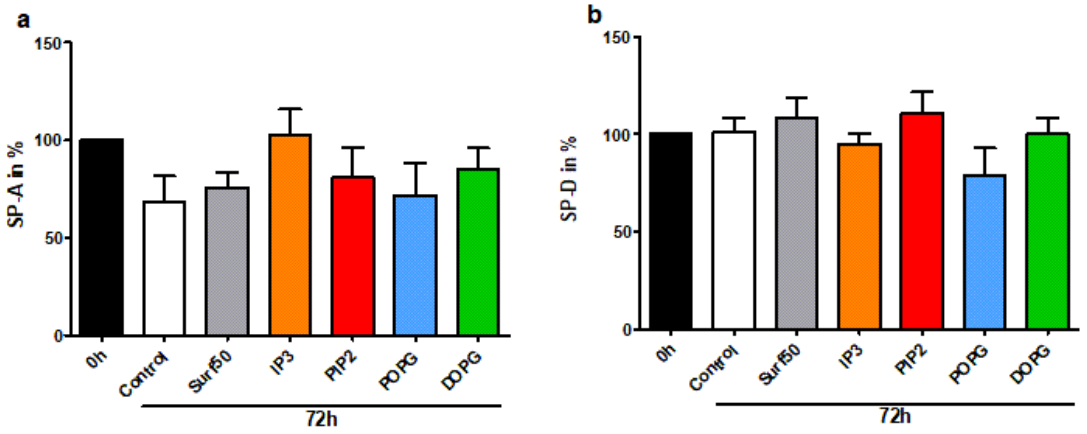

Figure 4.4: Surfactant protein A and D in piglet BALF at time points 0h and 72h. a) SP-A and b) SP-D concentrations were detected in in cell-free porcine BALF by Western blot. Band intensities were quantified with ImageJ image processing software. All sample data were normalized to a loaded human SP-D control. Afterwards, each 72h sample was normalized to its respective 0h control sample. Data of all 0h BALF-samples were pooled. Data are expressed as mean±SD. N = 7-8.

The surfactant proteins SP-A and SP-D are secreted by AECII and are an integral component of the pulmonary surfactant layer. Their most prominent functions are of anti-inflammatory nature, such as LPS neutralization, bacterial recognition and attenuation of macrophages. To analyze a possible modulation of surfactant protein concentration by the supplement lipid species, the concentrations of SP-A and SP-D were analyzed in the piglet BALF by Western blotting, see Figure 4.4.

The SP-A concentration in BALF slightly decreased in all piglet groups at time point 72h compared to the BALF from healthy piglets at time point 0h, apart from the IP3 treatment group: SP-A concentration remained at the healthy level, which may contribute to the positive clinical outcome seen in piglets treated with Curosurf®+IP3. In contrast to SP-A, there was no strong alteration of SP-D concentration detected in piglet BALF at time point 72h.

4.3. The modulation of the TLR4/NFκB and canonical inflammasome pathway in macrophages by anionic phospholipids

Above, the ability of the porcine alveolar macrophages to activate pro-inflammatory cytokine production in response to LPS was tested to determine if they are still responsive to LPS after 72h of disease progression and if that responsiveness is altered by the intervention lipids. The next step was to determine the direct effect the intervention lipids have on the activation of macrophages by LPS. As piglet macrophages were scarce, human macrophages differentiated from healthy volunteers PBMCs were used for this study, thereby connecting the piglet model to the human disease.

The first LPS-induced macrophage activation pathway discovered was the TLR4/NFκB pathway. As described in chapter 1.2.3, only one signal (provided by LPS) is required to initiate this particular signaling cascade which leads to the secretion of TNFα. Rather recently, another way of macrophage activation by LPS, termed the *canonical inflammasome pathway*, has been uncovered which not only requires the binding of LPS to the TLR4 receptor complex, but is also conditional on the presence of a second signal, such as ATP or other "danger" signals. The intervention substance Curosurf® and its anionic supplements come in direct contact with the alveolar macrophages. Thus, Curosurf® can directly exert its anti-inflammatory effects, which are known for pulmonary surfactant, on these cells.

In the following, the regulatory effect of Curosurf® on macrophage activation was confirmed. Furthermore, the inhibitory potential of the anionic phospholipids on the TLR4/NFκB pathway and canonical inflammasome activation of macrophages was quantified.

4.3.1. Curosurf® dampens the TNFα response of macrophages to LPS

It has been described in the literature that pulmonary surfactant exerts anti-inflammatory effects in the alveolar space. Therefore, the anti-inflammatory modulation of the LPS-induced macrophage activation by the porcine pulmonary surfactant preparation Curosurf® used in this porcine model of nARDS was tested. To that end, macrophages differentiated from human peripheral blood monocytes were incubated with Curosurf® and subsequently with LPS. As a measure of TLR4/NFκB-pathway activation, the concentration of TNFα in the cell-free supernatant was measured by human TNFα ELISA (see Figure 4.5). Macrophages incubated LPS-free showed no activation (TNFα secretion) and therefore Curosurf® itself showed no

activating effect towards the TLR4/NFκB pathway activation. The macrophages did show a concentration-dependent TNFα secretion in response to LPS (cells incubated without Curosurf®) as expected. However, the macrophages from each donor reacted to LPS to a different degree, a well-known behavior of primary immune cells in response to LPS, accounting for high variances. Incubation with 1 µg/mL Curosurf® had no significant attenuating effect on the macrophage response elicited by any of the tested LPS concentrations. 10 µg/mL Curosurf® had a small inhibitory effect on the LPS-induced TNFα secretion (significant only for 100 ng/mL LPS) and incubation with 100 µg/mL Curosurf® completely abrogated the TNFα secretion in response to all tested LPS concentrations and therefore completely attenuated the TLR4/NFκB pathway in these human macrophages.

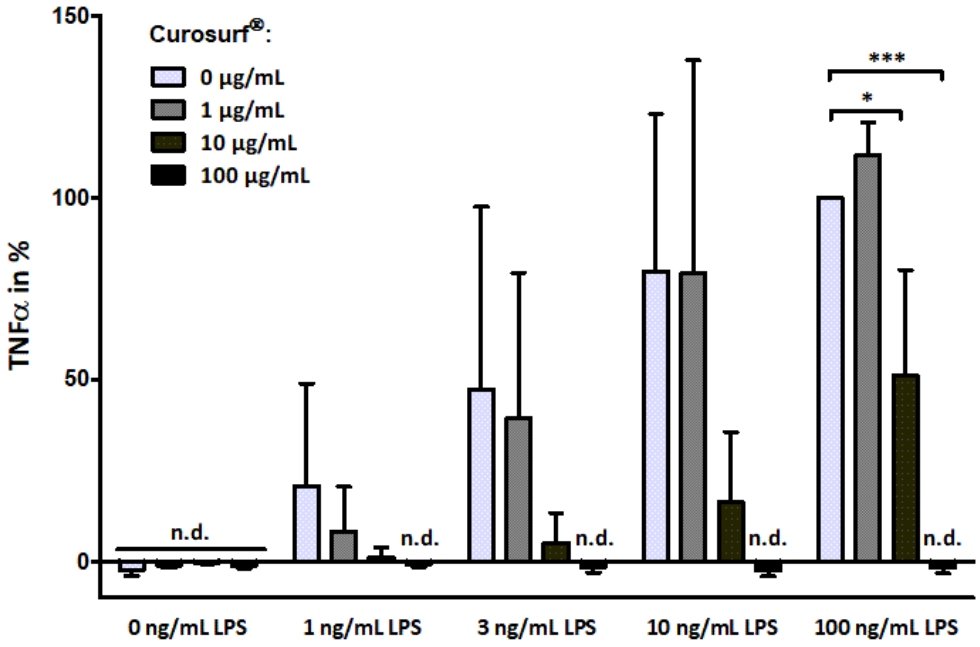

Figure 4.5: Curosurf® dampens the LPS-response of human PBMC-derived macrophages in a concentration dependent manner. Peripheral blood monocytes from human volunteers were differentiated into macrophages for 7 days, seeded at $1x10^5$ cells per well and incubated with Curosurf® at the indicated concentrations for 30 min at 37°C. LPS was added for 4h and TNFα concentration was subsequently measured in cell-free culture supernatant by ELISA. Data are expressed as mean±SD. n.d. = non detectable. Data are normalized to 100 ng/mL LPS + 0 µg/mL Curosurf®. One-way ANOVA with Dunnett's Multiple Comparison Test: *p≤0.05, ***p≤0.001. N=3 independent experiments with cells from different donors.

Prior to statistical analysis, the data were normalized to account for the donor-specific difference of the overall LPS-responsiveness. The macrophages incubated with 100 ng/mL LPS without addition of Curosurf® (100/0 control) were set as the 100% control in regards to macrophage LPS response and the read-out was thus defined as the maximum reaction to LPS in this assay. From previous experiments in the lab it is estimated that 100 µg/mL LPS is close

or at the threshold of LPS response saturation. Unfortunately it was not possible to verify this threshold for every donor by titrating the LPS concentration needed for maximum TNFα secretion for every set of donor macrophages before the actual experiment due to the fact that the macrophages used in this assay were primary cells that could not be kept in cultivation for more than 8 days (duration of the differentiation from monocytes). Therefore, the LPS concentrations used in the experiments had been titrated on donor macrophages before beginning of the actual experiments and from that the here applied concentrations had been determined.

In summary, incubation with 100 µg/mL Curosurf® completely suppressed TNFα secretion in response to all tested LPS concentrations, even to the highest LPS concentration (100 ng/mL). Incubation with 10 µg/mL Curosurf® exerted a smaller inhibitory effect on stimulation with every tested LPS-concentration. 1 µg/mL Curosurf® appeared to be a below-threshold concentration for macrophage stimulation by LPS concentrations above 3 ng/mL.

That below-threshold concentration of 1 µg/mL Curosurf® was initially used for the following experiments, in which the inhibitory potential of the intervention lipids PIP2, POPG and DOPG, as well as the headgroup variant IP3 was tested in regards to the activation of the TLR4/NFκB pathway and the canonical inflammasome pathway. Therefore, the macrophages were first incubated with Curosurf® and subsequently with the test substances and LPS. That below-threshold concentration of Curosurf® was chosen in order to specifically show the effects of the test substances without them being overshadowed by the inhibitory effects of Curosurf®. As these initial experiments had shown that the effect of the phosphoglycerols and –inositols were *not* significantly altered by the presence of 1 µg/mL Curosurf®, it was omitted in the following experiments (see supplementary Figure A1).

4.3.2. Macrophages are dampened in their LPS-response by anionic phospholipids

The porcine pulmonary surfactant Curosurf® used in this study was fortified with phospholipid species that are found as such in natural surfactant to determine their therapeutic benefit in the treatment of nARDS. The previous experiment corroborated the anti-inflammatory effect pure Curosurf® has on human macrophages. In line with that, also the anti-inflammatory potential of the phospholipid supplements (PIP2 and the headgroup variant IP3, as well as POPG and DOPG) was assessed on the TLR4/NFκB and canonical inflammasome pathway of

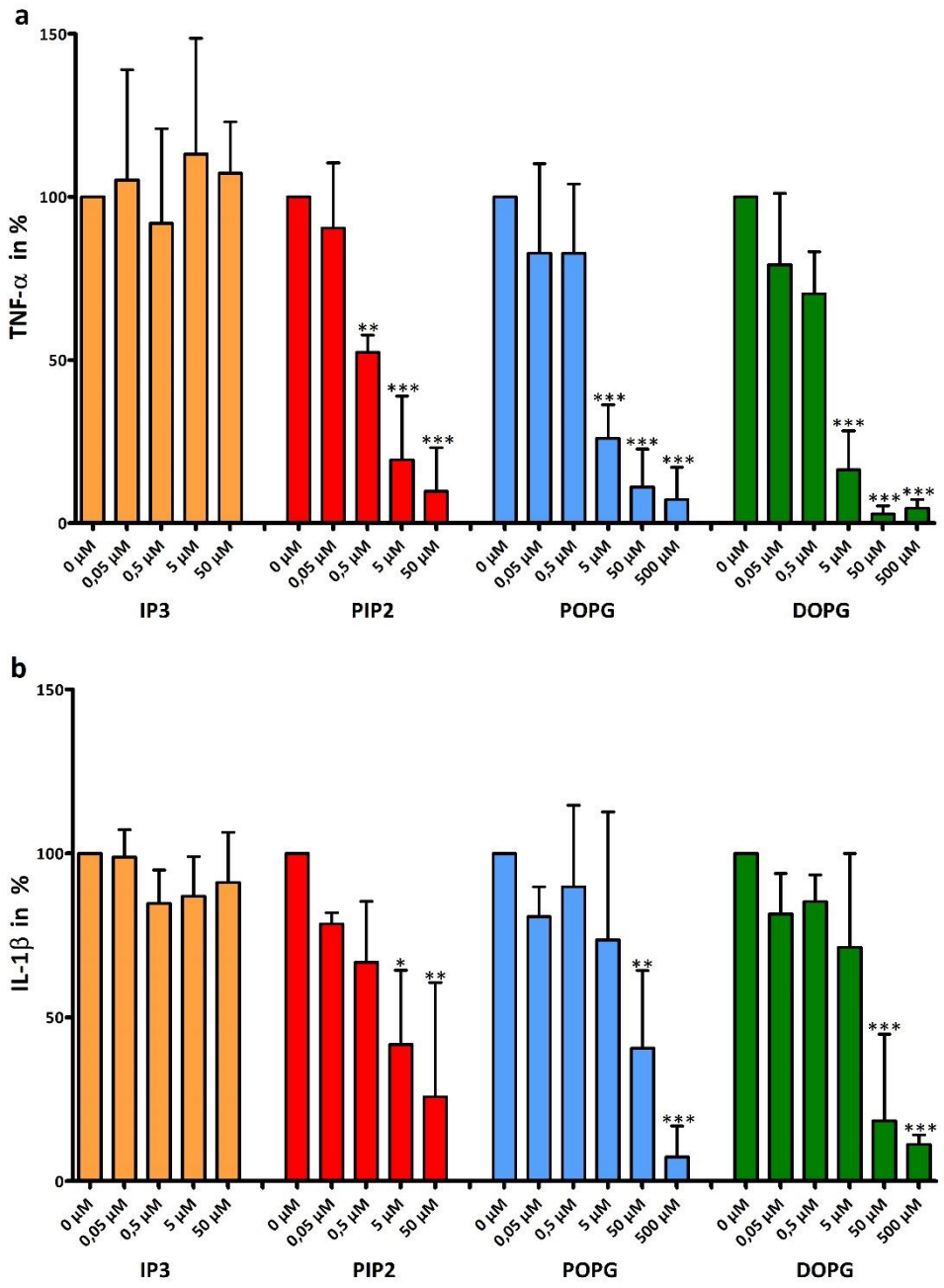

Figure 4.6: PIP2, POPG and DOPG, but not IP3, decrease the human macrophage TNFα and IL-1β secretion upon LPS-stimulation in a concentration-dependent manner. Peripheral blood monocytes from human volunteers were differentiated into macrophages for 7 days, seeded at $1x10^5$ per well and incubated with the indicated concentrations of IP3, PIP2, POPG or DOPG for 30 min at 37°C. LPS was added to a final concentration of 10 ng/mL for 4 h, after which TNFα concentration was measured in cell-free culture supernatant by ELISA (A). After an additional 19h, 5 mM ATP was added for 1 h. Human IL-1β concentration was measured in cell-free culture supernatant by ELISA (B). Data are expressed as mean±SD. Data are normalized to the respective control (incubation without addition of lipid species). One-way ANOVA with Dunnett's Multiple Comparison Test: *p≤0.05, **p≤0.01, ***p≤0.001. N=3-5 independent experiments with cells from different donors.

human macrophages. Macrophages differentiated from human peripheral blood monocytes were incubated with the respective anionic phospholipids and subsequently with LPS to determine the potential of the tested lipid species to inhibit TNFα and IL-1β secretion by LPS-activated macrophages, see Figure 4.6. Incubation without the addition of the lipid species

served as control (100% activation by LPS) and were thus set to 100% TNFα secretion for normalization purposes. Incubation of human macrophages with 0.5 µM, 5 µM and 50 µM PIP2 prior to LPS-stimulation resulted in significantly decreased TNFα secretion: 48%, 81% and 90% inhibition, respectively (see Figure 4.6a). The half maximal inhibitory concentration (IC50) of PIP2 for TNFα was determined to be 0.62 µM (see Table 4.1). In strong contrast, incubation of the human macrophages with IP3 resulted in no significant decrease of TNFα secretion upon LPS-stimulation whatsoever for all tested concentrations.

Incubation with POPG and DOPG had a similar inhibitory effect on the activation of the TLR4/NFκB pathway as PIP2 (see Figure 4.6a): TNFα secretion was significantly decreased. 5 µM, 50 µM and 500 µM POPG resulted in 74%, 89% and 93% inhibition of TNFα, respectively. And similar, incubation with 5 µM, 50 µM and 500 µM DOPG resulted in 84%, 97% and 95% inhibition of TNFα, respectively. Half maximal inhibitory concentration of POPG and DOPG for TNFα were calculated to be 1.96 and 1.01 µM, respectively, see Table 4.1.

Next, to determine the inhibitory effect of the four intervention substances on human macrophage inflammasome activation, human macrophages were again pre-incubated with IP3, PIP2, POPG and DOPG and subsequently stimulated with LPS. Whereas the TLR4/NFκB macrophage activation pathway leads to the secretion of TNFα, the canonical inflammasome activation induces the secretion of IL-1β. Therefore, this time IL-1β was chosen as read-out for the inhibition of human macrophage activation by LPS (see Figure 4.6b).

Analog to what was already seen for human TNFα secretion, none of the four IP3 concentrations had any discernable effect on the secretion of IL-1β by human macrophages in response to LPS stimulation. In contrast, yet again, incubation of human macrophages with 5 µM and 50 µM PIP2 prior to LPS-stimulation resulted in 58% and 74% inhibition of IL-1β-secretion, respectively. The IC50 of PIP2 for IL-1β is 2.61 µM (see Table 4.1). Human macrophages incubated with 50 µM and 500 µM POPG showed a secretion of IL-1β upon LPS-stimulation that was decreased by 60% and 96%, respectively. 50 µM and 500 µM DOPG resulted in 82% and 89% inhibition of IL-1β secretion, respectively. The IC50 for POPG was 23.78 µM and the IC50 for DOPG was 11.53 µM (see table 4.1).

The canonical inflammasome pathway was 9-fold more sensitive to inhibition by PIP2 compared to POPG and 4-fold more sensitive compared to DOPG. However, the partial inhibition of human IL-1β secretion only started being significant for concentrations of 5 µM PIP2 and 50 µM POPG/DOPG. That stands in contrast to 0.5 µM PIP2 and 5 µM POPG/DOPG

for human TNFα secretion. Therefore, PIP2 was 4 times more effective in reducing human TNFα secretion upon LPS-stimulation than human IL-1β secretion. The difference is even more pronounced for the glycerophospholipids: DOPG inhibited TNFα secretion when given in 10-times lower concentration compared to IL-1β secretion, and POPG even 12-times lower. So the TLR4/NFκB pathway is more sensitive to attenuation by PIP2, POPG and DOPG than the canonical inflammasome pathway.

Table 4.1: Half maximal inhibitory concentrations (IC50) of the anionic phospholipids PIP2, POPG and DOPG. IC50 values were calculated with GraphPad Prism 5.04 by non-linear regression of the log transformed cytokine concentration data.

In µM	**Human TNFα**	**Human IL-1β**
IC50 PIP2	0.62	2.61
IC50 POPG	1.96	23.78
IC50 DOPG	1.01	11.53

Considering necessary dilution factors of the tested lipid species within the experimental protocol, the stock concentration of PIP2 (2.5 mg/mL = 2.411 mM) that was received from the lab of Prof. Dr. Martin Krause did not allow for higher experimental concentrations than 50 µM. IP3 (2.5 mg/mL = 5.143 mM) was adjusted accordingly.

An MTT test for cell viability verified that the different results between IP3 and PIP2 were not due cytotoxicity of the lipid compounds (Figure 4.7).

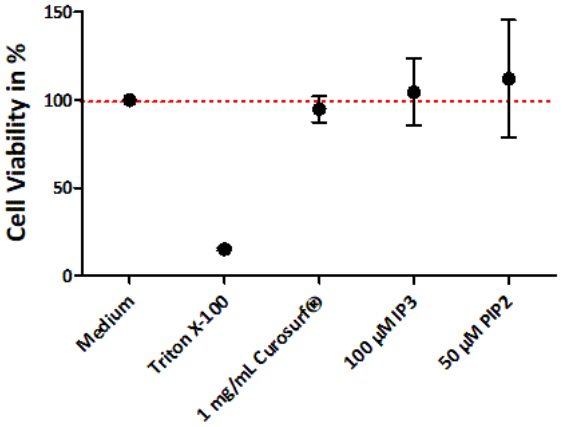

Figure 4.7: Distinct effects of the IP3 and PIP2 preparations were not due to cytotoxicity of the lipid compounds. Peripheral blood monocytes from human volunteers were differentiated into macrophages for 7 days, seeded at $1x10^5$ per well and incubated with the indicated concentrations of Curosurf®, IP3 and PIP2 for 30 min at 37°C. LPS was added to a final concentration of 10 ng/mL for 4 h. Cell viability was tested by MTT assay. N=2 independent experiments.

PBMC-derived macrophages are readily available from healthy volunteers but are differentiated *in vitro*, which makes them only a model of macrophages *in vivo*. Therefore, the

inhibitory effects of PIP2, POPG and DOPG were verified in primary human lung interstitial macrophages (see Figure 4.8) and primary human alveolar macrophages (see Figure 4.9). Due to a limited number of cells it was not possible to titrate the lipid concentrations as was done for the PBMC-derived macrophages. Therefore, the highest tested concentrations of the intervention lipids were chosen. The anti-inflammatory effects of the tested lipids seen in

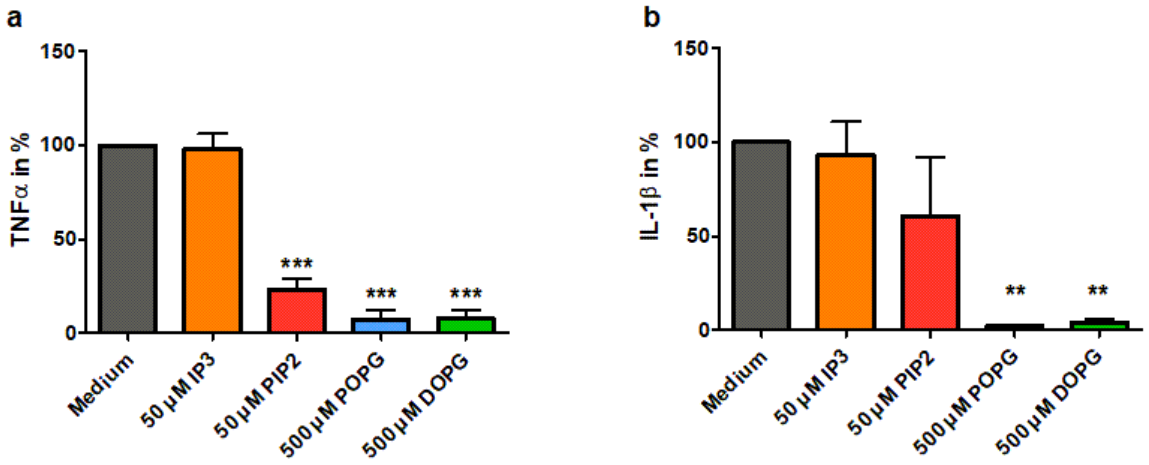

Figure 4.8: Primary human interstitial lung macrophages show inhibition by PIP2, POPG and DOPG. Primary lung interstitial macrophages isolated from surgical pneumonectomy or lobectomy material from cancer patients were seeded at $1x10^5$ in serum-free conditions and incubated with the indicated concentrations of IP3, PIP2, POPG or DOPG for 30 min at 37°C. LPS was added to a final concentration of 10 ng/mL for 4 h, after which TNFα concentration was measured in cell-free culture supernatant (a). After an additional 19h, 5 mM ATP was added for 1 h. Human IL-1β concentration was measured in cell-free culture supernatant (b). Data are expressed as mean±SD. Data are normalized to the respective medium control (incubation with LPS but without lipid species). One-way ANOVA with Dunnett's Multiple Comparison Test: **p≤0.01, ***p≤0.001. N=3 independent experiments.

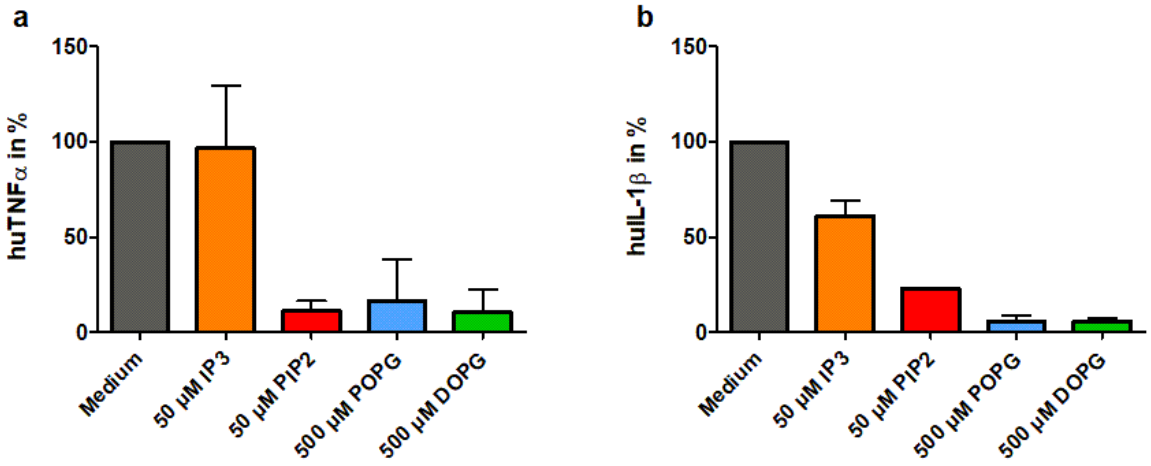

Figure 4.9: Primary human alveolar macrophages show inhibition by PIP2, POPG and DOPG. Primary alveolar macrophages isolated from BALF of healthy human volunteers were seeded at $1x10^5$ in serum-free conditions and incubated with the indicated concentrations of IP3, PIP2, POPG or DOPG for 30 min at 37°C. LPS was added to a final concentration of 10 ng/mL for 4 h, after which TNFα concentration was measured in cell-free culture supernatant (a). After additional 19h, 5 mM ATP was added for 1 h. Human IL-1β concentration was measured in cell-free culture supernatant (b). Data are expressed as mean±SD. Data are normalized to the respective medium control (incubation without lipid species). N=2 independent experiments (no statistical testing).

In summary, PIP2 decreased the secretion of TNFα (TLR4/NFκB pathway) and IL-1β (canonical inflammasome pathway) in response so LPS starting at lower concentrations compared to both phosphoglycerols POPG and DOPG. All three lipids inhibited the TNFα secretion more efficiently than IL-1b secretion.

IL-1β is initially expressed as its pro-form upon TLR4 activation and translocation of the transcription factor NFκB into the nucleus. To detect whether the expression of the pro-form is also inhibited, the cell lysates were analyzed for pro-IL-1β via Western Blotting (Figure 4.10).

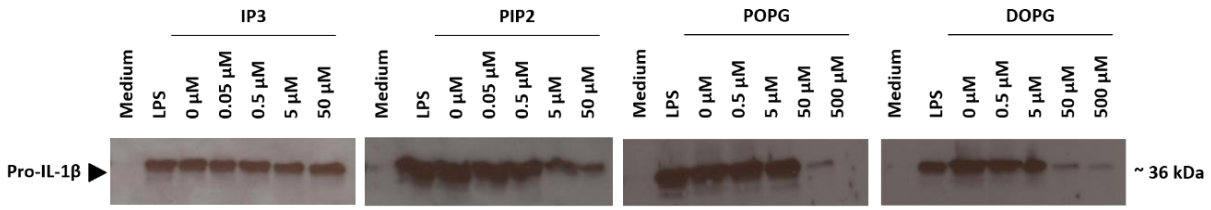

Figure 4.10: PIP2, POPG and DOPG attenuate LPS-induced pro-IL-1β expression in human PBMC-derived macrophages. Peripheral blood monocytes from human volunteers were differentiated into macrophages for 7 days, seeded at $1x10^5$ per well and incubated with the indicated concentrations of IP3, PIP2, POPG or DOPG for 30 min at 37°C. LPS was added to a final concentration of 10 ng/mL for 23 h. 5 mM ATP was added for 1 h. Cell lysates were analysed for pro-IL-1β by Western Blotting. Data from one donor.

A dose-dependent reduction ofpro-IL-1β was detected in lysates of macrophages treated with all three anionic lipids (PIP2, POPG, DOPG), but not IP3. Just as well, PIP2 again showed a stronger inhibitory activity compared to POPG and DOPG: Starting at 5 µM PIP2, less pro-IL-1β was detected in the cell lysates. This result indicates an inflammatory regulation upstream of pro-IL-1β expression.

4.3.3. IP3 and PIP2 effects on the LPS-induced response of human macrophages is comparable to porcine macrophages

In order to connect the aforementioned results of the lipid species on human macrophage activation by LPS to the nARDS piglet model, the same experimental setup was used with macrophages that were differentiated from *porcine* peripheral blood monocytes. Blood samples of two piglets (designated piglet 85 and piglet 86) were tested. Due to the low volume of porcine blood and accordingly monocytes, only the effects of IP3 and PIP2 (no effect on human macrophages versus strongest effect, respectively) were tested in the highest possible concentration. Also, macrophages from piglet 86 were seeded in triplets, but macrophages from piglet 85 could only be seeded in doublets. Again, the porcine macrophages were incubated with IP3 or PIP2 for 30 min followed by LPS-stimulation for 4h. As seen in

Figure 4.11, incubation of the porcine macrophages (from piglet 86) with 50 µM PIP2 prior to LPS-stimulation led to a nearly complete inhibition of porcine TNFα secretion and thus confirms the results in human macrophages for that particular PIP2 concentration. In contrast, again comparable to human macrophages, incubation with 50 µM IP3 triggered no reduction in porcine TNFα secretion. Interestingly, 500 µM IP3 triggered an 1.5-fold increase in TNFα

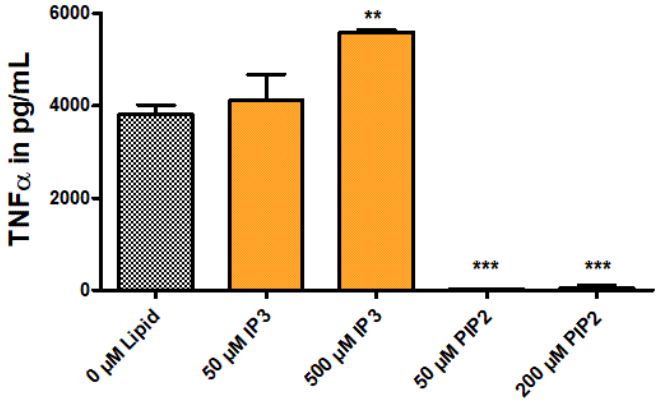

Figure 4.11: PIP2 inhibits TNFα secretion upon LPS-stimulation in porcine macrophages. Peripheral blood monocytes from two piglets were differentiated into macrophages for 7 days, seeded at $1x10^5$ per well and incubated with the indicated concentrations of IP3 and PIP2 for 30 min at 37°C. LPS was added to a final concentration of 10 ng/mL for 4 h, after which porcine TNFα concentration was measured in cell-free culture supernatant. Data are expressed as mean±SD. Paired T- Test: **p≤0.01, ***p≤0.001. N=3 (technical replicates). Data are representative of the same experiment for both piglet samples.

secretion for both piglets compared to the control without lipids. The parallel results of the macrophages derived from peripheral blood monocytes from piglet 85 (data not shown) corroborate the increase in TNFα secretion when pre-incubated with 500 µM IP3. Repetitions of the experimental setup with finer concentration intervals would be necessary to confirm any kind of antithetic IP3-induced TLR4/NFκB pathway activation enhancement. In summary, the attenuation of the TLR4/NFκB pathway by PIP2, and the lack thereof by IP3 (up to 50 µM), is inherent to both human and porcine macrophages.

4.3.4. The anionic headgroup, and not the lipid tail, conveys the inhibitory effect on macrophage TLR4/NFκB and canonical inflammasome activation

To determine if the inhibitory effect of the anionic lipids is conveyed by the anionic headgroup or the lipid acyl chain of POPG and DOPG, a comparison experiment was drafted with lipids that were comprised of the same acyl chains but with neutral headgroup charge (palmitoyl-oleoyl phosphatidylcholine [POPC], dioleoyl phosphatidylcholine [DOPC], natural mixture of egg phosphatidylcholine [Egg-PC]). The same experimental procedure as above was applied. Macrophages differentiated from human peripheral monocytes were incubated with the

intervention lipids and the neutral counterparts prior to stimulation with LPS. Again, the TNFα- and IL-1β secretion from LPS-stimulated macrophages without added lipids were set as 100% secretion control and was thus used to normalize the data (see Figure 4.12).

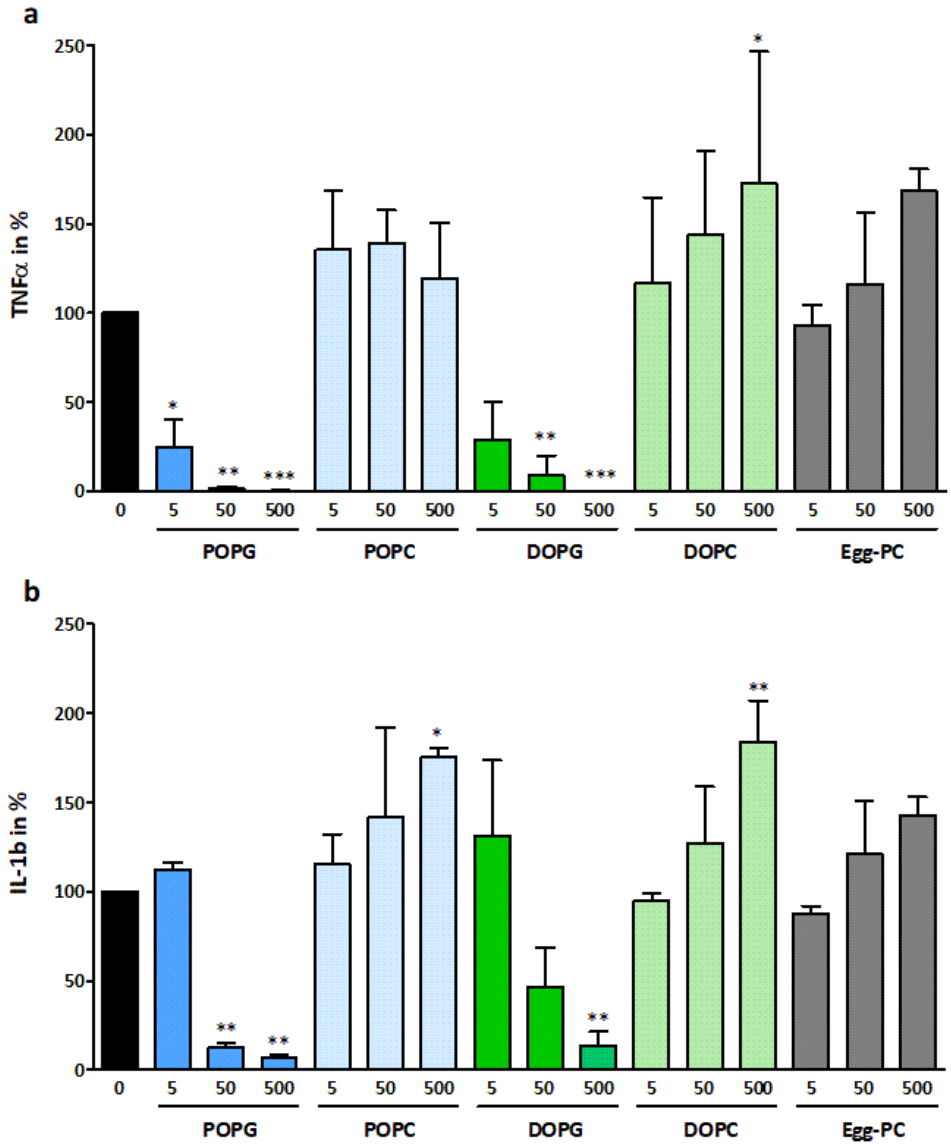

Figure 4.12: DOPC increases TNFα and IL-1β secretion in human macrophages upon LPS-stimulation. Peripheral blood monocytes from human volunteers were differentiated into macrophages for 7 days, seeded at $1x10^5$ per well and incubated with the indicated concentrations of IP3, PIP2, POPG, DOPG, DOPC, POPC or egg-PC in µM for 30 min at 37°C. LPS was added to a final concentration of 10 ng/mL for 4h, after which TNFα concentration was measured in cell-free culture supernatant by ELISA (a). After an additional 19h 5 mM ATP was added for 1h. Human IL-1β concentration was measured in cell-free culture supernatant by ELISA (b). Data are expressed as mean±SD. Data are normalized to the respective control without addition of lipid species. One-way ANOVA with Dunnett's Multiple Comparison Test: *p≤0.05, **p≤0.01, ***p≤0.001. N=3 independent experiments.

As seen in the previous experiments, incubation with 5, 50 and 500 µM POPG and DOPG again led to a significantly decreased TNFα- and IL-1β secretion. In absolute contrast, incubation of the macrophages with the corresponding neutral PC-lipid species POPC, DOPC and Egg-PEC

did not reduce the macrophage response to LPS for either TNFα or IL-1β secretion. In fact, a reverse macrophage response to LPS was observed: both TNFα and IL-1β secretion increased, especially in response to the addition of DOPC. Incubation with 500 µM DOPC led to a significant increase in TNFα and IL-1β secretion by 72% and 83%, respectively. Incubation with 500 µM POPC led to an increase in IL-1β secretion by 75%.

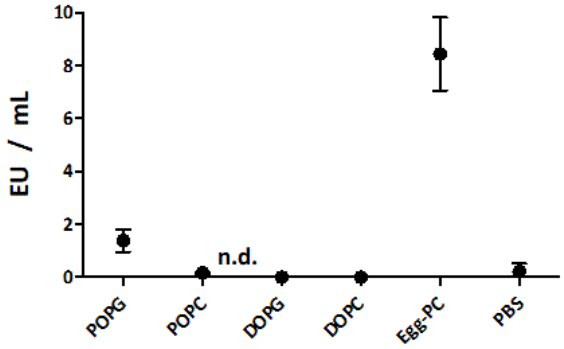

Figure 4.13: PC preparations did not show endotoxin contamination as analyzed by LAL test. The assay was performed as described in [157]. Phospholipids at 5 mM in PBS. N=2 (technical replicates).

An increase in macrophage activation, as seen for 500 µM DOPC, can be initiated by many factors, such as pyrogen contamination of the lipids used in these experiments. To verify that

Table 4.2: Approximated endotoxin levels in the lipid preparations. Phospholipids at 5 mM in PBS. N=2 (technical replicates).

Lipid preparation	EU / mL	Approx. pg LPS/mL in reaction well
POPG	1.38	13.8
DOPG	0	0
DOPC	0.01	0.1
POPC	0.16	1.6
EggPC	8.4	84

the observed increase in cytokine secretion upon incubation with PC-species is not a result of endotoxin contamination, the endotoxin levels in the lipid preparations were measured by LAL (limulus-amebocyte assay) test, see Figure 4.13. The endotoxin level in the samples measured by the LAL-test is given in endotoxin units per mL sample (EU/mL). 1 EU/mL corresponds roughly to 0.1 ng LPS/mL. The results from the LAL-test were converted to the approximate amount of LPS per well for every tested lipid preparation. PBS was used as negative control. The results can be seen in Table 4.2. The LAL test revealed very little endotoxin contamination of the used lipid preparations. The highest endotoxin concentration

was measured in the egg-PC preparation with 8.4 EU/mL, which corresponds to roughly 84 pg/mL LPS in the final reaction well. That is an increase in LPS concentration in the well by 0.84 % (macrophages were incubated with 10 ng/mL LPS). DOPC and POPC lipid preparations showed an endotoxin concentration of 0.01 EU/mL and 0.16 EU/mL, respectively, which approximates to an equivalent of 0.1 pg/mL LPS and 1.6 pg/mL LPS, respectively. POPG had an endotoxin contamination of 1.38 EU/mL, corresponding to 13.8 pg/mL LPS, which is also negligible in terms of macrophage stimulation. The observed increase in LPS-induced TLR4/NFκB and canonical inflammasome pathway upon incubation with POPC and DOPC were therefore not due to endotoxin contamination of the lipid preparations and would therefore need further study in order to conclude on mechanistic details.

4.4. LBP is upregulated in the lung during nARDS and conveys LPS-induced non-canonical inflammasome activation

LBP is mainly secreted by hepatocytes and rapidly upregulated during the acute phase response to an infection, and is crucial for the detection of LPS by macrophages. To answer the question whether or not LBP also has a pulmonary role in the inflammatory processes in nARDS, the LBP protein levels of the piglet BALF before treatment at time point 0h and after 72h of disease progression were analyzed by ELISA. Figure 4.14 depicts the LBP concentrations

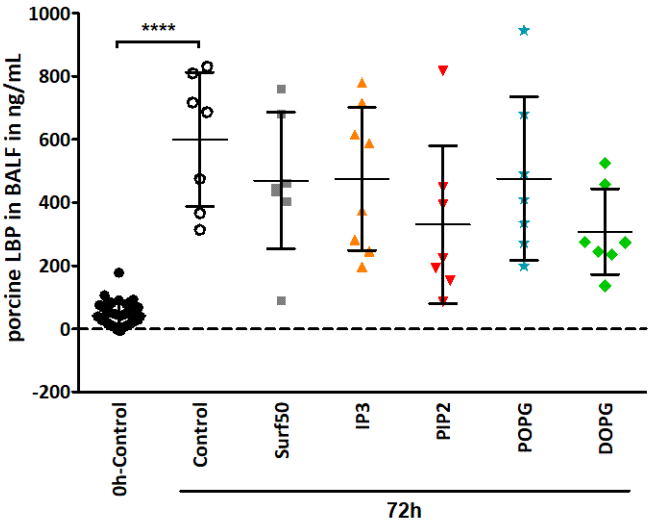

Figure 4.14: Porcine LBP in porcine cell-free broncho-alveolar lavage fluid before injury at 0h and after 72h. LBP levels were measured in ELISA in duplicates. Data of all 0h BALF-samples were pooled. Data are expressed as mean±SD. Unpaired, one-tailed T-Test: ****0h-control vs. 72h control p<0.0001.

in the porcine BALF samples. As all piglets were unchallenged and untreated before the initial diagnostic lavage at 0h, the data of these samples were pooled. Very low levels of LBP were detected in the BALF of healthy, unchallenged piglets at time point 0h (43.1 ±36.5 ng/mL). Mean LBP-levels increased 14-fold after 72h of disease progression, which corresponds to 24h after LPS-challenge, in the untreated 72h control BALF samples (599.6 ±212.4 ng/mL). Curosurf® application without (Surf50) or with IP3, PIP2, POPG or DOPG supplementation provoked no significant difference in LBP levels compared to the untreated 72h control. BALF samples from piglets treated with Curosurf® + PIP2 and Curosurf® + DOPG showed slightly lower mean LBP concentrations (330 ±250.3 ng/mL and 307.3 ±135.8 ng/mL, respectively) compared to Curosurf® alone. Yet again, there are considerable biological variances within the piglet groups.

LBP is a crucial component in LPS recognition by immune cells. Its increased presence in the lungs of the piglets after 72h of nARDS disease progression may indicate an immune regulatory function beyond the transport and presentation of LPS to immune cells. Previous data from our lab group [29] had shown the internalization of LBP in human macrophages and co-localization with human Caspases, which are associated with canonical and non-canonical inflammasome activation.

Thus, the possibility that LBP may convey macrophage activation independently from the danger signals of the canonical pathway was subsequently investigated. To this end, macrophages differentiated from human peripheral blood monocytes were primed with 10 ng/mL LPS for 16 hours. Afterwards they were incubated for 20 hours with LPS and LBP in increasing concentrations in absence of ATP to check for activation of the non-canonical inflammasome pathway. Lactate dehydrogenase (LDH) activity as an indicator of pyroptosis and IL-1b secretion were measured in cell-free supernatant. The data were normalized to IL-1β concentrations from macrophages primed with LPS and incubated with ATP for 4 hours (canonical inflammasome activation control). As seen in Figure 4.15a, neither LPS nor LBP alone provoked significant IL-1β secretion. Unprimed cells incubated with 10 µg/mL LPS and LBP, as well as primed cells incubated with 10 µg/mL LBP released a mean of 5,8% IL-1β. Primed cells that were incubated with 5 µg/mL LPS showed 15.7 % IL-1β secretion. The addition of 1 µg/mL LBP did not change IL-1β secretion yet. However, IL-1β secretion increased to 25.5% and 27.3% when primed cells were incubated with 5 µg/mL LBP and 10 µg/mL LBP, respectively, in combination with 5 µg/mL LPS. Incubation of primed macrophages with

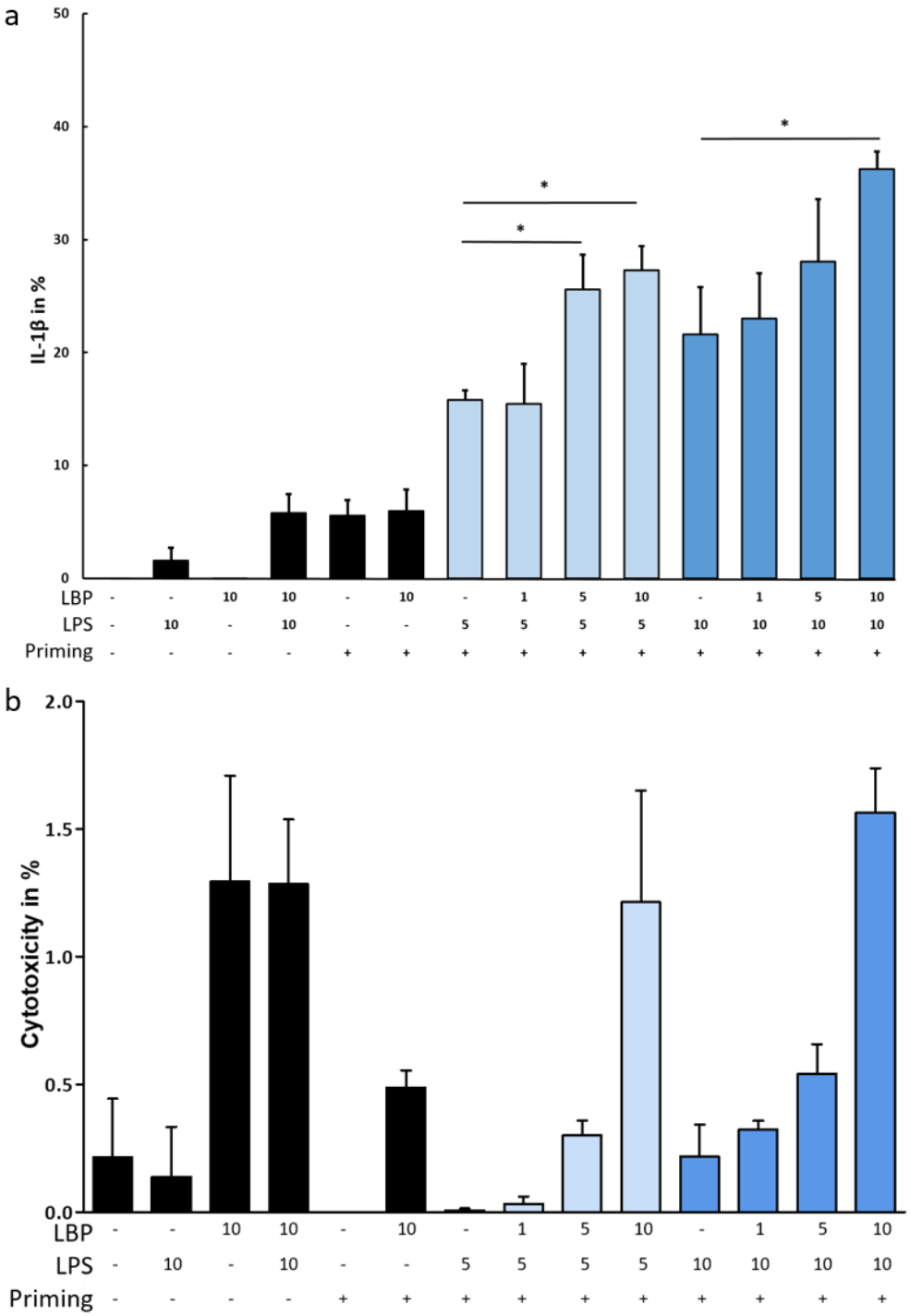

Figure 4.15: LBP enables LPS-induced IL-1β release in human PBMC-derived macrophages in a dose dependent manner. Peripheral blood monocytes from human volunteers were differentiated into macrophages for 7 days, seeded at $1x10^5$ per well and incubated for 2h at 37°C. The respective cells were primed with 10 ng/mL LPS for 16h. After washing, LPS and/or LBP was added to the cells at the indicated concentrations (in µg/mL) and spun down onto the cells. After 20 h of incubation cell-free supernatant was harvested to be analysed for IL-1β by ELISA (a). Data are expressed as mean±SD. Data are normalized to ATP inflammasome activation control (not shown). N=2-3. One-tailed T-test. *p<0.05. Cell-free supernatant was also analyzed for LDH concentration as a measure for cytotoxicity (b). Data expressed as mean±SD. Data are normalized to 100% lysis control (not shown). N=2-3 independent experiments.

10 µg/mL LBP alone led to an IL-1β secretion of 21.6%. The addition of 1 µg/mL and 5 µg/mL LPS to 10 µg/mL LBP increased the IL-1β response slightly, yet not statistically significant, to 23% and 28%, respectively. However, the IL-1β secretion was significantly increased to 36.2% when primed macrophages were incubated with the combination of LPS and LBP, 10 µg/mL

each (p=0.0181). The secretion of IL-1β in primed cells incubated with only 5 or 10 µg/mL LPS (without addition of LBP) may be connected to residual ATP or LBP on the cells.

As mentioned above, the same cell culture supernatants were tested for LDH activity. This cytosolic enzyme which is only released into the cell culture media when the cell membrane is damaged. It is thus used as an indicator of cellular toxicity. Cell lysis via pyroptosis has been published to be a consequence of canonical and non-canonical inflammasome activation. It was therefore tested whether the same experimental setting, namely IL-1b secretion by primed macrophages induced by LPS-LBP complex, also leads to cell lysis. The LDH activity was normalized to the lysis control (100% cytotoxicity). As can be seen in Figure 4.15b, no significant level of cell lysis has been detected in the unprimed or primed macrophages. Even though the increase in LBP concentration (1, 5 and 10 µg/mL) in combination with 5 or 10 µg/mL LPS seemed to evoke a concentration-dependent increase in cytotoxicity in primed macrophages, the maximum cytotoxicity reached was only 1.6 % for 10 µg/mL LPS/LBP. In conclusion, more than 98% of the cells were viable 20 hours after stimulation.

4.5. The piglet surfactant lipid*ome*

The treatment regime in this piglet model of nARDS is based on the application of the endogenous porcine surfactant preparation Curosurf® with the supplementation of the anionic phospholipids POPG, DOPG, PIP2 or the headgroup variant IP3. As the surfactant layer in the mammal lung is composed mainly of phospholipids, a possible alteration of the intrinsic piglet pulmonary surfactant composition by the application of substantial amounts of additional anionic lipids into the lung was hypothesized. To obtain detailed data on the piglet surfactant composition for an in-depth analysis, a detailed analysis of the pulmonary surfactant lipid profile (lipid*ome*) in healthy piglets (0h) was essential. Data on that healthy lipid*ome* was then compared to the surfactant lipid profile after 72h of disease progression

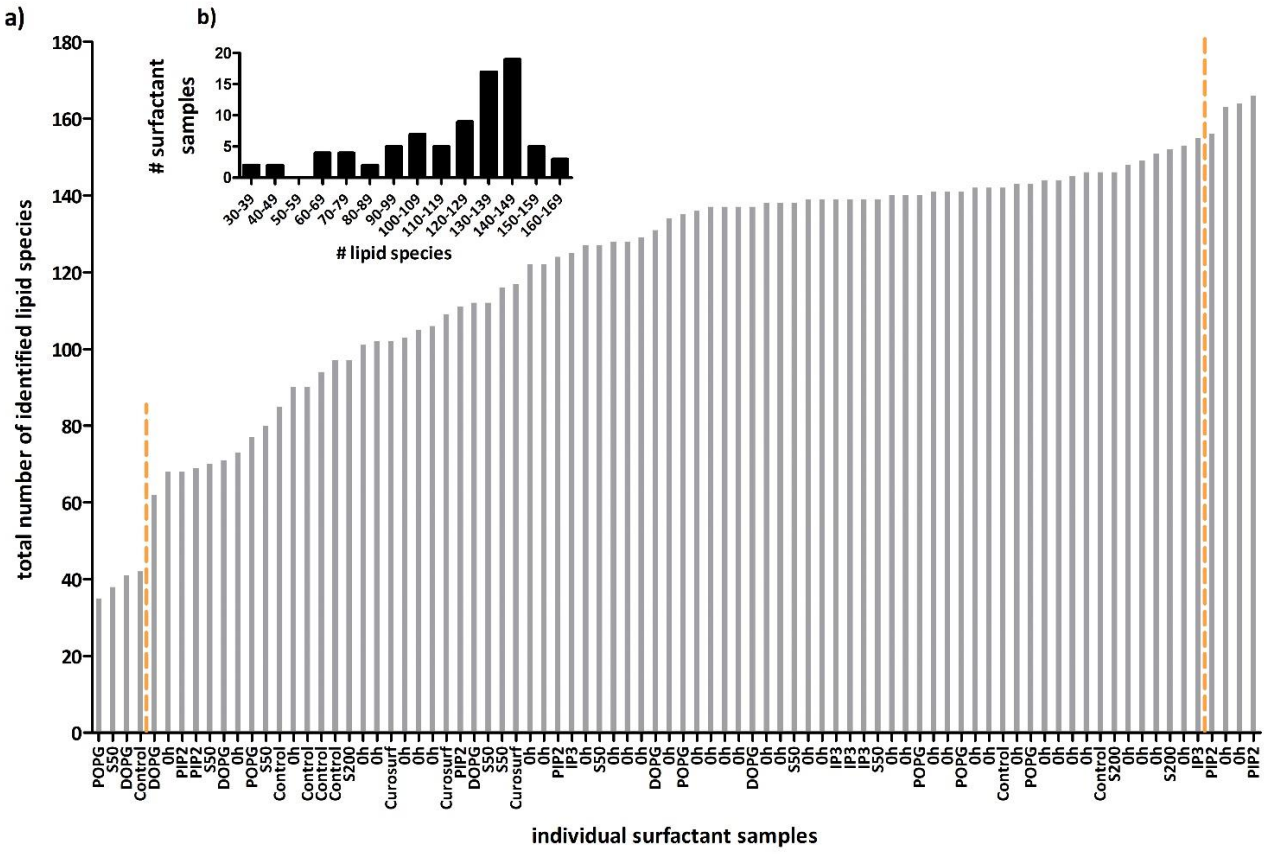

Figure 4.16: Total amount of lipid species in piglet pulmonary surfactant from BAL samples. a) Number of total lipid species identified in the individual surfactant samples. Orange dashed lines indicate selected cutoff for further data analysis. b) Histogram of total number of lipid species detected. Displayed are raw data without cutoff. N = 84 (including Curosurf® triplicates).

with or without treatment/intervention. To that end, surfactant was obtained from the untreated healthy piglets prior to any intervention at time point 0h and from all control and treatment groups after 72h of disease progression by repeated broncho-alveolar lavage and

subsequent centrifugation of the lavage fluid. The surfactant lipids were further extracted by the Bligh-and-Dyer method and then identified and quantified by a LC-MS/MS.

As the first step, the lipid content of all piglet pulmonary surfactant samples was assessed. The sample set included 81 piglet surfactant samples and one aliquot of the Curosurf® sample used in this study (in technical triplicates). The amount of total lipid species found in each surfactant sample is depicted in Figure 4.16a. Figure 4.16b shows the distribution of total number of lipid species detected. A strong variation in the total number of lipid species per sample is apparent (mean 120±32). Half of the samples contained ≥130 lipid species (median 134.5).

In total, 181 different lipid species were detected in the 84 samples analyzed, originating from 7 classes of phospholipids (phosphatidic acid [PA], phosphatidylcholine [PC], phosphatidylethanol [PE], phosphatidylglycerol [PG], phosphatidylinositol [PI], phosphatidylserine [PS], Cardiolipin), two classes of Sphingolipids (Sphingomyelin [SM], Ceramide) and free cholesterol, see Table A1 in the supplementary information. As a side note, triglycerides (13 additional species) detected in the piglet surfactant samples were not considered in any analysis.

Three distinct lipid species were not detected in both healthy piglet samples at 0h and in the 72h untreated control piglet samples: PC-O [39:1], PE [48:6] and SM [38:1;1]. These three lipid species were however detected in Curosurf® samples and all treatment group samples. It can

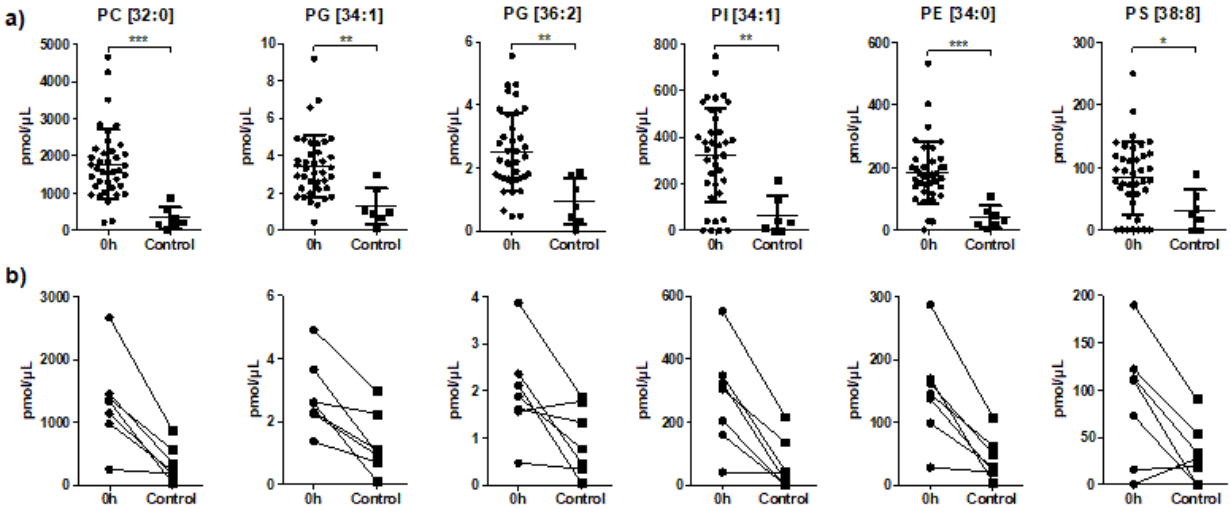

Figure 4.17: The absolute lipid abundance in piglet surfactant is strongly decreased after 72h of disease progression in the untreated control group. Differences in absolute abundance of the major lipid species per lipid class between 0h surfactant samples of all piglets and 72h surfactant samples of the piglets in the untreated control group. Lipid abundance was normalized to an internal MS standard. a) Complete sample population, 0h n=40, Control n=7. b) Grouped sample pairs, n=7. Raw data are shown (no cutoff). Two-tailed t-test: ***p≤0.001; **p≤0.01; *p≤0.1

therefore be assumed that these three 'new' lipid species were introduced into the piglet surfactant system by Curosurf® application, rather than changed metabolic pathways.
Long chained PC species above [38:5] and long-chained PI species above [41:0] were not detected in Curosurf®, neither were any of the PE-O species. One species of phosphatidic acid was detected (PA [34:1]).

A hallmark of nARDS is the secondary surfactant deficiency [161]. Therefore it was first analysed whether a reduction in lipid content after 72h in the diseased piglets had occurred. Exemplarily, results for the most abundant lipid species per main lipid class (PC, PG, PI, PE, PS) are shown in Figure 4.17a and 4.17b. A significant decrease in absolute lipid content per sample from 0h to 72 was calculated for all depicted lipids. The most abundant lipid species in pulmonary surfactant, PC [32:0] (DPPC), decreased by a whooping 70%. PG [34:1] and PG [36:2] decreased by 60% each, PI [34:1] by 80%, PE [34:0] by 75% and PS [38:8] by 60%.

Unfortunately, it was not possible to normalize this initial data due to the lack of a sample internal control, such as surfactant volume per BALF sample or similar. Therefore, only compositional changes in relative abundance were analyzed in the following, not absolute changes.
Thus, in order to introduce a quality control for the piglet pulmonary surfactant samples, a cutoff was set that excludes the four samples with the least total amount of lipid species and the four samples with the highest total amount of lipid species, indicated in Figure 4.16a by orange dashed lines (cutoff 1a). See Table A2 in supplementary information for sample details. These eight samples were excluded from any further data analysis with this cut-off. For these resulting 73 surfactant samples, an additional 80%-threshold (cutoff 1b) was defined: Every individual lipid species had to be detectable in ≥80% of the surfactant samples (irrespective of sample group) to be included in further analysis. After data curation, 80 different lipid species in 76 surfactant samples (from piglets, and Curosurf® in technical triplicate) were applicable for further statistical analysis (see Table 3.5 in the Methods chapter).

4.5.1. Curosurf® lipid composition differs from endogenous piglet surfactant in this study

To compare the piglet surfactant lipid*ome* of healthy and diseased piglets, pulmonary surfactant samples of healthy piglets at time point 0h, 72h untreated control piglets and Curosurf® were prepared and analysed, as described above, applying the 1st and 2nd sample

cut-offs. As depicted in Figure 4.18a, the surfactant lipid composition of the healthy piglets at 0h was dominated by PC species (57 mol%), which is also described as the main phospholipid class in pulmonary surfactant in the literature. Next in abundance was PI with 20 mol%, PS with 10 mol%, PE with 8%. PG and SM made up 0.3 mol% and 0.2 mol%, respectively. The 0h piglet pulmonary surfactant sample contained about 30% negatively charged phospholipids (PI, PS, PG). The general distribution of the major lipid classes in the pulmonary surfactant of the untreated control piglet group at 72h was very similar, with 59 mol% PC, 18 mol% PI, 10 mol% PS and 9 mol% PE. Only SM abundance was significantly different: p=0.0004 *** (two-tailed unpaired t-test). In contrast, Curosurf® contained 79 mol% PC, while PI and PS together only added up to 2.3 mol%. The amount of PE in Curosurf® was similar to the piglet surfactant with 6 mol%. Interestingly, the Curosurf® preparation contained higher amounts of PG and SM compared to the piglet surfactant: 2 mol% and 8 mol%, respectively. The higher PG abundance is most likely explained by the fact that Curosurf® is extracted from pulmonary surfactant of adult pigs which naturally have a higher PG concentration in their pulmonary surfactant, along with a lower PI content [5].

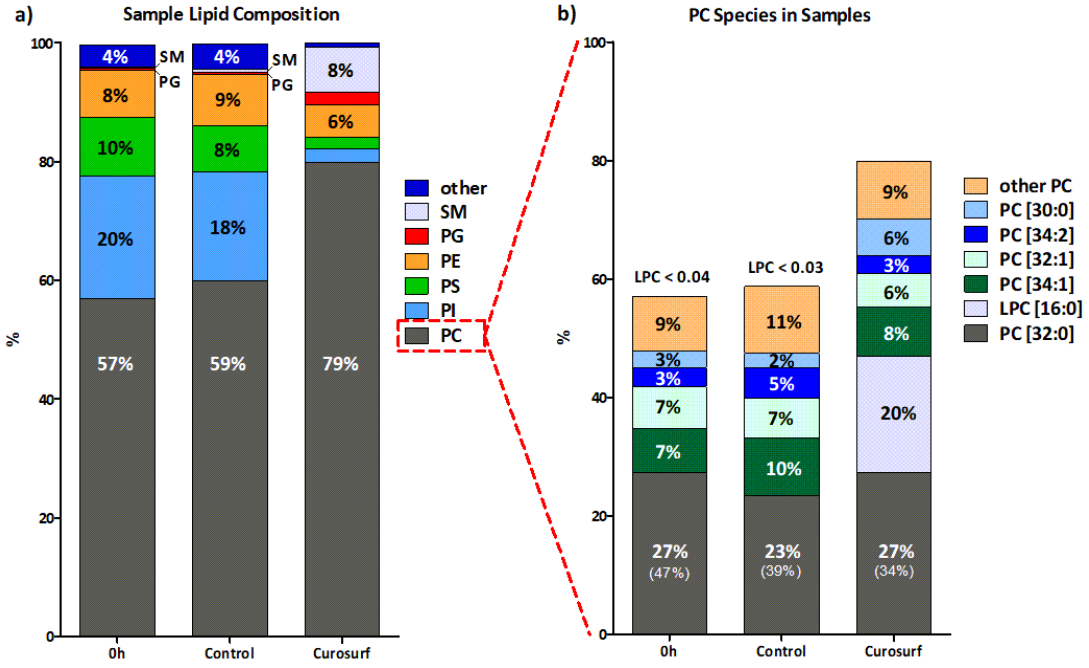

Figure 4.18: The lipid composition of Curosurf® differs from the endogenous piglet pulmonary surfactant composition. Individual Curosurf® and piglet pulmonary surfactant samples were filtered according to the abundance of lipid species: The 4 samples with the lowest and 4 samples with the highest total amount of lipid species were excluded. Furthermore, lipid species were excluded that were not detected in at least 80% of the remaining samples. Lipid abundance was normalized to an internal MS standard and afterwards to the total amount of lipids per sample (relative abundance in mol%). A) Distribution of major lipid classes. B) Distribution of most abundant PC species in samples relative to total lipid abundance. Percentages in brackets are relative to the total PC pool. 0h n= 38; Control n=6; Curosurf® n=3 (technical replicates). "other" contains Cardiolipin, Diacyglycerol, Phosphatidic Acid, Ceramide and free Cholesterol.

It is generally accepted in the literature that PC is the most abundant lipid class in pulmonary surfactant. And among the PC species, PC [32:0] (DPPC; Dipalmitoylphosphatidylcholine) is the most abundant lipid. In line with that, the total lipid pool of the healthy piglet pulmonary surfactant at 0h as well as Curosurf® contained 27 mol% DPPC (Figure 4.18b). The 72h control surfactant samples contained slightly less DPPC (23 mol%). That equals 47% of the total PC pool in the 0h samples and 39% in the 72h control samples. The relative abundances of PC [34:1], PC [32:1], PC [34:2] and PC [30:0] were similar between all three groups: 7-10 mol%, 6-7 mol%, 3-5 mol% and 2-6 mol%, respectively. Interestingly, Curosurf® contained 20 mol% lyso-phosphatidylcholine (LPC) [16:0], whereas the relative abundance of LPC in the piglet surfactant samples is negligible in comparison (<0.04 mol%). Of note, these differences were qualitative. As mentioned above, a proper normalization of each sample would be required to allow for a definite quantification of the lipid species. In summary, no major changes were observed in the piglet pulmonary surfactant composition on a lipid class level.

4.5.2. Compositional changes in the pulmonary surfactant of piglets treated with supplemented Curosurf® preparations

Compositional differences between the healthy piglet surfactant (0h) and the untreated control piglet surfactant sampled at 72h were compared to the Curosurf® preparation above. Next, potential changes in the piglet pulmonary surfactant lipid composition after administration of different fortified Curosurf® preparations were evaluated. For that evaluation of the piglet surfactant sample data, the above-mentioned 1st and 2nd sample cut-offs were applied. Figure 4.19 shows the resulting distribution of the main phospholipid classes in the piglet surfactant samples for all treatment groups. The significances were calculated by comparing the healthy 0h group and the S50 and S200 group to the untreated control group, and by comparing the different treatment groups (IP3, PIP2, POPG and DOPG) to the S50 control group. That way it was possible to evaluate a) changes occurring in the lipid*ome* of untreated sick piglets, b) changes due to Curosurf® application and c) changes due to the supplement lipids compared to the standard therapy with non-supplemented Curosurf®.

The lipid classes PC, PC-O, PE, PI and PS were overall not significantly changed in relative abundance, as shown in Figure 4.19a. PE-O relative abundance increased in all treatment groups compared to the healthy 0h sample and the 72h untreated control, but only the S200

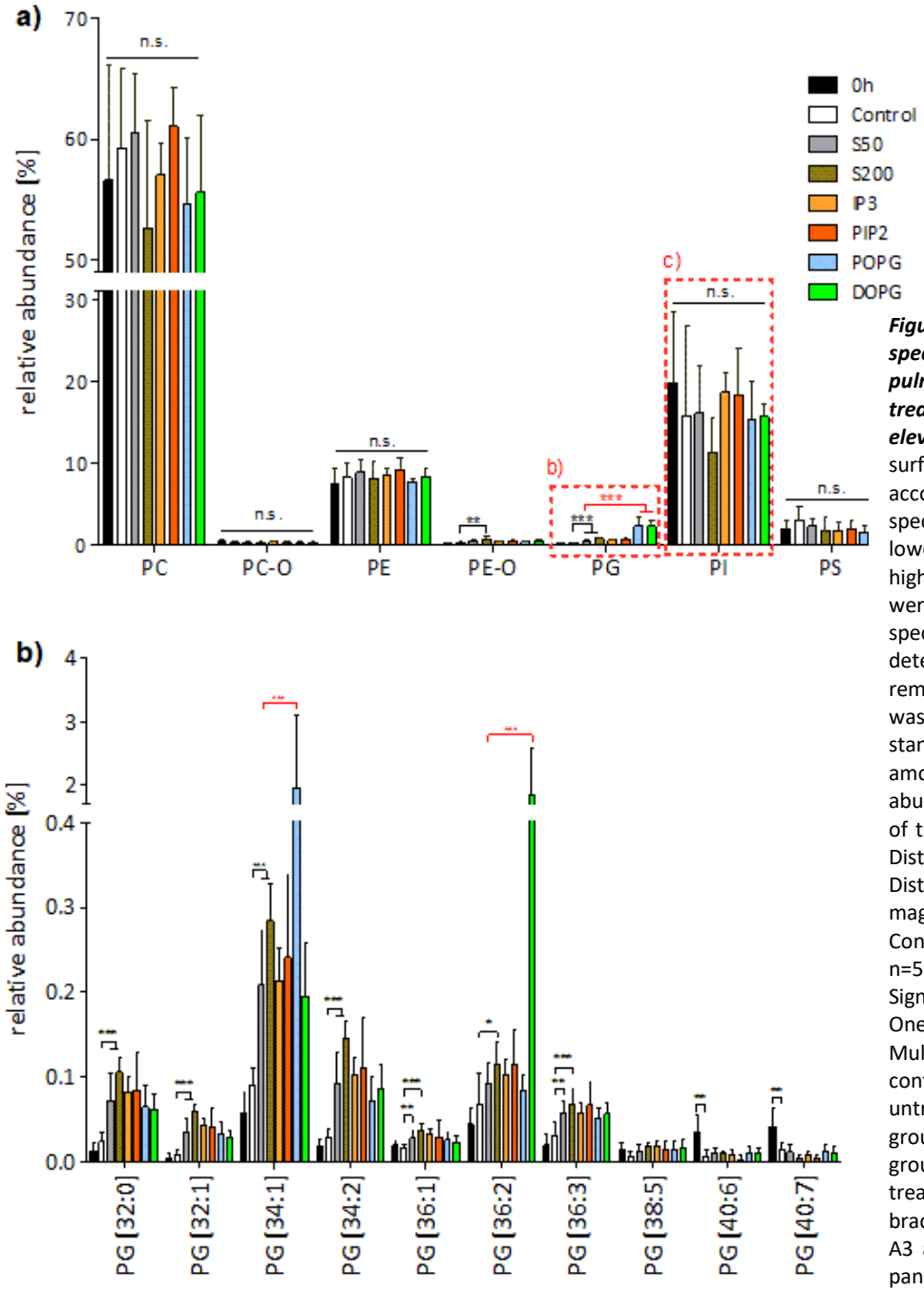

Figure 4.19: Supplemented lipid species can be detected in piglet pulmonary surfactant samples treated with fortified Curosurf® at elevated levels. Individual piglet surfactant samples were filtered according to the abundance of lipid species: The 4 samples with the lowest and 4 samples with the highest total amount of lipid species were excluded. Furthermore, lipid species were excluded that were not detected in at least 80% of the remaining samples. Lipid abundance was normalized to an internal MS standard and afterwards to the total amount of lipids per sample (relative abundance in mol%). a) Distribution of the main phospholipid classes. b) Distribution of PG-species. c) Distribution of PI-species with d) magnification of PI [32:0]. 0h n= 38; Control n=6; S50 n=7; S200 n=3; IP3 n=5; PIP2 n=4; POPG n=5; DOPG n=5. Significances were calculated with One-Way ANOVA with Dunnett's Multiple Comparison Test. 72h control group was compared to 0h untreated sample and S50/S200 groups (black brackets). S50 control group was compared to all four treatment groups and to S200 (red brackets). See supplementary Figure A3 and A4 for enlarged versions of panels b and c, respectively.

control showed a significant (2.7-fold) increase, see Figure 4.19b and Figure 4.21b. This cannot be attributed to the 4-fold higher Curosurf® amount that the S200 piglets received, since Curosurf® is virtually PE-O free (Table A1 in supplementary information). The PG-species increased significantly in the S50 and S200 control groups compared to the 72h untreated control (2-fold and 2.8-fold, respectively), which is explained by the fact that PG is nearly 7-times more abundant in Curosurf® than in pulmonary surfactant of the healthy 0h or the sick 72h untreated control group (see Figure 4.18a). Importantly, the abundance of PG-species was specifically increased in the POPG and DOPG treatment groups (3.7-fold each). Both observations are explained in Figure 4.19b in which the PG lipid class is split into the individual PG-species. PG [32:0] up to PG [36:3] were nearly all significantly increased in their relative abundance in the S50 and S200 control groups compared to the 72h untreated control group. The exceptions were the two long-chained PG-species PG [40:6] and PG [40:7] which show the opposite trend: a decrease was seen for all 72h samples. Additionally, the relative abundance of the two PG-species used for the supplementation of Curosurf® in this study were significantly elevated in their respective treatment group (Figure 4.19b): PG [34:1] was increased 9.4-fold in the POPG treatment group and PG [36:2] was increased 20-fold in the DOPG treatment group, both compared to the S50 control group.

The abundance of the overall PI lipid class did not show significant differences between treatment groups, as seen in Figure 4.19a. However, at the level of the individual PI species, one important change can be seen in Figure 4.19c: PI [32:0] abundance showed a 4.5-fold increase in PIP2 treatment group (magnified Panel d). By means of the here employed MS-approach it was unfortunately not possible to detect the PIP2 molecular mass. A possible explanation is the fragmentation of the molecule which may have led to the loss of the two phosphate groups bound to the inositol ring and the resulting phosphatidylinositol was detected. Considering that the PI that was used in this study as supplement for Curosurf® contained saturated C16:0 fatty acids at the sn1 and sn2 positions (1,2-dipalmitoyl), it can be assumed that the increase in PI [32:0] is a direct consequence from the supplementation with PIP2.

With the employed MS-approach 39 different PC species were detected in the surfactant samples, of which 25 remained after data curation with the 1st and 2nd sample cut-offs, see Figure 4.20a. The lipid species PC [32:0] comprised ±25% of the PC pool for all groups, compare with the overview in Figure 4.18. Next in abundance are the unsaturated species PC [34:1], PC

[32:1] and PC [34:2]. In total about 30% of the PC species are saturated. While the main PC species decreased, most of the longer chained PC species increased in relative abundance from the 0h healthy piglet surfactant samples to the 72h untreated control samples, such as the unsaturated species PC [34:1] and PC [34:2].

Most treatment groups showed no change in relative abundance of PC species compared to the S50 control group. Interestingly, the S200 control samples appeared to have lower relative abundances compared to S50 control samples for several unsaturated PC-species.

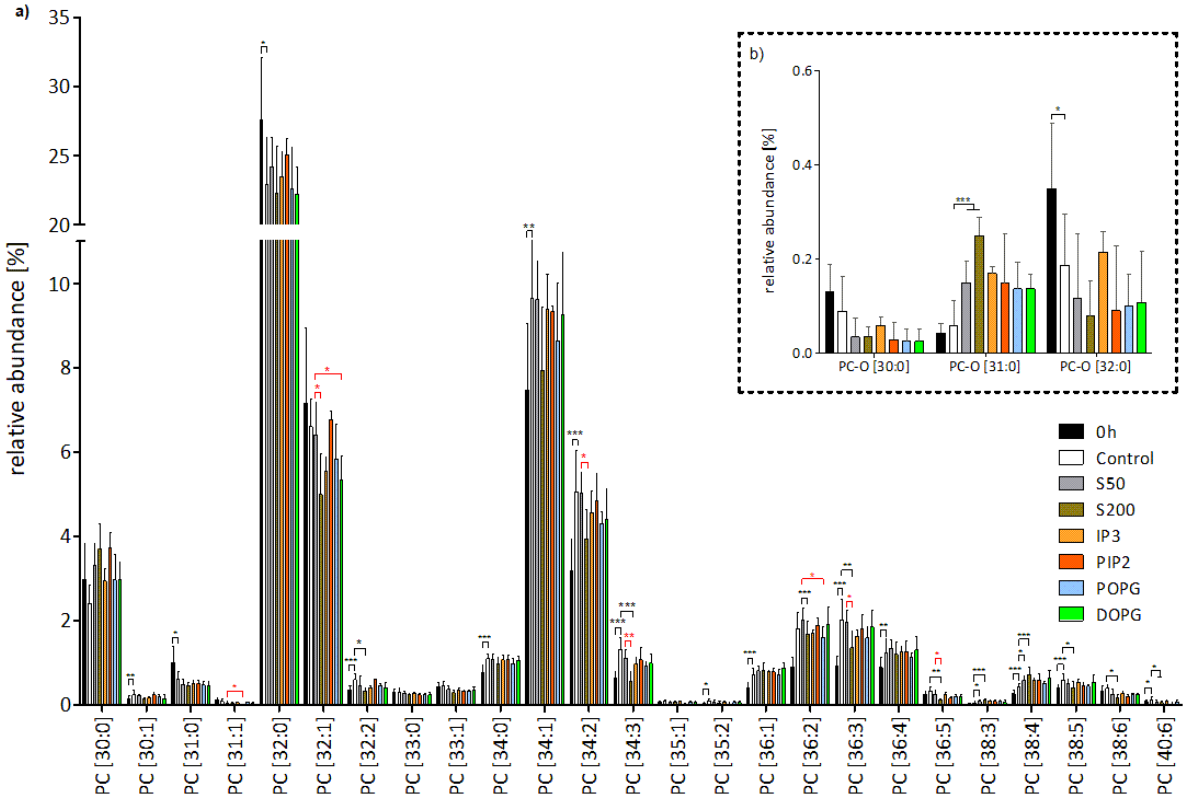

Figure 4.20: Relative abundance of PC species and PC ethers in piglet pulmonary surfactant samples. Individual piglet surfactant samples were filtered according to the abundance of lipid species: The 4 samples with the lowest and 4 samples with the highest total amount of lipid species were excluded. Furthermore, lipid species were excluded that were not detected in at least 80% of the remaining samples. Lipid abundance was normalized to an internal MS standard and afterwards to the total amount of lipids per sample (relative abundance in mol%). a) Distribution of PC species. b) Distribution of PC-ethers. 0h n= 38; Control n=6; S50 n=7; S200 n=3; IP3 n=5; PIP2 n=4; POPG n=5; DOPG n=5. Significances were calculated with One-Way ANOVA with Dunnett's Multiple Comparison Test. 72h control group was compared to 0h untreated sample and S50/S200 groups (black brackets). S50 control group was compared to all four treatment groups and to S200 (red brackets). See supplementary Figure A5 for enlarged version of panel a.

Only minor changes were seen in the distribution of PE species in the piglet pulmonary surfactant (see Figure 4.21a). PE [36:0], PE [36:1], PE [36:2] and PE [38:2] were significantly increased in relative abundance in the untreated control group compared to the 0h healthy piglet group. Interestingly, for all control groups (control, S50, S200) and nearly all treatment groups the relative abundance of the PE ether species increased compared to the untreated

0h group (see in Figure 4.21b). That effect was most pronounced in the S200 piglet surfactant samples. This effect cannot be attributed to the application of Curosurf® as it did not contain any PE-ether (see supplementary Table A1). No change was detected for PS species (see Figure 4.21c).

The sphingomyelin relative abundance was significantly increased in the untreated 72h control samples and again increased in the S50 and S200 control groups, see Figure 4.21d. When comparing again with the stacked chart in Figure 4.17a, this latter increase can be explained by the fact that Curosurf® had 16-times higher SM abundance compared to the untreated 72h control group.

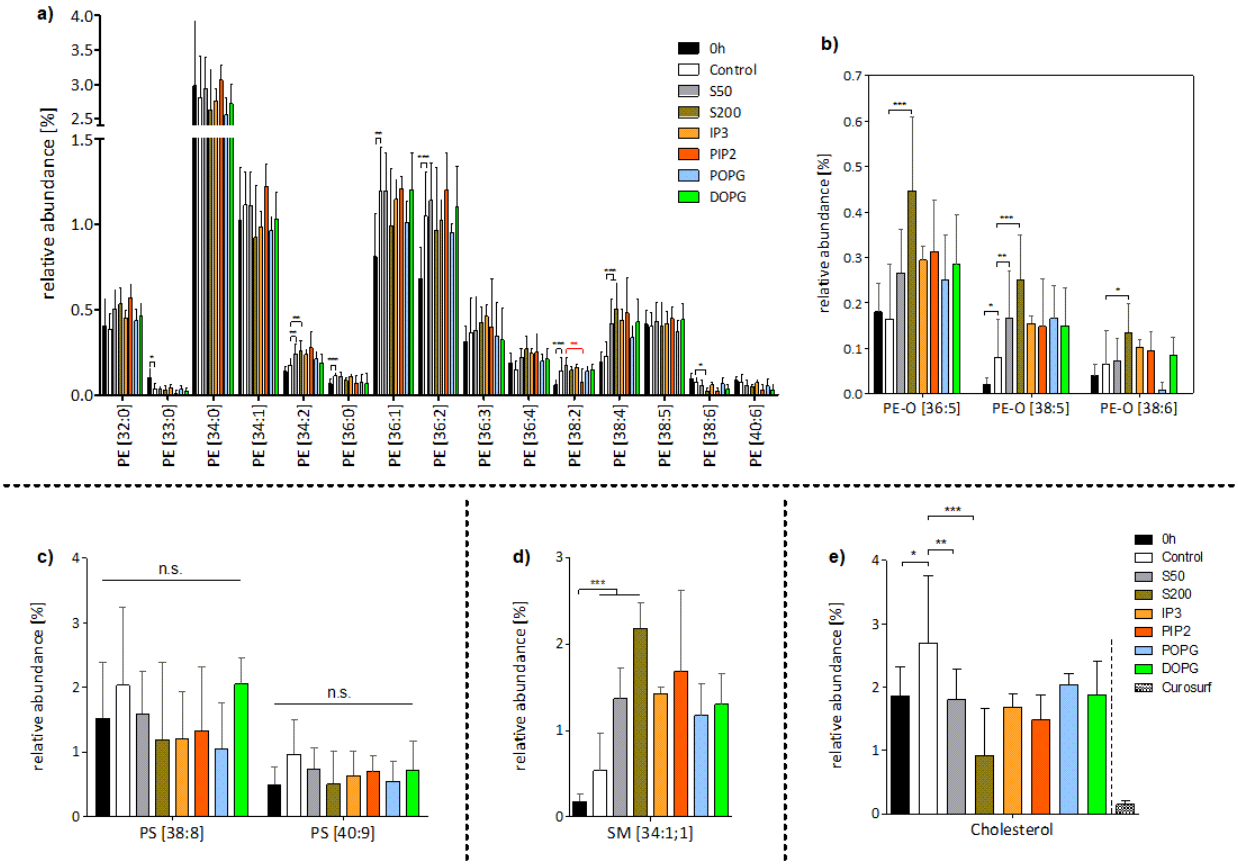

Figure 4.21: Relative abundance of PE and PE-ether, PS, SM species and free cholesterol in piglet pulmonary surfactant samples. Individual Curosurf and piglet surfactant samples were filtered according to the abundance of lipid species: The 4 samples with the lowest and 4 samples with the highest total amount of lipid species were excluded. Furthermore, lipid species were excluded that were not detected in at least 80% of the remaining samples. Lipid abundance was normalized to an internal MS standard and afterwards to the total amount of lipids per sample (relative abundance in mol%). a) Distribution of PE species. b) Distribution of PE-ethers. c) Distribution of PS species. d) Distribution of SM [34:1;1]. e) Distribution of Cholesterol 0h n= 38; Control n=6; S50 n=7; S200 n=3; IP3 n=5; PIP2 n=4; POPG n=5; DOPG n=5; in Panel e) Curosurf n=3 (technical replicates). Significances were calculated with One-Way ANOVA with Dunnett's Multiple Comparison Test. 72h control group was compared to 0h untreated sample and S50/S200 groups (black brackets). S50 control group was compared to all four treatment groups and to S200 (red brackets). Cholesterol content in Curosurf® was excluded from statistical analysis. See Supplementary Figure A6 for enlarged version of panel a.

As a general trend, the lipid abundance decreased with decreased degree of saturation. The common trend of increased lipid abundance in S50 and S200 samples could often be explained by the fact that the specific lipid species was found in higher abundance in Curosurf®, i.e. sphingomyelin or phosphatidylglycerol. In contrast, the cholesterol abundance was decreased in the S50 and S200 samples compared to the 72h control group (see Figure 4.21e). In comparison, the Curosurf® sample contained very low amounts of cholesterol (±0.15%). It may

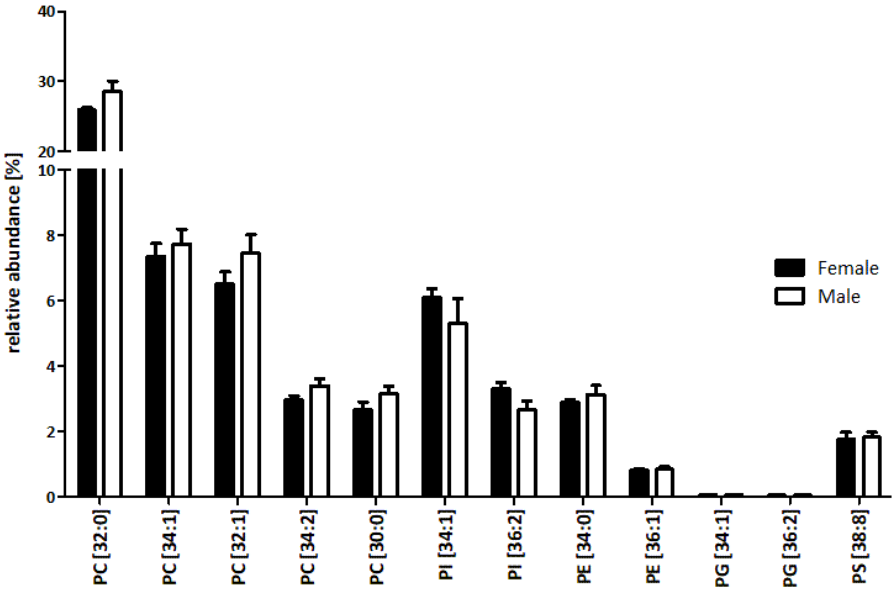

Figure 4.22: Mean lipid abundance in the 0h piglet pulmonary surfactant samples does not appear to be gender-dependent. Lipid abundance was normalized to an internal MS standard and afterwards to the total amount of lipids per sample (relative abundance in mol%). 0h samples from piglets with unknown gender were omitted from this analysis. Female n=12 (blank bars), male n=18 (black bars). No significances by two-tailed T-test.

be noted here that the origin of the cholesterol in the piglet surfactant samples may not only lie in the piglet pulmonary surfactant but some enrichment may be caused by cell debris due to the clinical intubation and BAL procedure.

Correlation analysis of relative abundances of different lipid species with acyl chains [34:1] and [36:2] did not give a strong indication of a possible head group exchange, for example between PG 34:1 (POPG) and PC 34:1 (POPC), or between PG 36:2 (DOPG) and PC 36:2 (DOPC) (see supplementary Figure A2).

Considering that male prematurely born babies have a higher morbidity [162], it was relevant to address possible piglet gender-related differences. Figure 4.22 shows the most abundant lipid species for the main lipid groups in the piglet surfactant samples, sorted by gender of the piglets. There were no differences in relative abundance of the main lipid species in relation to the gender of the piglets. It is known that pulmonary surfactant composition switches

changes after birth and that lung development continues steadily after birth [5]. However, no age-dependent differences could be detected in the absolute *and* relative abundance of the main lipid classes in the surfactant samples of the 0h piglets which were 2, 3, 4 or 5 days of age (see supplementary Figures A3 and A4).

In summary, most of the changes that occurred in the relative abundance of the single lipid species were seen between the pulmonary surfactant from healthy piglets at 0h and the surfactant of untreated, control piglets at 72h, as well as between the untreated and Curosurf®-treated piglets (S50 and S200 control samples). The supplementation of Curosurf® with the tested lipids did not lead to high-level alterations in relative abundance of the piglet surfactant lipid species. However, the supplementation with POPG, DOPG and PIP2 led to their accumulation in the piglet pulmonary surfactant of the respective treatment group.

4.5.3. Hierarchical clustering reveals distinct alterations in the piglet pulmonary surfactant lipid*ome* between healthy piglets and sick piglets

In the above chapter, the different sample groups were compared on a single lipid species level, which provides a fragmented picture of the piglet surfactant. Now, the data on the detected lipid species were combined in one hierarchical clustering (HC) analysis in order to create a snapshot of the complete piglet surfactant lipid*ome*, including all the detected lipid classes. HC analysis employs an algorithm that groups observations (lipid species in this study) that behave similarly into clusters. These clusters are then again grouped into higher order clusters. Eventually a final picture of several distinct clusters is created, in this study depicted as a heat map, where the observations within show a behavior which is different from other clusters. A higher data quality is required for such an analysis. Therefore only samples with a minimum of 100 identified lipid species were included in the HC analysis (cutoff 2a, n = 60 samples). Based on these 60 samples, only lipid species that were detected in at least 60% of these samples were included for analysis (cutoff 2b, n = 100 lipid species). S200 samples were not considered in this analysis because the treatment with 200 mg/kg Curosurf® showed adverse clinical effects and was therefore discontinued after three piglets. So the influence of the S200 groups in the lipid clustering was omitted from this analysis.

As shown in the HC dendrogram of Figure 4.23b, all but two pulmonary surfactant samples (95%) taken from healthy piglets at 0h formed a distinct cluster on the left side of the dendrogram (correlation coefficient of 0.63), indicating a very similar lipid*ome*. A sub-branch

is formed by one 0h sample together with the two 72h untreated control samples and two 72h S50 samples. Apart from these three samples, all other 72h samples, treated or untreated, form the second, separate cluster (correlation coefficient of 0.67). Every treatment group (IP3, PIP2, POPG, DOPG) formed an individual sub-cluster, except for one PIP2 sample found in the IP3 cluster. The other S50 control samples scattered throughout the IP3 and POPG sub-cluster.

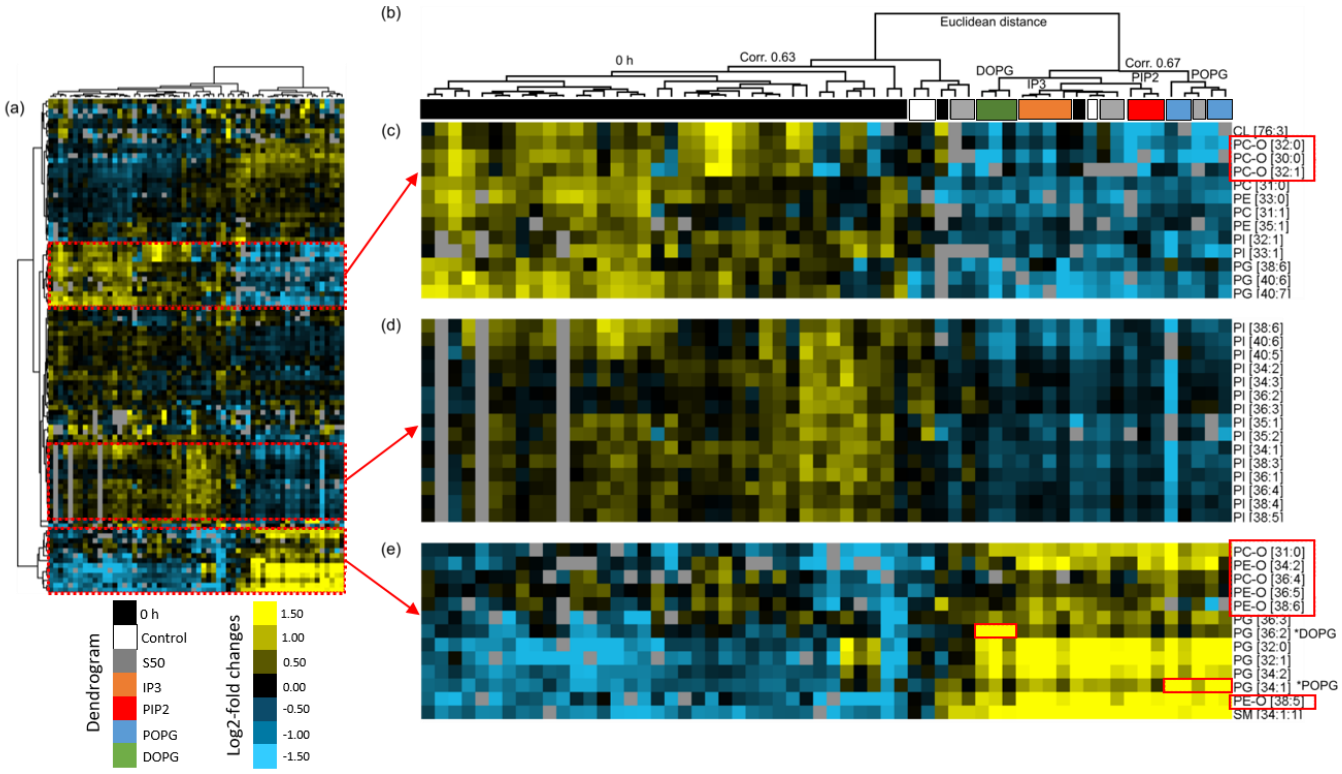

Figure 4.23: Healthy piglet pulmonary surfactant lipidome clearly separates from 72h treated surfactant lipidome. Hierachical clustering was calculated from piglet surfactant samples with at least 100 identified and quantified lipid species (n=60). Furthermore, lipid species detected in at least 60% of these samples were included in the present analysis (n=100). HC was performed for individual samples and lipids using Euclidean Distance metric and Complete Linkage clustering method. The heat-map shows adjusted lipid quantities (log2-fold changes compared to lipid species mean). Yellow marks an increase in abundance compared to the lipid-species mean and blue marks a decrease in abundance. (a) Overview of the complete analysis. Red squares are magnified in c)-e). b) HC dendrogram groups the samples into clusters based on their similarity. Colored squares between the HC tree and heat map define the sample types, see figure legend. Red squares on the right side of the magnified heat map areas indicate lipid ethers. Green squares in panel e) indicate the accumulation of DOPG and POPG in the 72h DOPG and POPG treatment group sample. 0h n=37; Control n= 2; S50 n= 5; IP3 n=5; PIP2 n=4; POPG n=4; DOPG n=3.

Certain lipid species showed similar behavior amongst the samples, as indicated by three sub-clusters, which are detailed in Figure 4.23c, d and e. The 0h samples had a larger abundance of the PC-species [31:0] and [31:1] (panel c), which are minor PC species compared to general concentrations of PC [32:0], [34:1], [32:1] and [34:2] (see Figure 4.20 histogram for comparison). Furthermore, the 0h samples were enriched in PE species [33:0] (compare with Figure 4.21a) and [35:1], as well as in the longer chained PG-species [38:6], [40:6] and [40:7] (compare with Figure 4.19b). Another lipid sub-cluster is formed by the majority of PI species (Panel d), which were found in larger quantity in the 0h samples compared to the 72h samples

from the treatment groups. 3 piglets were devoid of PI species (indicated by grey squares in the heat map). Only two of these piglets came from the same litter, all three were male. This may have been a measuring artefact.

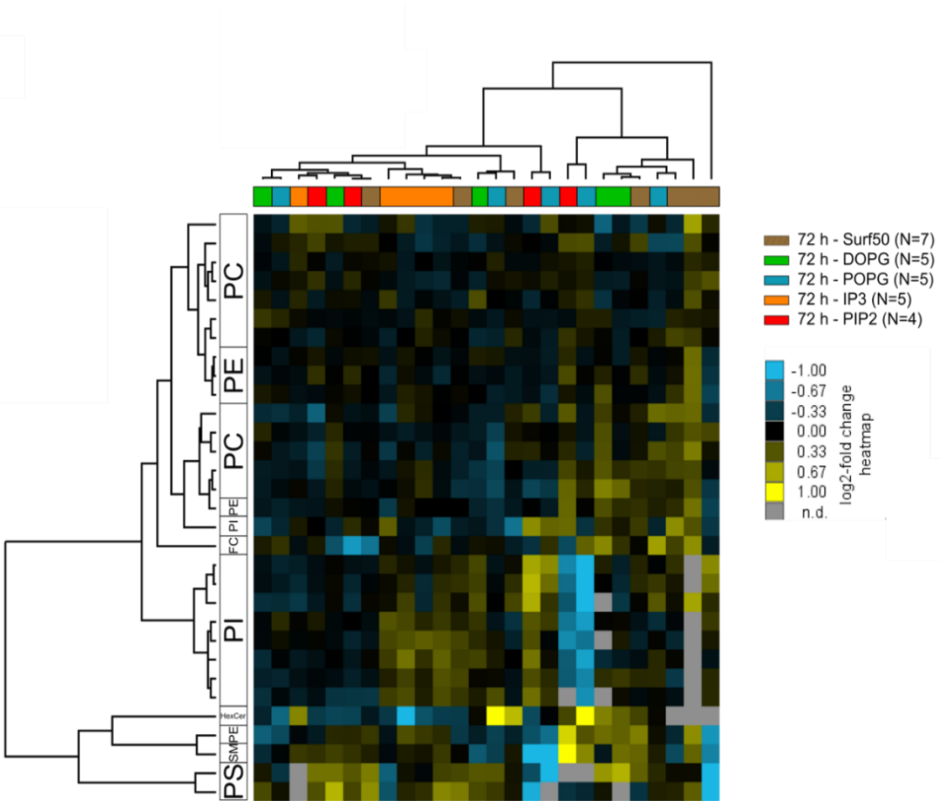

Figure 4.24: Exclusion of the supplemented lipid species abrogates the treatment group-specific hierarchical clustering. The three specific treatment lipid species PI [32:0], PG [34:1] and PG [36:2] were excluded from the clustering, as well as lipids that showed less than 10% variance between the samples. With the filtered and normalized data HC was performed for individual samples as well as for lipids using Euclidean Distance metric and Complete Linkage clustering method. The heat-map shows adjusted lipid quantities (log2-fold changes compared to mean per lipid species). Yellow marks an increase compared to the lipid-species mean and blue marks a decrease in abundance. N= 31 lipid species.

A third distinct sub-cluster (Panel e) was formed mainly by the shorter-chained PG species (compared to Panel c), which were enriched in the 72h treatment groups (compare with Figure 4.19b). The 72h surfactant samples from piglets treated with either DOPG or POPG were clearly enriched in their respective lipid species (red squares in Panel e), compare also with Figure 4.19 histogram. Interestingly, the same third cluster was also populated by PE-O species, which also show an increased abundance in the 72h treatment groups, as described above, intermingled with PC-O species. Here it is worth pointing out again that no PE-O species were detected in the Curosurf® preparation used. The PC-O behavior varied: whereas PC-O [30:0], [32:0] and [32:1] were found increased in abundance in the 0h samples (Panel c), the PC-O species [36:4] and especially [31:0] were enriched in the treatment samples (Panel e).

That may be explained by the amount of PC-O [31:0] detected in Curosurf®: It makes up on average 44.5% of the total PC-O abundance in Curosurf®. In contrast, Curosurf® contains nearly no PC-O [30:0] (0.4%) and little PC-O [32:0] (6%) (data not shown), and PC-O [32:1] was not detected at all (see Table A1 in supplementary information). These latter PC-O species would therefore not have been replenished in the 72h treatment groups and probably contribute to the separate hierarchical clustering.

As mentioned above, all samples from the DOPG and POPG treatment groups were enriched in their respective phospholipid (red squares in Panel e). Therefore, it may be assumed that the specific anionic phospholipid with which the Curosurf® preparation was fortified highly dominates the HR clustering of these respective samples. To test this, another hierarchical clustering of the 72h S50 control and IP3/PIP2/POPG/DOPG samples was calculated with the exclusion of the three supplemented phospholipid species PI [32:0], PG [34:1] and PG [36:2]. Furthermore, and in order to detect the strongest similarities, lipids that showed a variance between the samples of less than 10% were omitted from the analysis (cutoff 2c).

As hypothesized, the formation of the samples into treatment lipid-specific sub-clusters is nearly completely abolished for these three treatment groups (see dendrogram in Figure 4.24). Of note, four out of five IP3 samples form a minor sub-cluster. As stated above, IP3 was not detected in this mass spectrometric approach. However, its accumulation in the IP3-treated samples may contribute to the behavior of the respective samples. This corresponding lipid dendrogram again shows a distinct sub-cluster for PI-species.
In summary, the hierarchical clustering approach demonstrated a clear change in surfactant lipid*ome*s upon Curosurf® application. It further demonstrated that the differences observed in the piglet surfactant lipid*ome* between piglets treated with Curosurf® alone and treated with POPG/DOPG/PIP2-spiked Curosurf® were predominantly driven by the spiked anionic phospholipids. Also, the analysis supported that the overall pulmonary surfactant lipid*ome* of the piglets in the 72h treatment groups remained intrinsically unchanged by the accumulation of these lipids.

The HC findings were further confirmed by principal component analysis (PCA) of the same data set. Principal component analysis reduces the amount of variables in a data set into a structured data cluster depending on the variances in the data set. The ‘principal component’ (PC) is thereby a linear representation along which the samples have the greatest variation.

As shown in Figure 4.25a and b, the 0h samples clearly separated from the 72h treatment samples along principle component 1 (PC1). The untreated 72h control samples clustered in between both groups. PC1, 2 and 3 together comprised 55% of the variance in the data set (Panel c). The data set was therefore well represented by this model.

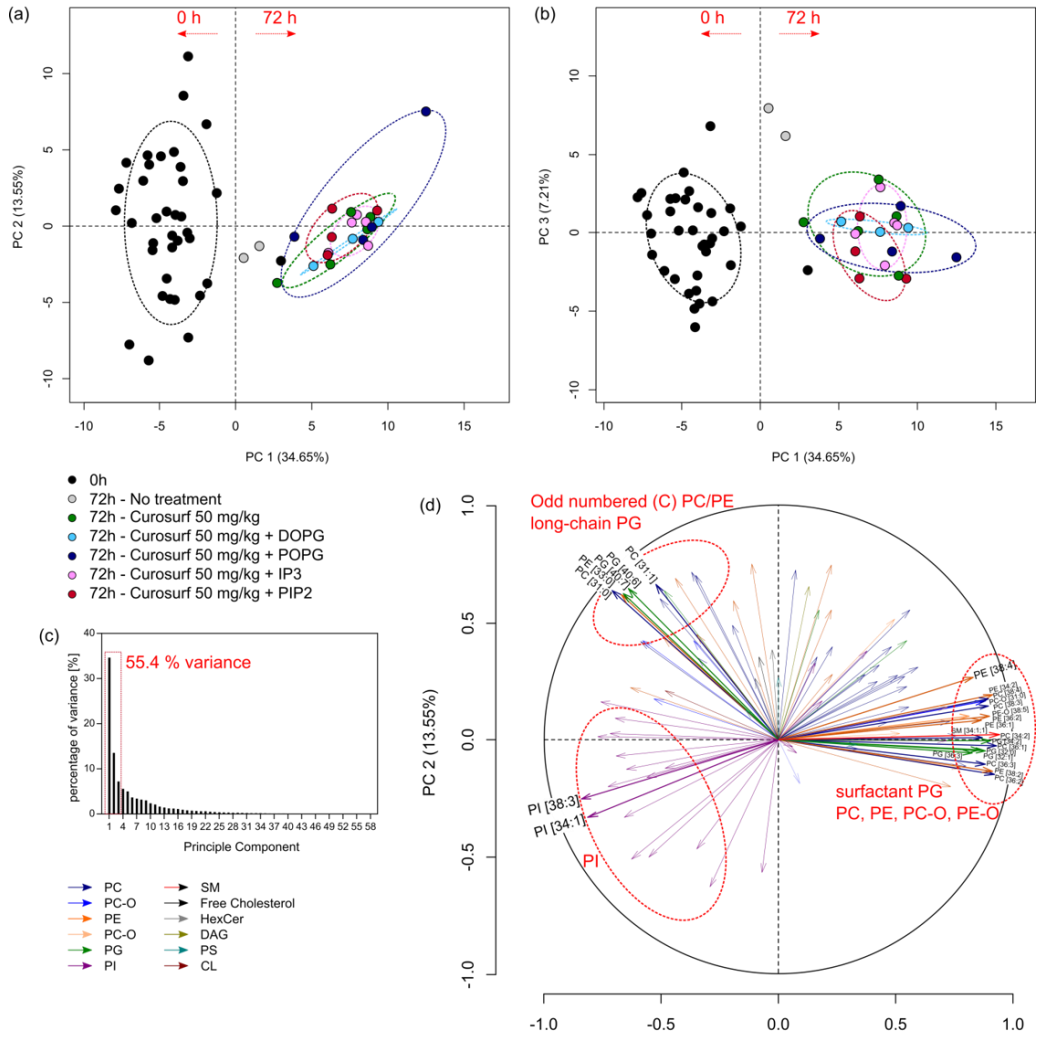

Figure 4.25: Principle component analysis confirms distinct lipidome differences before and after treatment. For this principle component analysis (PCA) the same data set as for the heat map was used (60 samples, 100 lipids). A) PCA factor map of the piglet sample lipid*ome*s showing pC1 vs. PC2, color-coded according to the sample treatment group. B) PCA factor map of the same analysis showing PC1 vs. PC3. C) The first three principle components (PC1 to PC3) cover 55.4% of the variance within the data set. D) Correlations of the relative abundances of the lipid species, color-coded by lipid group. The angles between vectors indicate the respective correlation: Positive correlation is indicated by a small angle, negative correlation by an angle close to 180° and an angle close to 90° indicates no correlation. The longer the vectors the better they contribute to this model. The 25 strongest lipids are labeled.

The PCA also underlined the above-mentioned association of PI-species with the 0h untreated samples (both correlate negatively to PC1, see Figure 4.25d). The 72h treatment samples correlated positively with PC1, as did a group of several unsaturated PC, PE and PE-ether species, as well as several PG species, among them PG [32:0], PG [32:1] and PG [34:2]

(compare with heat map in Figure 4.23e). A group of odd-numbered PC species as well as longer-chained PG species were also well represented by this factor map but were not correlated to the other clusters (1st quadrant in Panel d).

In conclusion, the hierarchical clustering and principal component analysis showed a distinct separation of lipid profiles from 0h healthy piglet surfactant versus 72h treated piglet surfactant. Clustering of the 72h treated samples were mainly defined by the absence or presence of the three treatment lipid species in the samples PIP2, POPG and DOPG.

5. Discussion

The application of Curosurf® has become the gold-standard in the therapy of neonatal respiratory distress syndrome. Can an enrichment of the Curosurf® preparation with the anionic lipid species POPG, DOPG, PIP2 and headgroup variant IP3 bring a therapeutic advantage in the treatment of acute respiratory distress syndrome in neonates? That is the central question around which our cooperation study, based on a triple-hit piglet nARDS study, revolved. As part of that big study, this present work specifically addressed the following four questions: 1) While the piglets clinical parameters indicate a positive therapeutic impact, is such an improvement mirrored in the alveolar macrophage inflammatory response state and disease-relevant cytokine levels in broncho-alveolar lavage fluid? 2) What is the effect of the intervention lipids on the macrophages activation pathways in regard to LPS and can the results be transferred from piglets to humans? 3) Does the application of substantial amounts of additional anionic lipids alter the piglet pulmonary surfactant lipid*ome* in this nARDS model? And 4) Can the results of this piglet model be predictive of a possible therapy outcome in human neonates?

At the center of this study stood a preclinical triple-hit animal model to investigate the application of Curosurf® supplemented with the anionic lipid species DOPG, POPG, PIP2 and headgroup variant IP3 as a novel therapeutic approach for neonatal ARDS. Acute lung injury was artificially induced in newborn piglets by means of three insults: 1) repeated broncho-alveolar lavage to remove endogenous surfactant and induce atelectasis and edema (1st hit at 0h), 2) mechanical overventilation to cause tissue injury/trauma (2nd hit at 24h) and 3) instillation of intratracheal LPS to mimic bacterial infection (3rd hit at 48h). Two hours after each hit the piglets received either an air bolus (control group), Curosurf® alone (S50 group) or Curosurf® plus the supplementation of one of the anionic lipids POPG, DOPG, PIP2 or the headgroup variant IP3. In the following, the answers to the above mentioned core questions will be discussed.

5.1. Macrophage regulation by Curosurf® and anionic phospholipids in the context of nARDS

At the forefront of the innate immune system, the macrophages produce pro-inflammatory cytokines such as TNFα and IL-1β in response to bacterial infection, inflammation and tissue injury in order to orchestrate the local and systemic response. As a consequence, the alveolar macrophages, as primary resident immune cells in the lung, play an important role in the pulmonary immune response to nARDS and lipid metabolism in the lung and were as such a key player in the present study. Therefore, the anti-inflammatory effect of the supplemented anionic phospholipids on piglet and human macrophages were investigated in the context of nARDS.

5.1.1. Porcine alveolar macrophages are in a refractive state 24h after the LPS instillation in the context of the nARDS model

Alveolar macrophages are at the front line when fighting microbial infections, but the alveolar tissue must be fiercely protected from destructive side-effects to ensure undisturbed and effective respiration. Accordingly, macrophages (and monocytes) have an intrinsic mechanism to halt their pro-inflammatory activation pathways, especially in context of protection against shock after endotoxin exposure. This so-called *Endotoxin tolerance* is defined as the reduced response to LPS due to previous exposure to the same stimulus. In human monocytes, even as little as 1h of LPS exposure can lead to tolerance induction, and starting at 6h or more after the initial LPS exposure, the subsequent TNFα secretion in response to a secondary LPS exposure can be nearly abrogated [163].

Representing the 3rd hit in the animal model of nARDS, the porcine macrophages in this study were challenged with LPS *in vivo* 24h prior to their extraction by the final lavage. Therefore, the capability of the alveolar macrophages from the piglets of all test groups to react to a second exposure of LPS 24h after the 3rd hit (= initial LPS exposure) was evaluated. The observed lack of a significant inflammatory response to the 2nd LPS stimulation *in vitro* (measured by level of TNFα secretion), compared to the macrophages from the healthy, untreated piglets at study initiation (0h), is likely to be an expression of ongoing LPS tolerance induced by the first encounter with endotoxin *in vivo*. All treatment groups showed a similar degree of inactivity in response to LPS and therefore the intervention lipids showed no

modulating effect on the reduced TNFα production as a consequence of LPS tolerance. This is, however, only a snap-shot of the macrophage state 24h after initial LPS exposure and it is therefore not possible to draw any conclusions about possible kinetics.

Tolerance is characterized by negative regulation of the transcription factor NFκB via the formation of inactive p50 dimers and subsequent abrogation of TNFα and IL-1β secretion, endocytosis of the TLR4-complex, increased IL-10 and CCL18 secretion and upregulation of vascular endothelial and fibroblast growth factors (VEGF and FGF-2). Analysis of these parameters could support the theory of the piglet macrophages being in LPS-tolerance. With that it can be argued that the macrophages have turned into anti-inflammatory, repair and remodeling-promoting M2-similar macrophages [164]. As a side note, it has been widely discussed that the *in vitro* differentiation of M1/M2 macrophages is not altogether representative of the *in vivo* situation where many in-between-stages of macrophage polarization can be observed as well. A flow cytometric characterization of the $CD38^{low}/Egr2^{high}$ phenotype could provide further insight into the polarization state of the piglet alveolar macrophages 24h after initial LPS exposure, as well as measurement of typical M2 chemokines in the porcine macrophage culture supernatant (e.g. CCL-24, CCL-22) [164,165].

While further analysis of the porcine macrophages, as discussed above, would be preferable, porcine alveolar macrophages retrieved from BALF in this study were oftentimes too scarce to allow for a more extensive approach. Note that the subsequent LPS challenge of the macrophages did not take place immediately after the isolation from BALF, but was undertaken about 8 hours after extraction of the BALF. These logistic challenges should be addressed in potential follow-up studies. Also, it needs to be considered that the response of the alveolar macrophages after re-exposure to LPS *ex vivo* may not be fully representing the situation *in vivo*, as this study looked at alveolar macrophages taken out of their microenvironment.

As mentioned above, macrophage immune activation is halted by endocytosis of the TLR4-receptor and with that by interference with the mobilization of TLR4 into lipid rafts [166]. As discussed in the next chapter, the clinical surfactant preparation Infasurf® was shown to block raft formation, which could lead to the conclusion that the application of Curosurf® indeed contributed to the initiation of immune tolerance in the piglet alveolar macrophages.

5.1.2. Curosurf® attenuates macrophage activation by LPS

Lipid metabolism is seen as an accessory function of macrophages. One example is their role in clearing up apoptotic cells, for which lipid metabolism is of utter importance. A second example is the role in pulmonary surfactant metabolism by alveolar macrophages. In line with the latter, alveolar macrophages (as well as Kupffer cells in the liver) have a constitutively high rate of lipid metabolism [167]. Several transcription factors are involved in lipid metabolism and can influence macrophage polarization, regulate (pro-) inflammatory gene expression or cellular cholesterol levels. Cholesterol in turn is important for the assembly of lipid rafts and consequent activation of TLR4 in presence of LPS [167], see Figure 5.1a. It is therefore not surprising that lipid surfactant can influence macrophages in their immune activation. In fact it has been published that pulmonary surfactant has an anti-inflammatory effect on alveolar macrophages [5]. In our *in vitro* experiments Curosurf® also attenuated the TNFα secretion in response to LPS in human macrophages in a concentration-dependent manner, starting at 10 µg/mL. Therefore, in line with published results, Curosurf® has an inhibitory effect on the

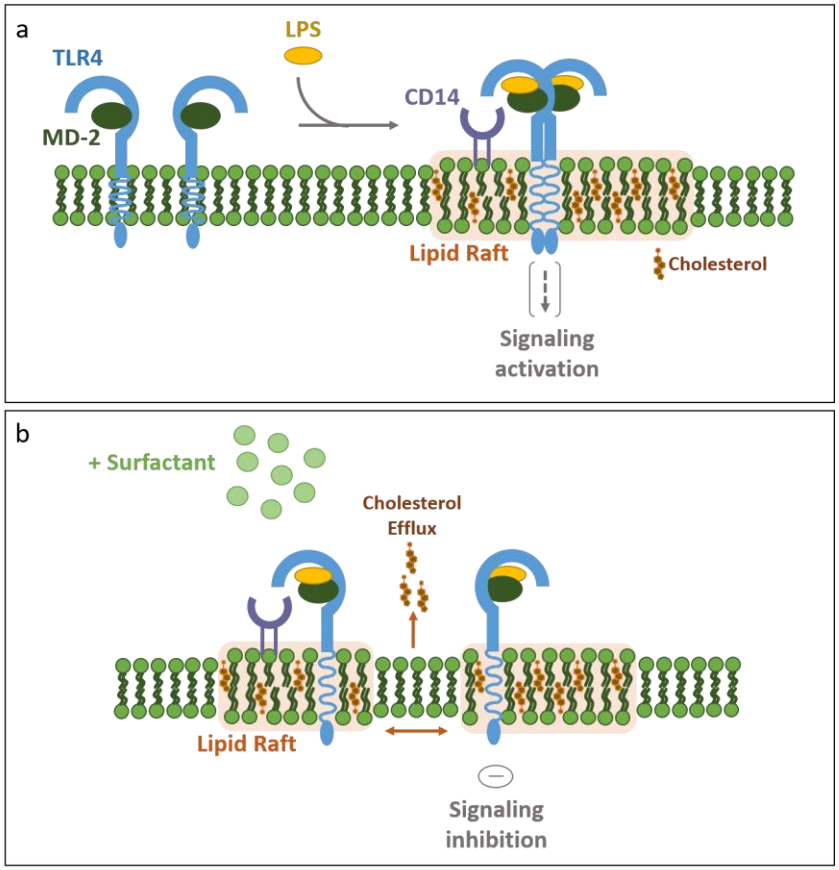

Figure 5.1: Surfactant inhibits raft formation and TLR4 signaling. A) Raft formation in the macrophage membrane in response to LPS exposure leads to TLR4 dimerization and activation of TLR4/NFκB signaling cascade. B) Surfactant supports cholesterol efflux from the membrane which inhibits raft formation and TLR4-signaling.

TLR4/NFκB-pathway and is with that attenuating the activation of macrophages in response to LPS. Importantly, no macrophage activation (measured by TNFα secretion) was observed in response to exposure to Curosurf® in absence of LPS, which is another sign that treatment with Curosurf® has no significant immune-activating activity itself. It has been shown that the clinical surfactant preparation Infasurf® (calfactant) aids in cholesterol removal from alveolar macrophages and as such reduces the formation of rafts and thus TLR4-dependant activation [168]. While Infasurf® is extracted from calf lungs, it has a very similar composition to the porcine lung surfactant preparation Curosurf®, with roughly a third of the surfactant lipids being DPPC and with associated hydrophobic surfactant proteins SP-B and SP-C [169]. It can therefore be hypothesized that Curosurf® has the same inhibitory effect as Infasurf® on raft formation, see Figure 5.1b. Disruption of raft formation has also been shown to be an effector mechanism of DPPC in A549 cells [170]. DPPC is the major constituent of the pulmonary surfactant, responsible for the low surfactant surface tension, and is thus additionally assigned a role in homeostatic control of TLR4 activation in the lung.

It is common knowledge that Curosurf® application improves the symptoms of respiratory distress, which is why it is the gold standard in clinical nARDS therapy up to now. A randomized clinical study with pre-term infants, which compared the initial application of a low dose of Curosurf® (100 mg/kg) versus a high dose (200 mg/kg) followed by identical repeated application of 100 mg/kg, showed similar clinical parameters with only a significant decrease in dependency on oxygen supplementation in the high dose group. The Curosurf® monograph therefore recommends either prophylactic or rescue treatment with at least 100 mg/kg which subsequent doses of 100 mg/kg [171].

In the present study, initially two different concentrations of Curosurf® were given to the piglets (50 mg/kg and 200 mg/kg). However, application of 200 mg/kg Curosurf® did not result in improved clinical parameters compared to 50 mg/kg. In contrast, piglets of the S200 group showed a general clinical outcome which was partly inferior (oxygenation index, ventilation efficiency index) even to those of the untreated control group which only received air boli. The S200 group was therefore discontinued after three piglets. Determination of the responsible underlying mechanisms compared to the S50 group where not subject of this study, but it would be an obvious conclusion that application of 3x 200 mg/kg Curosurf® has exceeded the beneficial amount of surfactant in piglet lungs. Application of excessive quantities of surfactant preparation have been demonstrated to lead to toxic reactions in the

pulmonary space due to i.e. excessive accumulation of phagocytes but reduced phagocytosis of apoptotic cells [5], [171].

It is thus to be concluded that the answer to an improved therapy with Curosurf® does not simply lie in the therapeutical application of excessive Curosurf® amounts. This work highlights, that supplementation of Curosurf could indeed be a promising strategy to an improved nARDS therapy.

5.1.3. The macrophage TLR4/NFκB-activation pathway is an order of magnitude more receptive to inhibition by DOPG, POPG and PIP2 compared to the canonical inflammasome pathway

Disaturated phosphatidylcholine is not the only phospholipid that shows the ability to directly or indirectly interrupt LPS-signaling through TLR4. Anionic phospholipids found in pulmonary surfactant such as POPG and PI are competitive antagonists of LPS due to structural similarities: Their negative net charge enables binding to positively charged proteins, such as LBP [173]. PI binds to LBP which transports it to CD-14, the co-receptor of TLR4, and POPG binds to the LPS-binding sites of MD-2 and CD14 [94,174]. These anionic phospholipids are thus competitive inhibitors of LPS. The group of Dennis R. Voelker has shown that POPG efficiently inhibits TLR4 dependent lipid mediator (arachidonic acid [AA]) release in murine RAW264.7 macrophages and in human alveolar macrophages in response to *Mycoplasma pneumoniae* and that it exhibits anti-viral activity in the context of infection with respiratory syncytial virus and Influenza A Virus [142,143,145]. DOPG, a minor component of the pulmonary surfactant pool concentration-wise, was shown to interfere with NFκB-dependant type II sPLA2 production in LPS-stimulated guinea pig macrophages.

The accumulation of PG species is unique to pulmonary surfactant in mammals, which in itself already indicates a specific role in surfactant and lung homeostasis. In the last two decades more and more studies have indicated a strong role in innate pulmonary immunity. While POPG is the most abundant PG in pulmonary surfactant, DOPG is one of the less abundant ones, and increases in concentration during post-natal lung development. Therefore, the reasons why PI and PG species (PIP2, POPG, DOPG) were chosen as supplement for Curosurf® in this piglet model of nARDS are manifold.

In line with known anti-inflammatory properties of POPG, our study also showed an efficient down-regulation of the activation of human PBMC-derived macrophages in response to LPS, not only for the TLR4/NFκB-dependant pathway for TNFα secretion, but also for the canonical

inflammasome pathway for IL-1β production ($IC50_{TNFα}$ 1.9 µM; $IC50_{IL-1β}$ 23.8 µM). The structurally very similar lipid DOPG (saturated palmitic acid [16:0] of POPG replaced by a second unsaturated oleic acid [18:1]) showed an equivalent result as it also significantly, even more efficiently, inhibited macrophage secretion of TNFα and IL-1β in response to LPS ($IC50_{TNFα}$ 1 µM; $IC50_{IL-1β}$ 11.5 µM). Note that the same is true for PIP2, as discussed in the later chapter 5.1.5.

Western blotting analysis of macrophage cell lysates in this study showed that POPG and DOPG effectively reduced the expression of pro-IL-1β in response to LPS stimulation. Pro-IL-1β is expressed in macrophages in response to TLR4-activation by LPS, without the need of a second signal [175]. Therefore, reduction of secreted mature IL-1β is not by itself a definite sign that PIP2, POPG or DOPG actively interfere with the canonical inflammasome pathway per se, as it may be the sole direct result of reduced production of its pro-form. Therefore, it should be further investigated, whether DOPG and POPG also have a direct inhibitory effect on either the assembly of the NLRP3-inflammasome or cleavage of pro-caspase-1 into its active form, possibly even the assembly of GSDMD membrane pores – so the steps downstream of pro-IL-1β expression. The Western blot analysis of pro-Caspase-1 were inconclusive and could not define whether any of the four lipid substances could inhibit secretion of pro-caspase-1. While POPG elicits its inhibitory actions indirectly by binding to MD-2 and thereby blocking the LPS-binding site, it has been shown only very recently (in 2019) that DOPG, on the other hand, acts further downstream by inhibiting the nuclear translocation of the transcription factor NFκB [176].

In regards to the inhibition of LPS-initiated TNFα- and IL-1β secretion, in this experimental *in vitro* setting POPG showed an IC50 which is 2-fold higher than that of DOPG. It may therefore be hypothesized that the combination of antagonistic activity and a direct, downstream inhibitory function of DOPG is more efficient than blocking of LPS-binding site at the receptor complex by POPG. In the bigger context of respiratory distress syndrome, LPS (and with that microbial exposure) is not the only inflammation-promoting factor. Mechanical ventilation just as example, also leads to pro-inflammatory cytokine release [177]. Therefore, blocking the signaling cascade downstream of the TLR4-receptor complex is likely to inhibit a wider range of pro-inflammatory signals.

Inhibition of the TLR4/NFκB-pathway required significantly lower anionic phospholipid concentrations compared to the canonical pathway. TNFα secretion via the TLR4/NFκB-

pathway demands only one signal (PAMP binding) for inflammatory gene expression. However, canonical inflammasome activation is not only reliant on PAMP recognition, but also on a second stress signal, ATP in this study. Thus the higher complexity of the activation cascade may necessitate higher inhibitory concentrations.

5.1.4. Both the headgroup charge and the acyl chain composition are dictating the immunological function of the anionic phospholipids

The inhibitory activity of both DOPG and POPG is mediated on the one hand by the negatively charged PG headgroup, as their equivalents with neutral net charge but identical acyl chains (DOPC and POPC) did not attenuate the LPS-induced TLR4/NFκB or canonical inflammasome pathway under identical conditions in this study. On the other hand, as DOPG and POPG share an identical headgroup, the final binding site that dictates the specific regulatory function would therefore additionally be dependant on the specific acyl chain. However, studies showing the distinct anti-inflammatory effects of DOPG and POPG did not always corroborate their findings with the respective other PG species, but only with the corresponding PC species (same acyl chains but PC as headgroup). So the notion that DOPG and POPG have overlapping molecular mechanisms cannot be easily dismissed. As an example, CD14 also binds just as efficiently to DPPG and to PI [146], which could indicate again that the negative charge of the headgroup is the stronger factor rather than small differences in length and level of saturation of the corresponding acyl chain.

In 2017 it was published by Backhaus et al. that the surfactant component DPPC inhibits IL-1β release by effectively blocking the activation of the ATP-dependant P2X7 receptor in LPS-primed human monocytic U937 cells and LPS-primed human PBMCs (while POPG does not) [178]. In this present study however, the structurally very similar PC species DOPC and POPC did *not* reduce the ATP-induced IL-1β secretion of LPS-primed human PBMC-derived macrophages. On the contrary, a slight concentration-dependant increase in IL-1β concentration in cell supernatant was detected upon incubation with DOPC and POPC. DPPC has two palmitoyl (16:0) chains while DOPC has two oleoyl (18:1) chains and POPC has one of both (16:0 – 18:1). Backhaus et al. concluded that the DPPC headgroup must be the immune modulating structure when considering that lipids such as DPPE (same acyl chain composition, different headgroup) did not inhibit IL-1β release. However, compared to DOPC and POPC in this present study, all three PC lipids share the identical headgroup and yet DOPC and POPC

did not elicit IL-1β release impairment. It could be concluded that here again, the small but mighty difference in lipid acyl chain composition between DPPC and DOPC/POPC, namely the presence of at least one unsaturated acyl chain, confers an additional level of molecular regulation. The additional double bond in POPC compared to DPPC leads to a 'kink' in the acyl chain conformation which could result in steric hindrance that effectively prevents POPC from binding. However, the difference could also be contributed to differences in IL-1β pathway regulation in monocytes and macrophages. This goes to show that the immune-regulatory functions of surfactant phospholipids are of great complexity and specificity.

5.1.5. PIP2 attenuates both the TLR4/NFκB pathway and canonical inflammasome pathway more efficiently than DOPG and POPG

As mentioned above, PIP2 is another anionic surfactant phospholipid with immune-regulatory function. It has been described by Wang et al. that phosphatidylinositol (PI) effectively competes with LPS for LBP-mediated binding to CD14 in human monocytes and therefore has the ability to inhibit LPS mediated pro-inflammatory signaling at the receptor level [174]. PIP2, just like other bi- and tri-phosphorylated PI family members, is a strong inhibitor of acid sphingomyelinase (aSMase) which is responsible for lysosomal degradation of sphingomyelin to ceramide [156]. This is important as ceramide is upregulated upon LPS or TNFα signaling and the elevated ceramide concentration in the cytoplasm activates the NLRP3 inflammasome, increases endothelial permeability and epithelial apoptosis [179]. So ceramide acts as a pro-inflammatory mediator.

As PIP2 was chosen as one of the therapeutic compounds in this piglet nARDS study, also the direct effect PIP2 has on human PBMC-derived macrophages was tested. Comparable to the anti-inflammatory effects that were shown for DOPG and POPG, PIP2 attenuated TNFα and IL-1β release by LPS-stimulated macrophages and it did so in a concentration dependant manner. However, PIP2 was required in a lower concentration to exert these effects than DOPG and POPG. Especially noticeable is this observation for the inhibition of the canonical inflammasome pathway as measured by IL-1β secretion: PIP2 IC50 was observed to be 5-fold and 10-fold lower than DOPG and POPG, respectively. PIP2 is a bulky molecule compared to DOPG/POPG, due to its inositol headgroup. So while both POPG and PIP2 bind to CD14, only POPG binds to MD-2 [146], so the different effector functions may be attributed to the different headgroup, even though POPG has more binding partners in this pathway.

PIP2 allows for location-dependant signaling functions as it is mainly located in the inner leaflet of the macrophage membrane where it allows for assembly of adaptor proteins TIRAP/MAL to the activated TLR4 receptor complex and subsequent MyD88 and NFκB signaling [180]. PIP2 phosphorylation to PIP3 by PI3K initiates TLR4-receptor complex translocation into endosomes of dendritic cells where the adaptor molecules TRIF/TRAM initiate anti-inflammatory signaling (IL-10, IFN-β secretion) [181].

The anti-inflammatory effector functions tested in this study, which are directly exerted on macrophages, were corroborated in primary human lung macrophages, making these results clinically even more relevant.

5.1.6. The *in vitro* effects of PIP2 and IP3 on macrophage activation are profoundly distinct

PIP2 was not the only PI family member identified as a good candidate for therapeutic application as described above: IP3 is a strong inhibitor of the acid sphingomyelinase as well. LPS leads to increased expression of the IP3 receptor (IP3R2) in murine peritoneal macrophages [182]. All IP3-receptors are Ca^{2+}-channels in the ER membrane and their activation releases Ca^{2+} into the cytoplasm. Upon LPS-binding to the TLR4 receptor complex, PI(4,5)P2 is upregulated and cleaved by phospholipase C (PLC) into IP3 and DAG. IP3 binds to IP3R2 on the ER membrane which initiates a Ca^{2+} efflux from the ER into the cytosol. Ca^{2+} increase and DAG activate PKCα which initiates the JNK/NFκB pathway leading to pro-inflammatory cytokine release [183]. Interestingly, the Ca^{2+} influx into the cytosol also mediates the endosomal uptake of the TLR4-complex and consequent anti-inflammatory signaling, initiating inflammation resolution [184,185].

PIP2 had a strong attenuating effect on the LPS-induced secretion of TNFα and IL-1β by human and porcine macrophages *in vitro* in this study. IP3 however, essentially being the free, tri-phosphorylated inositol headgroup of PIP2, did not inhibit macrophage secretion of TNFα or IL-1β in response to LPS. Therefore it did not inhibit the TLR4/NFκB- or canonical inflammasome pathway. Even the highest concentration of IP3 (50 µM and 500 µM) did not show any inhibition and cytokine production remained uninterrupted. This result was then corroborated in porcine macrophages, so it is not a species-specific peculiarity of macrophages. Wang et al. showed in the human monocytic THP-1 cell line that the capability of phosphatidylinositols to bind CD14 may at least partly be dependant on the glycerol moiety,

which is lacking in IP3, as well as positioning of phosphorylation on the inositol ring, whereby C3- and C4-phosphorylation display higher affinity [174]. The IP3 used in this study was phosphorylated on C1, 2 and 6, while the PIP2 used also has the potentially favorable C3 phosphorylation. Furthermore, PIP2 does not penetrate the cell membrane [186], whereas IP3 can diffuse through the membrane to its intracellular receptor. So the lack of anti-inflammatory action of IP3 on macrophages in response to LPS may indicate a regulatory role of the lipid moiety of PIP2 in addition to the inositol headgroup and the subcellular location. It would be interesting to assay other PI species with phosphorylations on varying hydroxyl groups, such as the unphosphorylated precursor, tri-phosphorylated PI or even the unphosphorylated inositol headgroup only, and compare their immunological effect with the PI(3,5)P2 used in this study. Indeed, the cleavage product and phosphorylated headgroup IP3 will be discussed in the next chapter.

5.1.7. Piglets treated with IP3 and POPG display the greatest therapeutic improvement *in vivo*

The anionic lipids PIP2, POPG and DOPG showed different inhibitory concentrations for inhibition of TNFα and IL-1β secretion in LPS-primed PBMC- derived macrophages. The potent direct anti-inflammatory action that all three phospholipids exerted in this study would also benefit the alveolar environment for several reasons: The attenuated macrophages release less pro-inflammatory cytokines which would otherwise attract further inflammatory cells, not just macrophages but also neutrophils and monocytes. Less activated immune cells also means less tissue damage, because it is well known that the pro-inflammatory mediators also lead to vascular permeability and leakage into the alveolar space. Cytokine-induced leukocyte respiratory burst also leads to direct tissue damage. Increased TNFα-levels can effectively attenuate SP-A production and mediate epithelial cell death [185], [186].

Supplementation with DOPG and POPG led to a strong decrease in alveolar epithelial cell apoptosis, compared to Curosurf® (S50) alone (full results reported in[157]). Consequently, a stronger attenuation of macrophages by the intervention lipids should contribute to a better clinical outcome in the context of this nARDS study. Additionally, inhibition of the TLR4/NFκB-pathway by anionic lipids specifically in the lung would be an effective therapy option while not exhibiting systemic side effects such as increased risk of other infections, which has been shown for current anti-TNFα antibody therapies [50].

This piglet study of nARDS made it very clear, already from the *in vivo* data alone, that *all* four phosphatidylglycerol and inositol intervention substances show a significant, measurable and positive therapeutic effect, while negative side effects of this treatment were not detected (apart from the S200 group). For most clinical parameters, supplementation with POPG and IP3 showed the more pronounced improvements (see additional *in vivo* data in [157]). Especially the oxygenation index, extravascular lung water index (EVLWI) and the compliance of the respiratory system were markedly improved after 72h. In accordance with that, the lung weight was significantly decreased for IP3 and POPG.

However, analysis of lung and liver tissue lysates revealed a more diverse picture. As mentioned above, IP3 has been well described as a highly potent inhibitor of the sphingolipid-ceramide-pathway. Accordingly, molecular analysis of the lung tissue has shown significantly decreased aSMase activity and in consequence a lower ceramide concentration. These results were mirrored in liver tissue lysates which indicates not only a located, pulmonary effect but also a systemic effect of IP3 supplementation on the ceramide-pathway (see data in [157]). Macrophage stimulation experiments in this study showed that only PIP2, POPG and DOPG inhibited the TLR4/NFκB- and the canonical inflammasome pathway presumably by direct interaction with LBP, MD-2 or CD14. IP3 showed no such inhibitory effect on LPS-stimulated macrophages. In contrast to these *in vitro* results, IP3 did indeed show a strong inhibitory effect by downregulation of IκB-kinase in lung tissue which in turn led to higher concentrations of total IκBα [157]. It is well known that IκBα in its unphosphorylated state is bound to NFκB. Upon IκBα phosphorylation and degradation, initiated by pro-inflammatory signaling such as TLR4-activation, NFκB is released and translocates into the nucleus for transcription of pro-inflammatory genes. Consequently, supplementation with IP3 led to potent blocking of the NFκB pathway in lung tissue. In line with that, IP3 supplementation also led to a reduction of canonical inflammasome activity in lung tissue, as shown by decreased concentrations of the inflammasome key proteins NLRP3, ASC and caspase-1. This discrepancy between *in vitro* results (no inhibition of TNFα/IL1β-release in LPS-stimulated PBMC-derived macrophages) versus *in vivo* results (downregulation of NFκB/inflammasome and ceramide pathway) indicates differentially regulated effects of IP3 and a systemic anti-inflammatory effector function, not directly targeted at macrophages. Human primary alveolar macrophages also were not attenuated by IP3 *in vitro*. Human primary interstitial macrophages showed a slight, yet statistically insignificant decrease in IL-1β in response to IP3, but these results would need

further verification. While both macrophages and pulmonary epithelial cells express TLR4, inflammatory signaling is not identical in regards to LPS sensing [189,190] and a further analysis of piglet pulmonary alveolar epithelial cells could provide further insights.

As a side note, compared to the identified IC50 concentrations on the macrophages, the anionic lipids PIP2, POPG and DOPG were applied in great excess to the piglet lungs *in vivo* (see calculation 7 in the supplementary information). These values are, of course, not directly comparable, as there are unknown dilution factors in the lung to be considered etc. But it may indicate that especially IP3 could need higher concentrations to show inhibitory effects on the macrophages *in vitro*.

5.2. BALF cytokine analysis has limited diagnostic relevance

Induction of TNFα gene transcription takes place within minutes of stimuli binding and is thus an example of an immediate early gene. In monocytes, the macrophage precursor, TNFα mRNA peaks between 2 and 4 hours post-stimulation with LPS and returns to background levels after approx. 8h. Actual secretion of the cytokine peaks after 4h and then slowly levels off, cut in half after approx. 24h. Even with persistent stimuli exposure TNFα expression is transient [191,192]. Similarly, IL-1b mRNA can already be detected in human PBMC-derived macrophages after 1h [193]. The stimulation of the piglets in this study by LPS-instillation into the airways preceded the final lavage, in which the porcine TNFα and IL-1β concentrations were measured, by 24 hours and thus, the time point measured in this study was many hours *after* TNFα and IL-1β concentration peaked. The mismatch in time along with the high biological variances and the fact that the alveolar content is highly diluted by the lavage procedure make it seem possible that cytokine concentration differences elicited by the presence of the intervention lipids were masked, if any did occur. The analysis of porcine BALF for TNFα and IL-1β concentrations only allows for the conclusion that there has indeed been an activation of alveolar macrophages or other alveolar cells due to the triple hits and especially due to the LPS-instillation and with it an increased inflammatory status in the lungs, as depicted by elevated cytokine and total protein concentration.

Both surfactant proteins A and D are produced by AECII and it is therefore not surprising, that the SP-A concentration in BALF was found reduced by 30% in the sick control piglets after 72h.

An increase in SP-A concentrations back to the healthy 0h level in the IP3 piglet group supported the *in vivo* observation that IP3 showed strong anti-inflammatory effects especially in correlation with the NFκB-pathway in the tissue samples and with the clinical parameters in general. The observed decrease of SP-A concentrations in the untreated control group was milder than what is known for human adult ARDS patients [194], but is in line with published reports that SP-A concentrations in children only slightly decreases, if at all [195]. Considering the premise that nARDS leads to the disruption of the alveolar epithelium und AECII apoptosis, one would expect SP-D concentrations to decrease along with SP-A. However, there was no concentration change observed between healthy and sick piglets for SP-D, independent of the treatment group. Some previous studies in ARDS patients corroborate these results [194], whereas other studies found significant changes in SP-D levels in BALF in ARDS patients [195,196]. In addition to surfactant proteins, apoptosis in BALF AECII was analysed as part of the cooperation nARDS piglet study [157]. This analysis did not reveal significant differences between untreated control piglets and healthy piglets. While this may be explained by the observation that in the first 24 months of life children exhibit increased AECII apoptosis anyway, which is believed to be necessary for tissue remodeling and differentiation [197], BALF cannot aid in a proper assessment of changes in AECII apoptosis during nARDS (see original paper [157] on AECII apoptosis data). Taking together all of these results, it could be concluded that BALF has a limited diagnostic usefulness in the context of nARDS and specifically in this piglet model.

5.3. Role of LBP in pulmonary inflammasome activation

The LPS binding protein (LBP) sensitizes immune cells to LPS by serving as a LPS sensor and by mediating LPS transport to the CD14/MD-2/TLR4 receptor complex. $LBP^{-/-}$ mice show suppressed production of inflammatory cytokines and impaired bacterial clearance [198,199]. Furthermore, LBP neutralizes LPS by transporting it to high-density lipoprotein [200]. Elevated LBP levels have been detected in the BALF of adult human patients with respiratory distress syndrome [201]. In this study, piglet BALF was also analysed by means of ELISA and highly elevated LBP levels were indeed detected in the final diagnostic lavage after 72h compared to BALF of the healthy piglets**.** Application of Curosurf® reduced the LBP content in BALF slightly, but the supplementation with IP3, PIP2, POPG, or DOPG did not lead to any further reduction.

It has been shown that not just hepatocytes, but also AECII cells express LBP [25], which points towards a direct pulmonary, anti-inflammatory role of LBP. In addition, our lab has shown that LBP mediates the intercalation of LPS into phospholipid bilayer, which leads to LPS neutralization, and transports it into the cell (TLR4-independent) where LBP co-localizes with human caspase-1 [29,173]. Intracellular LPS has been shown to activate human caspase-4 and -5 [74,202]. In that context, a side project of this study aimed to identify the possible involvement of LBP in activation of the non-canonical inflammasome activation in macrophages. To that end, human macrophages were incubated with LBP and LPS under serum-free conditions, but in the absence of ATP, to avoid activation of the TLR4-dependant canonical inflammasome. A background level of non-canonical inflammasome activation was observed in the macrophages upon LPS priming which could be attributed to the fact, that even though the macrophages were incubated in serum-reduced conditions, they initially had endogenous LBP bound to their membrane [29]. These macrophages were differentiated from peripheral blood monocytes which had indeed been in contact with serum LBP. It is thus very difficult to create a truly serum-free environment for cells harvested from blood or differentiated from primary blood cells even when using serum-free media and culture conditions.

Upon addition of LBP/LPS complex to the LPS primed macrophages, IL-1β secretion, and therefore non-canonical inflammasome activity, increased. Considering that a) LPS cannot intercalate into phospholipid membranes or cross them on its own, b) LBP most likely mediates LPS transport into macrophages and c) the macrophages in this experimental setup where not supplied with a second stimulus to activate the canonical inflammasome, the results of this study suggest a direct effect of LBP on non-canonical inflammasome activation by intracellular LPS. Since phosphatidylglycerol markedly suppresses LBP intercalation into phospholipid liposomes [173] (the initial step in the proposed mechanism of LBP-mediated intracellular LPS-sensing), it would furthermore be of interest, if co-incubation with the anionic phospholipid species used in this nARDS model has a regulatory effect on the LBP-mediated LPS-dependant non-canonical inflammasome activation in macrophages. The potential role of phospholipids as inhibitors has not yet been addressed in this context and could shed light on the regulation of LPS transport in the context of inflammasome activation. Bacterial LPS can enter the cell by several different mechanisms, some of which have only very recently been described. LPS can be introduced into the cytoplasm of the host cell by type 3 secretion systems, as seen for *Salmonella* or *Y.pestis* [203]. Outer-membrane vesicles (OMV's) of

Gram-negative bacteria are thought to act as direct transporters of LPS into the host cytoplasm. It was shown in 2017 that, in contrast to the pathogen-initiated LPS transport, LPS internalization can be mediated by the host cell protein high-mobility group box 1 (HMGB1). It binds LPS and the HMGB1-LPS complex is subsequently endocytosed [204]. Therefore, LBP-mediated transport of LPS into the cytoplasm could be an alternative entry route for LPS into the cell and an initiator of LPS-mediated non-canonical inflammasome activation. It is very likely that several pathways are simultaneously contributing to the activation of the non-canonical inflammasome, in which LBP could play an essential role.

5.4. The piglet pulmonary surfactant lipid*ome* in health and nARDS

This present study provides a detailed overview of the piglet lipid*ome* in a healthy state as well as in a state of acute respiratory distress. In the context of this piglet nARDS model, pulmonary surfactant was isolated from the piglet BALF from healthy (0h) and diseased (72h) piglets. By a mass spectrometric approach the piglet pulmonary surfactant was dissected to allow for a detailed analysis of its 181 detected lipid components. The aim was to define the composition of the healthy piglet surfactant lipid*ome* and its comparability to the human lipid*ome*, to determine the changes possibly occurring from the healthy state to a state of acute respiratory distress, and to identify possible modifications resulting from supplementation with Curosurf® and the anionic phospholipids POPG, DOPG, PIP2 and IP3.

In this nARDS study piglets were chosen as the model organism for the reason that pigs are much closer related to the human physiology than mice or rats. It was therefore not surprising that the grand scheme of the piglet pulmonary surfactant lipid*ome* corresponded to the human surfactant lipid*ome*: PC species made up about 60% of the phospholipid pool with DPPC (PC 32:0) being the most prominent PC species; minor components were PE, PS and SM species.

While pulmonary surfactant from human adults have a PG content of about 5-10% with a similar or lower PI amount, human neonates show a distinct composition: Upon birth, the PI/PG ratio is high, meaning that PG is nearly undetectable while the PI amount is elevated [5]. From a structural perspective, it has been suggested that the lack of PG is compensated by the higher PI amount. That is attributed to the fact that both PG and PI improve absorption of DPPC into the surfactant monolayer [205–207]. This PI/PG peculiarity was also shown for piglet

surfactant in this study, which again underlines the physiological relevance of using a piglet model to research a human disease.

When mentioning the PI/PG relationship it should be considered that not the entire PI amount must necessarily come from the pulmonary surfactant alone. It is an ubiquitous lipid found in the inner leaflet of mammal cell membranes, similar to PS [208]; while PG is basically restricted to pulmonary surfactant in mammals. Note that the membrane asymmetry is generally lost in aging platelets and in apoptotic cells [209,210]. Therefore, PI-rich membrane patches released from apoptotic cells or other membrane residues that were not completely removed by centrifugation could have contributed to the PI pool in the piglet surfactant samples. However, the surfactant samples contained little amounts of triglycerides, which would have been an indicator for a high number of apoptotic cell debris, supporting that the observed PI is neonatal PI of the surfactant phase. The piglet surfactant did not show an age dependant difference in total abundance of PI and PG, but the age range of the individual piglets in the analyzed groups was very narrow (2-5d at study start).

As will be discussed in chapter 5.5, the piglet model mimics well the physiological symptoms of nARDS in human children, which means that the surfactant system in the lungs is also compromised by the triple-hit model: The endogenous surfactant was removed by the initial lavage which is a chemical insult leading to high surface tension in the lung, overventilation is a mechanical insult leading to stress-induced inflammation, and LPS as a microbial insult leading to PAMP-induced inflammation, all resulting in an impacted surfactant pool. In line with that, the piglet surfactant data of the untreated control piglets (only air boli) at 72h showed decreased concentrations in many of the main and important lipid species, among them DPPC, POPG and DOPG. Decrease in PC content is correlated with upregulation of $sPLA_2$ during nARDS [211,212], a group of enzymes that cleave the sn-2 ester bonds of phospholipids which leads to the surfactant lipid degradation. However, the analysis of $sPLA_2$ in piglet BALF by ELISA did not reveal any significant change in $sPLA_2$ concentration in the piglet treatment groups compared to non-supplemented Curosurf®, neither was there any correlation with the total protein concentration per sample (data not shown). That can most likely be attributed to biological variances and varying dilution of the samples.

The piglet's endogenous surfactant pool was initially diminished by repeated lavage procedures at 0h. The clinical parameters did not return to the baseline upon the first Curosurf® application at 2h, partly probably due to already ongoing pulmonary inflammation

caused by the initial lavages, and partly because the administered Curosurf® probably did not fully replace the loss of endogenous surfactant. It can therefore not strictly be stated, that the main lipid species were 'degraded' after 72h, as a) they could have not been replaced in full by Curosurf® to begin with or b) the alveolar epithelium had reduced surfactant synthesis due to inflammation. Nevertheless, the intratracheal administration of surfactant preparation via a double lumen tube without discontinuation of ventilation is an established clinical method and while it has been critically discussed whether the applied surfactant spreads evenly throughout the alveoli, an immediate improvement of the clinical parameters, especially oxygenation, indicates a successful application of 50 mg/kg Curosurf®.

5.4.1. The surfactant lipid*ome* composition in sick piglets remains intrinsically stable during nARDS despite small changes on a single lipid level

The endogenous surfactant composition is complex, specific and tightly regulated by an abundance of interconnected metabolic pathways. A comparison of the healthy piglet surfactant at 0h with the surfactant of the untreated control piglets at 72h revealed that the overall surfactant lipid composition (qualitative, not quantitative) has remained unchanged, although the total amount was reduced. The split into the different main lipid species PC, PI, PS, PG etc. showed a distribution which was basically equivalent with that of surfactant from healthy piglets. The control piglets did not receive Curosurf®, so the detected lipid species must all originate from the piglet's endogenous lipid*ome*. Going into more details and analyzing the single lipid species led to the conclusion that the relative abundance of most species did not change. However, small changes on a single lipid level were indeed detected and should not be dismissed easily.

For one, an increase in the relative abundance for SM [34:1] in the 72h untreated control groups was seen. This observation may be directly connected to the increased ceramide concentration that was detected in whole lung tissue of the piglets [157]. SM[34:1] is specifically abundant in endothelial cells [213], as it regulates endothelial barrier function, and therefore its increase during disease progression may be related to alveolar-capillary damage. It could be of further interest to analyze the presence of SM precursors/metabolites such as S1P (reduces vascular permeability) and S3P (increases vascular permeability and promotes lung edema) [214]. SM, along with cholesterol, is of importance for cell signaling in response to DAMPs due to its enrichment in lipid rafts, so the increase may also stem from the onset of nARDS in the

control piglets. In this respect, cell-specific analysis of the specific lipid*ome* of the alveolar macrophages and AECII to determine cell-specific membrane composition changes during nARDS may provide further insight.

A slight increase in cholesterol relative abundance in the untreated control samples was also detected, and may as such contribute to the inflammatory state in the lungs. However, studies have shown that cholesterol in pulmonary surfactant is for the most part transported there by plasma lipoproteins and cleared via cholesterol efflux and HDL, instead of being de-novo synthesized in pulmonary tissue [94]. So cholesterol accumulation in the lung could be a result of defective alveolar-capillary barrier function which was shown in this piglet model by total protein concentration in BALF and increased serum albumin (see data in [157]).

In summary, the general piglet surfactant lipid*ome* composition in untreated sick piglets was likely impacted by the decline in its total amount, but not by grave compositional changes. As the intrinsic surfactant lipid*ome* configuration is most efficient in lowering surface tension and enabling proper respiration, a considerable change in its composition in addition to an already reduced total amount would possibly aggravate the nARDS symptoms even further. Therefore, the observed compositional stability of the lipid*ome* is in line with the functional requirements.

5.4.2. The surfactant lipid*ome* after treatment shows Curosurf®-specific alterations, but is not influenced in its composition by the supplemented anionic phospholipids

The piglets in this nARDS study received three Curosurf® interventions, with or without the anionic phospholipids, each 2h post-hit. While Curosurf® is extracted from the lungs of adult pigs (past the PI/PG switch age), it was not identical in composition with the piglet surfactant in this study. The 'modified natural surfactant' Curosurf® is obtained from whole pig lungs by organic solvent extraction, followed by liquid-gel column chromatography [215]. Therefore it is depleted in the hydrophilic SP-A and SP-D as well as cholesterol.

Generally, concentration increases of several lipid species that were seen in the pulmonary surfactant of the S50 group, but not of the untreated control group, were mainly due to the introduction of these lipids by Curosurf® application, such as many PG species: PG 32:0, PG 32:1, PG 34:1 (POPG). At the same time, the piglet surfactant lipid*ome* did not show an increase in PI concentration upon Curosurf® application because Curosurf® has a comparably small PI content (likely due to the fact that it was extracted from *adult* pigs, where the PI/PG-

ratio is smaller). However, there was no significant difference in qualitative surfactant PI-pool composition between healthy piglets and Curosurf® treated sick piglets which may indicate that the PI-pool decreases in total amount with aging, but remains similar in its composition.

A few specific lipid species were only detectable in the pulmonary surfactant of Curosurf®-treated piglets. Those lipid species were either below the detection limit in the untreated control piglet surfactant samples (a higher amount of sample would need to be extracted in further studies) or are related to maturation of the lung and are thus only present in adult pigs and therefore in Curosurf®.

The Curosurf® surfactant preparation contained high amounts of lysophatidylcholine (LPC; PC 16:0) as detected by mass spectrometry (mean ±10.9 mM = 5.4 mg LPC/mL; total Curosurf lipid content ±55,7 mM). Interestingly, Fornaiser et al pointed out a concentration of 0,56 mg/mL LPC in Curosurf [216]. This 10-fold difference is puzzling. It is unlikely that PC 16:0 spontaneously degraded to LPC during storage at +4°C as the ester bonds are relatively stable, nor is enzymatic contamination a likely explanation. Analysis of a different lot of Curosurf® could shed light on the issue, as last but not least, lot-dependant difference in LPC concentrations could be the culprit.
Nevertheless, it has been shown that LPC promotes a positive membrane curvature which blocks absorption into the bilayer [217] which in turn can lead to surfactant impairment and higher surface tension, and it was shown recently (in 2020) that LPC can also induce caspase-1 activation and pyroptosis in the human THP-1 monocytic cell line and HUVECs [218]. An intentional decrease in LPC-concentration in Curosurf® preparations may therefore be beneficial.

A few PC species with odd-chain fatty acids (PC [31:1], PC [31:0]) were detected in the piglet surfactant. As their relative amount was elevated in the pulmonary surfactant of the healthy piglets compared to the piglets after 72h of disease progression, these lipids cannot be Curosurf®-derived and are unlikely to be of blood plasma origin. However, research into the biological relevance of these odd-chain fatty acids has only really begun these last few years and was so far mainly investigated in contexts of metabolic or dietary backgrounds [219].

A further peculiarity in the piglet lipid*ome* results was the increase of the low-abundance PE-ether upon Curosurf® treatment, which was even more pronounced in the pulmonary surfactant of the S200 group. These glycerophospholipids possess an ether-bond at sn-1 and

sn-2 instead of the ester bond. As the Curosurf® sample did *not* contain any detectable PE-ether-concentration, these lipids probably stem from *de novo* synthesis in the peroxisomes of the alveolar cells. Ether lipids have been implicated in re-absorption of lipids from tubular myelin into the surfactant bilayer [220] and an increase in their concentration could therefore indicate a protective pathway to refill the pulmonary surfactant from the myelin storage pool.

The anionic PG and PI species used as supplements for Curosurf® in this study were clearly detectable in the surfactant of the piglets 24h after the 3rd Curosurf® application. It would be useful in further research to label the applied PG and PI species to determine their half-life *in vivo*, as it is unclear which ratio of the originally supplemented lipids remained after 24h (i.e. by quantification with deuterium-labeled PI and PG in mass spectrometry), and to determine how they are incorporated and distributed in the surfactant layer (i.e. by detection with the fluorescent TopFluor®PI(3,5)P_2). Either way, the lipids POPG, DOPG, and PIP2 (IP3 could not be detected with this mass spectrometric approach) were present in excess amounts in the piglet surfactant 24h after their final and 3rd application, which means that their immune protective effect may be exerted *in vivo* beyond that time frame.

Analysis of the lipid*ome* data by hierarchical clustering clearly showed that the healthy surfactant lipid*ome* was distinct from the Curosurf® treated lipid*ome*, but that the presence of the supplemented lipids did not further alter the lipid*ome* composition. The clinical pulmonary parameters definitely indicated that the supplemented anionic lipid species did improve the structural properties of the surfactant, as significant improvements in parameters such as compliance and resistance of the respiratory system were observed in the piglets. That leads to the conclusion that their presence may not have altered any surfactant metabolic pathway *per se*, but improved surfactant properties by promoting important parameters such as re-spreading and re-absorption and with that conferred the desired therapeutical effects on a biophysical/functional level.

5.5. nARDS piglet model benefits and challenges

The present model combined three of the main causes of respiratory distress, namely surfactant deficiency, mechanical stress due to artificial ventilation and microbial inflammation. It allowed for the comprehensive analysis of several treatment groups in a pre-

clinical set up, as well as the retrieval of biological samples, such as BALF, immune cells, and tissue, for *in-vitro* analysis. These samples were of extremely high value for this translational study due to the fact that it is nearly impossible to research the same samples from human newborns suffering from nARDs due to the obvious mechanical and chemical stress of the BAL procedure.

The current study mimicked the cumulative application of the porcine surfactant preparation Curosurf® as it is nowadays routinely applied in the clinical setting. It has been shown that a repetitive application of surfactant correlates with improved gas exchange and reduced risk of pneumothorax [5]. The clinical data of the piglets in this triple-hit model [157] confirmed the typical patterns known from human neonates with nARDS: acute onset, lung edema, increased oxygenation index, inflammatory response, neutrophil influx into the lung and pulmonary fibrosis [124] and is as such well suited as a piglet model of human nARDS.

As a first step in the animal model the term-born piglets were deprived of their endogenous surfactant. Then the inflammation was aggravated by the 2nd hit (mechanical ventilation) and 3rd hit (LPS challenge). Indeed, this satisfies the demands of the Montreux definition of nARDS from 2017 [122] for an acute onset of the disease (provided by the removal of endogenous surfactant by the first lavages) and a sustained inflammation by subsequent hits. This official definition of nARDS was not compiled until 2017 [122], at which point the experimental part of this study was finished. This definition clearly differentiates between the respiratory distress in *premature* infants (IRDS), with respiratory distress as a direct consequence of surfactant deficiencies due to immaturity of the lung, and neonatal ARDS (nARDS) in *term-born* infants, with lack of surfactant function and amount not as a primary cause but a subsequent result of lung damage due to exogenous factors such as bacterial or viral pneumonia, aspiration of meconium, blood or amniotic fluid during birth.

Either way, surfactant replacement therapy is the only effective therapy option, whether the surfactant deficiency is the primary cause (premature infants) or the secondary result (term-born) of lung damage leading to respiratory distress. The underlying mechanisms of immune activation by LPS and the effects of anionic phospholipids on the resulting inflammatory pathways are relevant for both disease definitions.

The pig genome has a remarkable similarity to the human genome and pigs are in this respect a more suitable disease model than the commonly-used mouse models. Pig macrophages show a high TLR4 sequence homology and similar reaction to LPS compared to human

macrophages [221,222]. Apart from the genome, piglets resemble newborn humans in body size (about 80%), as well as size and weight of the lung, which was central to the study of pulmonary diseases [124]. Keeping in mind the ethical implications and higher costs of research on non-human primates and the significant genomic/physiology differences between mice and humans, the usage of a porcine animal model is the method of choice in the context of nARDS research.

However, every study system can be further developed and improved.
Due to the use of non-inbred animals higher biological variances, and with it probably also variances in pulmonary surfactant amounts, were and are always an obstacle. An increase in animal numbers would be a possible solution to counteract the data 'blurring' due to variances. In the same context, increasing the number of piglets in each treatment group may have allowed for the retrieval of biological samples at additional time points between 0h and 72h and therefore may have provided further insight into the kinetics of the BALF cytokine concentrations, alveolar macrophage activation or changes in the pulmonary surfactant lipid*ome*. However, both these changes come in turn with an ethical dilemma, as it is the common wish and necessity to use as few test animals and animal models as possible.

It needs to be mentioned as well that all experiments were performed with the same lot of Curosurf® to avoid additional variance from biological variations of porcine surfactant lipid composition. The results can therefore only provide a snapshot of this particular Curosurf® batch and might be corroborated with additional batches.

Secondary endogenous surfactant deficiency is a pathological result of inflammation as part of nARDS in the neonatal lung, which then drives further inflammatory processes. In the present animal model however, removal of endogenous piglet surfactant represents the 1st hit in order to artificially cause respiratory distress in the piglets. So when the BALF samples were taken on day 3 of the procedure, the piglets had already gone through a surfactant depletion on day 1. It is unknown to which degree/amount the endogenous surfactant was replenished during the course of the three days and how much of it was degraded during disease progression. A possible solution would be additional control piglets that undergo BAL on day 1 and are afterwards simply monitored without any additional hits. On day 3 the amount of surfactant in the BALF could give an indication on the amount of the surfactant portion that was newly produced.

Broncho-alveolar lavage is a common, minimally invasive method used since the 1970's as a diagnostic tool for pulmonary pathology, in case of alveolar proteinosis it is even used as a treatment asset. It is a method of choice for absence/presence testing for i.e. asbestos, malignant cells, fungi and other microorganisms, or blood due to alveolar hemorrhage [223] or more recently also infections with SARS-CoV-2 [224]. In this study, BALF was employed in part to assess inflammatory cytokine concentration in the context of nARDS in the alveoli. Even though an expected, significantly increased amount of cytokines/proteins was detected in BALF of diseased piglets, the improvement of oxygenation index that were seen in piglets treated with fortified Curosurf® compared to pure Curosurf® were in the end not reflected in the BALF cytokine levels and thus the BALF data did not corroborate the clinical data. That may be in part explained by the biological variance of the piglet physiology, but also by an unknown degree of dilution of the alveolar epithelial fluid by the instilled saline which can lead to strong inaccuracies in BALF protein concentration compared to actual concentrations *in vivo* [225]. The BALF as such may not be the most appropriate indicator for disease stage or progression as a stand-alone measure. Furthermore, notation of the exact volume of recovered BALF or pulmonary surfactant per piglet was not part of the study protocol. Such a concentration factor (mg surfactant per mL recovered BALF or instilled saline) would be a valuable factor to normalize the detected amount of BAL proteins and total increase or decrease in lipid abundance as part of the piglet lipid*ome* study.

Peripheral blood monocytes, which can be differentiated into macrophages, can easily be obtained from adult human volunteers in abundant amounts. Even though using them for studies about human neonatal immunity is distinctly more relevant and comparable than using murine cells, as is common practice, the results must still be differentially examined. The inflammatory reaction in neonates differs somewhat from that in adult humans. Probably due to a "lack" of anti-inflammatory mediators, the prenatal and neonate pro-inflammatory immune response to endotoxin is significantly elevated compared to adults [5].

Last but not least, despite the genomic similarity, porcine physiology and immune response are not completely identical to humans. This should always be kept in mind when translating porcine study results for human disease pathology. While pigs harbor alveolar macrophages, respiratory tract macrophages and dendritic cells, just as humans do, another subpopulation of macrophages has been shown to be located in porcine lung capillary endothelium, the so-called Pulmonary Intravascular Macrophages (PIM). These were not found in humans or mice

in steady-state as of now. They are phagocytic, express TLR4 and take up LPS within minutes after exposure via the blood stream. While they are typically not removed by BAL (tight adherence to endothelium), and therefore no interference with the BALF AM stimulation with LPS is to be expected, they do contribute to the pulmonary and systemic immune response by secreting pro-inflammatory cytokines, even to airway-borne infection [226–228].

5.6. Future direction of surfactant replacement therapy

Since Avery and Mead described the underlying cause of respiratory distress syndrome in 1959, a great demand for a surfactant preparation that could be used therapeutically to replace the missing endogenous surfactant emerged. First trials in the 1960s used nebulizers to administer surfactant preparations that contained mostly DPPC and some other unsaturated lipids, but were unsuccessful. In 1980, Tore Curstedt and Bengt Robertson from the Karolinska Institute in Stockholm extracted pulmonary surfactant from minced porcine lungs for the first time. Curstedt and Robertson named their porcine surfactant preparation *Curosurf*, a combination of both their names (*CU*rstedt-*RO*bertson-*SURF*actant). Several studies in the 1980s and 1990s demonstrated the success of therapeutic application of Curosurf®: neonatal mortality decreased, reduction of intraventricular hemorrhage, pulmonary air leaks and chronic lung disease. A 2-year follow-up study of infants who had been enrolled in clinical trials with Curosurf® application revealed no immune responses to the porcine surfactant preparation [229].

Curosurf® was not the only commercial surfactant preparation at the beginning of this study in 2013. The first generation of synthetic surfactant preparations such as Pumactant® (pure DPPC and PG) and Exosurf® (synthetic lipids with alcohols to increase spreading) were devoid of surfactant proteins. Both preparations induced only a small improvement in respiration and mortality remained high [230,231].

Surfaxin® was a synthetic surfactant preparation of second generation which contained peptides with structural similarity to SP-B (imitating the cross-linking function of SP-B) and synthetic DPPC, POPG and palmitic acid. While it showed a similar improvement in oxygenation compared to modified natural surfactant preparations, its use was discontinued in 2015 due to difficult physical properties that entailed a problematic administration [230].

Venticute® with its functional SP-C analog was developed in 1998 but had poor *in vivo* surface activity. Different analogs have since been tested with different amino acid substitutions [232,233]. Curosurf® is also part of the second generation of modified natural preparations isolated from animal lungs, just like preparations from bovine lungs (Survanta®, Infasurf®, Alveofact®). These naturally contain SP-C and SP-D but their high batch variability and expensive production remain challenging.

Third generation preparations of pulmonary surfactant replacements trend towards synthetic peptides that resemble the *in vivo* activity of SP-C and SP-D. Synsurf® has completely synthetic components: SP-B mimicking polypeptides, a peptide complex made of poly-L-Lysine (positive charge), poly-L-glutamic acid (negative charge) which can carry the phospholipid components into the aqueous surrounding, DPPC and PG. It is administered via inhalation and had passed first animal studies in 2018 [234]. In 2017, Chiesi Farmaceutici S.p.A., Parma, Italy, passed first clinical studies in human neonates with a new, completely synthetic surfactant preparation (Elifactant®) containing peptide analogs of both SP-C and SP-D in a mixture of DPPC:POPG (1:1) [235–237].

A synthetic surfactant that has also passed phase I clinical trials is CHF5633. It simply contains equal amounts of DPPC and POPG, as well as 1.3% hydrophobic surfactant proteins SP-B and SP-C. While higher concentrations are needed for absorption properties comparable to Curosurf®, it shows greater resistance to inactivation by serum proteins which is very important in acute pulmonary inflammation [238]. Presence of SP-A in surfactant preparations seems to be a deciding factor for its success, as lack of that hydrophilic re-absorption-promoting surfactant protein seems to be greatly responsible for worse absorption performances. In conclusion, it could be worth to determine in an animal model if SP-A-spiking could potentially improve the currently used Curosurf® preparation (structurally and immunologically), maybe even in combination with the anionic lipids tested in this study.

There is still a great need for further development of synthetic surfactant preparation, as natural animal preparations are time- and money-consuming, and have a high batch-to-batch variability. However, natural surfactant is very complex in composition and the detailed functions of many of its compounds have yet to be determined. Simply the application of access amounts of natural surfactant preparations also do not bring a surplus in therapeutical advantage as was shown in this study (S200 piglet group). Furthermore, it is relatively clear that a too targeted approach of a single-lipid/single protein preparation is a poor replacement

for natural surfactant, while a synthetic identical copy may not be economically advantageous. Therefore supplementation of natural surfactant in order to boost its intrinsically optimum composition, as in this study, seems so far to be the best way to go. While synthetic surfactant preparations of a defined, but less complex composition are constantly improving and could in the future even be designed to boost very specific properties of surfactant, such as absorption, immune response, stability or drug delivering efficiency, fortified Curosurf® surfactant by the current stand is supported as a promising improvement of the established surfactant therapy.

5.7. Connection of this study to the current health crisis

As a last note, application of phosphatidylglycerol as supplement for endogenous surfactant preparations has received some new attention in the context of COVID-19. The novel coronavirus SARS-CoV-2 has rapidly spread the globe to create a pandemic with severe ARDS-like respiratory failure leading to a high mortality rate. SARS-CoV-2 infects AECII cells, leading to pulmonary edema, impaired gas exchange and reduces surfactant production and the so-called 'cytokine storm'. In the light of this ARDS-resemblance, it has been proposed and hypothesized that application of endogenous surfactant preparations, such as Curosurf®, possibly supplemented with additional PG, could serve as protective lung therapy in context of COVID-19, maybe even as prophylactic treatment [239,240]. So even though the practical work for this study was done between 2013 and 2017, the topic of improving surfactant preparations to treat respiratory distress, even with anionic lipids, is as urgent as ever.

5.8. Conclusion

This study had the anti-inflammatory modulation of nARDS-relevant pathways by the anionic phospholipids POPG, DOPG, PIP2 and headgroup variant IP3 as its core hypothesis. It employed a piglet model of acute respiratory distress in order to evaluate the therapeutical potential of Curosurf® supplemented with these anionic phospholipids. It can be confidently declared that this novel treatment venture has improved piglet pulmonary gas exchange and lung mechanics and was as such already successful in the clinical setting. On a cellular level, it

was shown that PIP2 has the strongest anti-inflammatory effect on the TLR4/NFκB- and canonical human macrophage pathways in order to counteract the pro-inflammatory effect of LPS/bacterial infection. Translation of these results to the piglet model was demonstrated. Furthermore, and to the best of our knowledge, this is the first time that all four anionic intervention lipids were employed in a piglet model of nARDS and that such a detailed overview of the piglet lipid*ome* with and without treatment was created. It has revealed that the pulmonary surfactant composition is robust and did not alter significantly upon mechanical, chemical and bacterial insults. Just as importantly, it was also demonstrated that treatment with Curosurf® and the intervention substances does not induce non-physiological alterations in piglet surfactant composition, even though the lipids strongly supported normal lung function. Ultimately, using substances for treatment that are in itself endogenous to the porcine and human lung was expected to show no adverse effects at best, and it didn't.

In summary, this study has presented ample evidence that Curosurf® enrichment with the anionic phospholipids POPG, DOPG, PIP2 and its headgroup variant IP3 is a valid future treatment candidate.

6. References

1. Fishman, A. P. *et al. Fishman's Pulmonary Diseases and Disorders*. (2008).
2. Jobe, A. H. & Ikegami, M. Lung Development and Function in Preterm Infants in the Surfactant Treatment Era. *Annu. Rev. Physiol.* **62**, 825–846 (2000).
3. Fehrenbach, H. Alveolar epithelial type II cell: defender of the alveolus revisited. *Respir. Res.* **2**, 33–46 (2001).
4. Barkauskas, C. E. *et al.* Type 2 alveolar cells are stem cells in adult lung. *J. Clin. Invest.* **123**, 3025–3036 (2013).
5. Wauer, R. R. *Surfactanttherapie: Grundlagen, Diagnostik, Therapie*. (Thieme, 2004).
6. Karnovsky, M. L. Metchnikoff in Messina: a century of studies on phagocytosis. *N. Engl. J. Med.* **304**, 1178–1180 (1981).
7. Merien, F. A Journey with Elie Metchnikoff: From Innate Cell Mechanisms in Infectious Diseases to Quantum Biology. *Front. public Heal.* **4**, 125 (2016).
8. Embleton, M. J. The Macrophage (2nd Edn). *Br. J. Cancer* **89**, 421 (2003).
9. Mills, C. D., Kincaid, K., Alt, J. M., Heilman, M. J. & Hill, A. M. M-1/M-2 Macrophages and the Th1/Th2 Paradigm. *J. Immunol.* **164**, 6166–6173 (2000).
10. Stein, M. Interleukin 4 potently enhances murine macrophage mannose receptor activity: a marker of alternative immunologic macrophage activation. *J. Exp. Med.* **176**, 287–292 (1992).
11. Jenkins, S. J. *et al.* Local macrophage proliferation, rather than recruitment from the blood, is a signature of Th2 inflammation. *Eur. PMC Funders Gr.* **332**, 1284–1288 (2011).
12. Hashimoto, D. *et al.* Tissue-resident macrophages self-maintain locally throughout adult life with minimal contribution from circulating monocytes. *Immunity* **38**, 792–804 (2013).
13. Schwartz, L. W. & Christman, C. A. Lung lining material as a chemotactant for alveolar macrophages. *Chest* **75**, 284–8 (1979).
14. Corrin, B. & Nicholson, A. G. *Pathology of the lungs*. (Churchill Livingstone/Elsevier, 2011).
15. Stark, J. M. & Mueller, G. A. Lung Defenses. in *Kendig & Chernick's Disorders of the Respiratory Tract in Children* 89–109 (Elsevier, 2012). doi:10.1016/B978-1-4377-1984-0.00007-3

16. Rietschel, E. T. & Cavaillon, J. M. Richard Pfeiffer and Alexandre Besredka: Creators of the concept of endotoxin and anti-endotoxin. *Microbes Infect.* **5**, 1407–1414 (2003).

17. Dofferhoff, A. S. M. *et al.* Effects of different types and combinations of antimicrobial agents on endotoxin release from gram-negative bacteria: An in-vitro and in-vivo study. *Scand. J. Infect. Dis.* **23**, 745–754 (1991).

18. Rietschel, E. T. *et al.* Bacterial endotoxin: molecular relationships of structure to activity and function. *FASEB J.* **8**, 217–25 (1994).

19. Jan, A. T. Outer Membrane Vesicles (OMVs) of gram-negative bacteria: A perspective update. *Front. Microbiol.* **8**, 1053 (2017).

20. Galanos, C. *et al.* Synthetic and natural Escherichia coli free lipid A express identical endotoxic activities. *Eur. J. Biochem.* **148**, 1–5 (1985).

21. Schumann, R. R. *et al.* Structure and function of lipopolysaccharide binding protein. *Science (80-.).* **249**, 1429–1431 (1990).

22. Schumann, R. R. & Zweigner, J. A novel acute-phase marker: Lipopolysaccharide binding protein (LBP). *Clin. Chem. Lab. Med.* **37**, 271–274 (1999).

23. Tobias, P. S., Soldau, K. & Ulevitch, R. J. Isolation of a lipopolysaccharide-binding acute phase reactant from rabbit serum. *J. Exp. Med.* **164**, 777–93 (1986).

24. Tobias, P. S. *et al.* Participation of Lipopolysaccharide-binding Protein in Lipopolysaccharide-dependent Macrophage Activation. *Am. J. Respir. Cell Mol. Biol.* **7**, 239–245 (1992).

25. Dentener, M. A. *et al.* Production of the Acute-Phase Protein Lipopolysaccharide-Binding Protein by Respiratory Type II Epithelial Cells. *Am. J. Respir. Cell Mol. Biol.* **23**, 146–153 (2000).

26. Schumann, R. R. *et al.* The Lipopolysaccharide-Binding Protein Is a Secretory Class 1 Acute-Phase Protein Whose Gene Is Transcriptionally Activated by APRF/STAT-3 and Other Cytokine-Inducible Nuclear Proteins. *Mol. Cell. Biol.* **16**, 3490–3503 (1996).

27. Wright, S. D. *et al.* CD14, a receptor for complexes of lipopolysaccharide (LPS) and LPS binding protein. *Science* **249**, 1431–3 (1990).

28. Tobias, P. S., Soldau, K. & Ulevitch, R. J. Identification of a lipid A binding site in the acute phase reactant lipopolysaccharide binding protein. *J. Biol. Chem.* **264**, 10867–71 (1989).

29. Kopp, F., Kupsch, S. & Schromm, A. B. Lipopolysaccharide-binding protein is bound and internalized by host cells and colocalizes with LPS in the cytoplasm: Implications for a role of

LBP in intracellular LPS-signaling. *Biochim. Biophys. Acta - Mol. Cell Res.* **1863**, 660–672 (2016).

30. Gutsmann, T., Haberer, N., Carroll, S. F., Seydel, U. & Wiese, A. Interaction between Lipopolysaccharide (LPS), LPS-Binding Protein (LBP), and Planar Membranes. *Biol. Chem.* **382**, 425–434 (2001).

31. Schromm, A. B. *et al.* Lipopolysaccharide-binding protein mediates CD14-independent intercalation of lipopolysaccharide into phospholipid membranes. *FEBS Lett.* **399**, 267–271 (1996).

32. Wurfel, M. M., Hailman, E. & Wright, S. D. Soluble CD14 acts as a shuttle in the neutralization of lipopolysaccharide (LPS) by LPS-binding protein and reconstituted high density lipoprotein. *J. Exp. Med.* **181**, 1743–1754 (1995).

33. Lamping, N. *et al.* LPS-binding protein protects mice from septic shock caused by LPS or gram-negative bacteria. *J. Clin. Invest.* **101**, 2065–71 (1998).

34. Cohen, J. The immunopathogenesis of sepsis. *Nature* **420**, 885–891 (2002).

35. Zweigner, J. High concentrations of lipopolysaccharide-binding protein in serum of patients with severe sepsis or septic shock inhibit the lipopolysaccharide response in human monocytes. *Blood* **98**, 3800–3808 (2001).

36. Gallay, P. *et al.* Lipopolysaccharide (LPS)-binding protein in human serum determines the tumor necrosis factor response of monocytes to LPS. *J. Infect. Dis.* **170**, 1319–1322 (1994).

37. Carswell, E. A. *et al.* An endotoxin-induced serum factor that causes necrosis of tumors. *Proc. Natl. Acad. Sci.* **72**, 3666–3670 (1975).

38. Spriggs, D. R., Deutsch, S. & Kufe, D. W. Genomic structure, induction, and production of TNF-alpha. *Immunol. Ser.* **56**, 3–34 (1992).

39. Black, R. A. *et al.* A metalloproteinase disintegrin that releases tumour-necrosis factor-α from cells. *Nature* **385**, 729–733 (1997).

40. Kriegler, M., Perez, C., DeFay, K., Albert, I. & Lu, S. D. A novel form of TNF/cachectin is a cell surface cytotoxic transmembrane protein: ramifications for the complex physiology of TNF. *Cell* **53**, 45–53 (1988).

41. Tartaglia, L. A., Pennica, D. & Goeddel, D. V. Ligand passing: the 75-kDa tumor necrosis factor (TNF) receptor recruits TNF for signaling by the 55-kDa TNF receptor. *J. Biol. Chem.* **268**, 18542–8 (1993).

42. Manna, S. K., Aggarwal, B. B., Maroto, B., Boscá, L. & Knaus, U. G. Lipopolysaccharide inhibits TNF-induced apoptosis: role of nuclear factor-kappaB activation and reactive oxygen intermediates. *J. Immunol.* **162**, 1510–8 (1999).

43. Takada, Y., Sung, B., Sethi, G., Chaturvedi, M. M. & Aggarwal, B. B. Evidence that genetic deletion of the TNF receptor p60 or p80 inhibits Fas mediated apoptosis in macrophages. *Biochem. Pharmacol.* **74**, 1057–64 (2007).

44. Witsell, A. L. & Schook, L. B. Tumor necrosis factor alpha is an autocrine growth regulator during macrophage differentiation. *Proc. Natl. Acad. Sci. U. S. A.* **89**, 4754–8 (1992).

45. Feng, X. Regulatory roles and molecular signaling of TNF family members in osteoclasts. *Gene* **350**, 1–13 (2005).

46. Feldmann, M., Brennan, F. M., Elliott, M. J., Williams, R. O. & Maini, R. N. TNF alpha is an effective therapeutic target for rheumatoid arthritis. *Ann. N. Y. Acad. Sci.* **766**, 272–8 (1995).

47. Kollias, G., Douni, E., Kassiotis, G. & Kontoyiannis, D. On the role of tumor necrosis factor and receptors in models of multiorgan failure, rheumatoid arthritis, multiple sclerosis and inflammatory bowel disease. *Immunol. Rev.* **169**, 175–94 (1999).

48. Nakao, S. *et al.* Tumor necrosis factor alpha (TNF-alpha)-induced prostaglandin E2 release is mediated by the activation of cyclooxygenase-2 (COX-2) transcription via NFkappaB in human gingival fibroblasts. *Mol. Cell. Biochem.* **238**, 11–8 (2002).

49. Rabinovici, R. *et al.* Platelet activating factor (PAF) and tumor necrosis factor-alpha (TNF alpha) interactions in endotoxemic shock: studies with BN 50739, a novel PAF antagonist. *J. Pharmacol. Exp. Ther.* **255**, (1990).

50. Mukhopadhyay, S., Hoidal, J. R. & Mukherjee, T. K. Role of TNFα in pulmonary pathophysiology. *Respir. Res.* **7**, 125 (2006).

51. Gery, I. & Waksman, B. H. Potentiation of the T-lymphocyte response to mitogens. II. The cellular source of potentiating mediator(s). *J. Exp. Med.* **136**, 143–55 (1972).

52. Beeson, P. B. Temperature-elevating effect of a substance obtained from polymorphonuclear leucocytes. *J. Clin. Invest.* **27**, 524 (1948).

53. Baumann, C. L. *et al.* CD14 is a coreceptor of Toll-like receptors 7 and 9. *J. Exp. Med.* **207**, 2689–701 (2010).

54. Fitzgerald, K. A., Rowe, D. C. & Golenbock, D. T. Endotoxin recognition and signal transduction by the TLR4/MD2-complex. *Microbes Infect.* **6**, 1361–1367 (2004).

55. Leifer, C. A. & Medvedev, A. E. Molecular mechanisms of regulation of Toll-like receptor signaling. *J. Leukoc. Biol.* **100**, 927–941 (2016).

56. Fujihara, M. *et al.* Molecular mechanisms of macrophage activation and deactivation by lipopolysaccharide: roles of the receptor complex. *Pharmacol. Ther.* **100**, 171–94 (2003).

57. Miyake, K. Innate recognition of lipopolysaccharide by CD14 and toll-like receptor 4-MD-2: unique roles for MD-2. *Int. Immunopharmacol.* **3**, 119–28 (2003).

58. Pugin, J. *et al.* Lipopolysaccharide activation of human endothelial and epithelial cells is mediated by lipopolysaccharide-binding protein and soluble CD14. *Proc. Natl. Acad. Sci. U. S. A.* **90**, 2744–8 (1993).

59. Park, B. S. *et al.* The structural basis of lipopolysaccharide recognition by the TLR4–MD-2 complex. *Nature* **458**, 1191–1195 (2009).

60. Schromm, A. B. *et al.* Molecular genetic analysis of an endotoxin nonresponder mutant cell line: A point mutation in a conserved region of MD-2 abolishes endotoxin-induced signaling. *J. Exp. Med.* **194**, 79–88 (2001).

61. O'Neill, L. A. J. & Bowie, A. G. The family of five: TIR-domain-containing adaptors in Toll-like receptor signalling. *Nat. Rev. Immunol.* **7**, 353–364 (2007).

62. Janssens, S. & Beyaert, R. A universal role for MyD88 in TLR/IL-1R-mediated signaling. *Trends Biochem. Sci.* **27**, 474–82 (2002).

63. Hoesel, B. & Schmid, J. A. The complexity of NF-κB signaling in inflammation and cancer. *Mol. Cancer* **12**, 86 (2013).

64. Martinon, F., Burns, K. & Tschopp, J. The inflammasome: a molecular platform triggering activation of inflammatory caspases and processing of proIL-beta. *Mol. Cell* **10**, 417–26 (2002).

65. Lu, A. *et al.* Unified polymerization mechanism for the assembly of ASC-dependent inflammasomes. *Cell* **156**, 1193–1206 (2014).

66. Stutz, A., Horvath, G. L., Monks, B. G. & Latz, E. ASC Speck Formation as a Readout for Inflammasome Activation. in *Methods in molecular biology (Clifton, N.J.)* **1040**, 91–101 (2013).

67. Latz, E. The inflammasomes: mechanisms of activation and function. *Curr Opin Immunol* **22**, 28–33 (2010).

68. Perregaux, D. & Gabel, C. A. Interleukin-1 beta maturation and release in response to ATP and nigericin. Evidence that potassium depletion mediated by these agents is a necessary and

common feature of their activity. *J. Biol. Chem.* **269**, 15195–203 (1994).

69. Pétrilli, V. *et al.* Activation of the NALP3 inflammasome is triggered by low intracellular potassium concentration. *Cell Death Differ.* **14**, 1583–1589 (2007).

70. Ferrari, D. *et al.* The P2X7 receptor: a key player in IL-1 processing and release. *J. Immunol.* **176**, 3877–83 (2006).

71. Shi, J. *et al.* Cleavage of GSDMD by inflammatory caspases determines pyroptotic cell death. *Nature* **526**, 660–665 (2015).

72. Man, S. M., Karki, R. & Kanneganti, T.-D. Molecular mechanisms and functions of pyroptosis, inflammatory caspases and inflammasomes in infectious diseases. *Immunol. Rev.* **277**, 61–75 (2017).

73. Bauernfeind, F. G. *et al.* Cutting edge: NF-kappaB activating pattern recognition and cytokine receptors license NLRP3 inflammasome activation by regulating NLRP3 expression. *J. Immunol.* **183**, 787–91 (2009).

74. Kayagaki, N. *et al.* Non-canonical inflammasome activation targets caspase-11. *Nature* **479**, 117–121 (2011).

75. Vanaja, S. K. *et al.* Bacterial Outer Membrane Vesicles Mediate Cytosolic Localization of LPS and Caspase-11 Activation. *Cell* **165**, 1106–1119 (2016).

76. Schromm, A. B. & Brandenburg, K. TLR4 Ligands: Single Molecules and Aggregates. in *Progress in Inflammation Research* **87**, 39–56 (Springer, Cham, 2021).

77. Kim, B.-H. *et al.* IFN-induced Guanylate Binding Proteins in Inflammasome Activation and Host Defense. **17**, 481–489 (2016).

78. Shi, J. *et al.* Inflammatory caspases are innate immune receptors for intracellular LPS. *Nature* **514**, 187–192 (2014).

79. Kayagaki, N. *et al.* Caspase-11 cleaves gasdermin D for non-canonical inflammasome signalling. *Nature* **526**, 666–671 (2015).

80. Stamme, C., Müller, M., Hamann, L., Gutsmann, T. & Seydel, U. Surfactant protein A inhibits lipopolysaccharide-induced immune cell activation by preventing the interaction of lipopolysaccharide with lipopolysaccharide-binding protein. *Am. J. Respir. Cell Mol. Biol.* **27**, 353–360 (2002).

81. Kuan, S. F., Rust, K. & Crouch, E. Interactions of surfactant protein D with bacterial

lipopolysaccharides. Surfactant protein D is an Escherichia coli-binding protein in bronchoalveolar lavage. *J. Clin. Invest.* **90**, 97–106 (1992).

82. Miyamura, K. *et al.* Surfactant protein D binding to alveolar macrophages. *Biochem. J.* **300 (Pt 1)**, 237–42 (1994).

83. McCormack, F. X. New concepts in collectin-mediated host defense at the air-liquid interface of the lung. *Respirology* **11**, S7–S10 (2006).

84. Chroneos, Z., Sever-Chroneos, Z. & Shepherd, V. Pulmonary surfactant: An immunological perspective. *Cell. Physiol. Biochem.* **25**, 13–26 (2010).

85. Wu, Y. *et al.* Accumulation of inhibitory κB-α as a mechanism contributing to the anti-inflammatory effects of surfactant protein-A. *Am. J. Respir. Cell Mol. Biol.* **31**, 587–594 (2004).

86. Sender, V., Lang, L. & Stamme, C. Surfactant Protein-A Modulates LPS-Induced TLR4 Localization and Signaling via β-Arrestin 2. *PLoS One* **8**, (2013).

87. Lopez-Rodriguez, E., Pascual, A., Arroyo, R., Floros, J. & Perez-Gil, J. Human Pulmonary Surfactant Protein SP-A1 Provides Maximal Efficiency of Lung Interfacial Films. *Biophys. J.* **111**, 524–536 (2016).

88. Perez-Gil, J. & Weaver, T. E. Pulmonary Surfactant Pathophysiology: Current Models and Open Questions. *Physiology* **25**, 132–141 (2010).

89. Masuda, S. *et al.* Expression of secretory phospholipase A2 enzymes in lungs of humans with pneumonia and their potential prostaglandin-synthetic function in human lung-derived cells. *Biochem. J.* **387**, 27–38 (2005).

90. Nicolson, G. L. The Fluid—Mosaic Model of Membrane Structure: Still relevant to understanding the structure, function and dynamics of biological membranes after more than 40 years. *Biochim. Biophys. Acta - Biomembr.* **1838**, 1451–1466 (2014).

91. Murakami, M., Taketomi, Y., Sato, H. & Yamamoto, K. Secreted phospholipase A2 revisited. *J. Biochem.* **150**, 233–255 (2011).

92. Orgeig, S. & Daniels, C. B. The roles of cholesterol in pulmonary surfactant: Insights from comparative and evolutionary studies. in *Comparative Biochemistry and Physiology - A Molecular and Integrative Physiology* **129**, 75–89 (Elsevier Inc., 2001).

93. Pinkwart, K. *et al.* Nanoscale dynamics of cholesterol in the cell membrane. *J. Biol. Chem.* **294**, 12599–12609 (2019).

94. Fessler, M. B. & Summer, R. S. Surfactant Lipids at the Host–Environment Interface. Metabolic Sensors, Suppressors, and Effectors of Inflammatory Lung Disease. *Am. J. Respir. Cell Mol. Biol.* **54**, 624–635 (2016).

95. Bunt, J. E. H. *et al.* Endogenous Surfactant Turnover in Preterm Infants Measured with Stable Isotopes. *Am. J. Respir. Crit. Care Med.* **157**, 810–814 (1998).

96. Voyno-Yasenetskaya, T. A., Dobbs, L. G. & Williams, M. C. Regulation of ATP-dependent surfactant secretion and activation of second-messenger systems in alveolar type II cells. *Am. J. Physiol.* **261**, 105–9 (1991).

97. Griese, M., Gobran, L. I. & Rooney, S. A. ATP-stimulated inositol phospholipid metabolism and surfactant secretion in rat type II pneumocytes. *Am. J. Physiol. Cell. Mol. Physiol.* **260**, L586–L593 (1991).

98. Wirtz, H. R. & Dobbs, L. G. Calcium mobilization and exocytosis after one mechanical stretch of lung epithelial cells. *Science* **250**, 1266–9 (1990).

99. Brown, L. A. & Longmore, W. J. Adrenergic and cholinergic regulation of lung surfactant secretion in the isolated perfused rat lung and in the alveolar type II cell in culture. *J. Biol. Chem.* **256**, 66–72 (1981).

100. Mettler, N. R., Gray, M. E., Schuffman, S. & LeQuire, V. S. beta-Adrenergic induced synthesis and secretion of phosphatidylcholine by isolated pulmonary alveolar type II cells. *Lab. Invest.* **45**, 575–86 (1981).

101. Rice, W. R. & Singleton, F. M. P2-purinoceptors regulate surfactant secretion from rat isolated alveolar type II cells. *Br. J. Pharmacol.* **89**, 485–91 (1986).

102. Gilfillan, A. M. & Rooney, S. A. Purinoceptor agonists stimulate phosphatidylcholine secretion in primary cultures of adult rat type II pneumocytes. *Biochim. Biophys. Acta* **917**, 18–23 (1987).

103. Gilfillan, A. M. & Rooney, S. A. Arachidonic acid metabolites stimulate phosphatidylcholine secretion in primary cultures of type II pneumocytes. *Biochim. Biophys. Acta - Lipids Lipid Metab.* **833**, 336–341 (1985).

104. Andreeva, A. V., Kutuzov, M. A. & Voyno-Yasenetskaya, T. A. Regulation of surfactant secretion in alveolar type II cells. *Am. J. Physiol. Cell. Mol. Physiol.* **293**, L259–L271 (2007).

105. Meyrick, B. & Reid, L. The alveolar wall. *Br. J. Dis. Chest* **64**, 121–140 (1970).

106. Schmitz, G. & Müller, G. Structure and function of lamellar bodies, lipid-protein complexes involved in storage and secretion of cellular lipids. *J. Lipid Res.* **32**, 1539–70 (1991).

107. Askin, F. B. & Kuhn, C. The cellular origin of pulmonary surfactant. *Lab. Invest.* **25**, 260–8 (1971).

108. Chakraborty, M. & Kotecha, S. Pulmonary surfactant in newborn infants and children. *Breathe* **9**, 476–488 (2013).

109. Poulain, F. R., Allen, L., Williams, M. C., Hamilton, R. L. & Hawgood, S. Effects of surfactant apolipoproteins on liposome structure: implications for tubular myelin formation. *Am. J. Physiol. Cell. Mol. Physiol.* **262**, L730–L739 (1992).

110. Kendig, E. L. & Wilmott, R. W. *Kendig and Chernick's disorders of the respiratory tract in children.* (Elsevier/Saunders, 2012).

111. Goerke, J. Pulmonary surfactant: functions and molecular composition. *Biochim. Biophys. Acta - Mol. Basis Dis.* **1408**, 79–89 (1998).

112. Schürch, S., Green, F. H. Y. & Bachofen, H. Formation and structure of surface films: captive bubble surfactometry. *Biochim. Biophys. Acta - Mol. Basis Dis.* **1408**, 180–202 (1998).

113. Putz, G., Walch, M., Van Eijk, M. & Haagsman, H. P. Hydrophobic lung surfactant proteins B and C remain associated with surface film during dynamic cyclic area changes. *Biochim. Biophys. Acta - Mol. Basis Dis.* **1453**, 126–134 (1999).

114. Dagan, M. P. & Hall, S. B. The Equilibrium Spreading Tension of Pulmonary Surfactant. *Langmuir* **31**, 13063–7 (2015).

115. Casals, C. & Cañadas, O. Role of lipid ordered/disordered phase coexistence in pulmonary surfactant function. *Biochim. Biophys. Acta - Biomembr.* **1818**, 2550–2562 (2012).

116. De La Serna, J. B., Perez-Gil, J., Simonsen, A. C. & Bagatolli, L. A. Cholesterol rules: Direct observation of the coexistence of two fluid phases in native pulmonary surfactant membranes at physiological temperatures. *J. Biol. Chem.* **279**, 40715–40722 (2004).

117. Osanai, K., Mason, R. J. & Voelker, D. R. Trafficking of Newly Synthesized Surfactant Protein A in Isolated Rat Alveolar Type II Cells. *Am. J. Respir. Cell Mol. Biol.* **19**, 929–935 (1998).

118. Tsuzuki, A., Kuroki, Y. & Akino, T. Pulmonary surfactant protein A-mediated uptake of phosphatidylcholine by alveolar type II cells. *Am. J. Physiol.* **265**, L193-9 (1993).

119. Ogasawara, Y., Kuroki, Y. & Akino, T. Pulmonary surfactant protein D specifically binds to phosphatidylinositol. *J. Biol. Chem.* **267**, 21244–9 (1992).

120. Ikegami, M., Na, C.-L., Korfhagen, T. R. & Whitsett, J. A. Surfactant protein D influences surfactant ultrastructure and uptake by alveolar type II cells. *Am. J. Physiol. Cell. Mol. Physiol.*

288, L552–L561 (2005).

121. Ikegami, M., Grant, S., Korfhagen, T., Scheule, R. K. & Whitsett, J. A. Surfactant protein-D regulates the postnatal maturation of pulmonary surfactant lipid pool sizes. *J. Appl. Physiol.* **106**, 1545–1552 (2009).

122. De Luca, D. *et al.* The Montreux definition of neonatal ARDS: biological and clinical background behind the description of a new entity. *Lancet. Respir. Med.* **5**, 657–666 (2017).

123. NIH National Heart, Lung, and B. I. Respiratory Distress Syndrome | National Heart, Lung, and Blood Institute (NHLBI). Available at: https://www.nhlbi.nih.gov/health-topics/respiratory-distress-syndrome. (Accessed: 17th November 2019)

124. Spengler, D., Rintz, N. & Krause, M. F. An Unsettled Promise: The Newborn Piglet Model of Neonatal Acute Respiratory Distress Syndrome (NARDS). Physiologic Data and Systematic Review. *Front. Physiol.* **10**, 1345 (2019).

125. Holm, B. A., Notter, R. H. & Finkelstein, J. N. Surface property changes from interactions of albumin with natural lung surfactant and extracted lung lipids. *Chem. Phys. Lipids* **38**, 287–298 (1985).

126. Holm, B. A. & Notter, R. H. Effects of hemoglobin and cell membrane lipids on pulmonary surfactant activity. *J. Appl. Physiol.* **63**, 1434–42 (1987).

127. Cockshutt, A. M. & Possmayer, F. Lysophosphatidylcholine sensitizes lipid extracts of pulmonary surfactant to inhibition by serum proteins. *Biochim. Biophys. Acta - Lipids Lipid Metab.* **1086**, 63–71 (1991).

128. De Luca, D. *et al.* Varespladib Inhibits Secretory Phospholipase A2 in Bronchoalveolar Lavage of Different Types of Neonatal Lung Injury. *J. Clin. Pharmacol.* **52**, 729–737 (2012).

129. Wolf, A. J. *et al.* Hexokinase Is an Innate Immune Receptor for the Detection of Bacterial Peptidoglycan. *Cell* **166**, 624–636 (2016).

130. Avery, M. E. & Mead, J. Surface Properties in Relation to Atelectasis and Hyaline Membrane Disease. *Arch. Pediatr. Adolesc. Med.* **97**, 517 (1959).

131. Chaussier, F. Appareil pour inhalations d'oxygene chez le nouveau-né. *Mem. la Socite R. Med.* (1791).

132. Stern, L., Ramos, A. D., Outerbridge, E. W. & Beaudry, P. H. Negative pressure artificial respiration: use in treatment of respiratory failure of the newborn. *Can. Med. Assoc. J.* **102**, 595–601 (1970).

133. Virchow, R. Ueber das ausgebreitete Vorkommen einer dem Nervenmark analogen Substanz in den thierischen Geweben. *Arch. für Pathol. Anat. und Physiol. und für Klin. Med.* **6**, 562–572 (1854).

134. Farber, S. & Sweet, L. K. Amniotic sac contents in the lungs of infants. *Am. J. Dis. Child.* **42**, 1372–1383 (1931).

135. Neergaard, K. Neue Auffassungen über einen Grundbegriff der Atemmechanik. *Z. Gesamte Exp. Med.* **66**, 373–394 (1929).

136. Macklin, C. C. The pulmonary alveolar mucoid film and the pneumonocytes. *Lancet (London, England)* **266**, 1099–1104 (1954).

137. Pattle, R. E. Properties, Function and Origin of the Alveolar Lining Layer. *Nature* **175**, 1125–1126 (1955).

138. Fujiwara, T. *et al.* Artificial surfactant therapy in hyaline-membrane disease. *Lancet (London, England)* **1**, 55–9 (1980).

139. Herting, E. Praxis der Surfactanttherapie. *Neonatol. Scan* **02**, 303–314 (2013).

140. Stillwell, W. *An introduction to biological membranes : composition, structure and function*. (Elsevier Science, 2016).

141. Ross, M., Krol, S., Janshoff, A. & Galla, H.-J. Kinetics of phospholipid insertion into monolayers containing the lung surfactant proteins SP-B or SP-C. *Eur. Biophys. J.* **31**, 52–61 (2002).

142. Numata, M., Chu, H. W., Dakhama, A. & Voelker, D. R. Pulmonary surfactant phosphatidylglycerol inhibits respiratory syncytial virus-induced inflammation and infection. *Proc. Natl. Acad. Sci.* **107**, 320–325 (2010).

143. Numata, M. *et al.* Phosphatidylglycerol Suppresses Influenza A Virus Infection. *Am. J. Respir. Cell Mol. Biol.* **46**, 479–487 (2012).

144. Numata, M. *et al.* Phosphatidylglycerol provides short-term prophylaxis against respiratory syncytial virus infection. *J. Lipid Res.* **54**, 2133–2143 (2013).

145. Kandasamy, P. *et al.* Pulmonary surfactant phosphatidylglycerol inhibits Mycoplasma pneumoniae-stimulated eicosanoid production from human and mouse macrophages. *J. Biol. Chem.* **286**, 7841–53 (2011).

146. Kuronuma, K. *et al.* Anionic pulmonary surfactant phospholipids inhibit inflammatory responses from alveolar macrophages and U937 cells by binding the lipopolysaccharide-interacting

proteins CD14 and MD-2. *J. Biol. Chem.* **284**, 25488–25500 (2009).

147. Kandasamy, P. *et al.* Structural analogs of pulmonary surfactant phosphatidylglycerol inhibit toll-like receptor 2 and 4 signaling. *J. Lipid Res.* **57**, 993–1005 (2016).

148. Berger, A. *et al.* Dioleylphosphatidylglycerol Inhibits the Expression of Type II Phospholipase A2 in Macrophages. *Am. J. Respir. Crit. Care Med.* **159**, 613–618 (1999).

149. Quintana, A., Griesemer, D., Schwarz, E. C. & Hoth, M. Calcium-dependent activation of T-lymphocytes. *Pflügers Arch. - Eur. J. Physiol.* **450**, 1–12 (2005).

150. Shaw, P. J., Qu, B., Hoth, M. & Feske, S. Molecular regulation of CRAC channels and their role in lymphocyte function. *Cell. Mol. Life Sci.* **70**, 2637–56 (2013).

151. Feske, S. Calcium signalling in lymphocyte activation and disease. *Nat. Rev. Immunol.* **7**, 690–702 (2007).

152. James, H. E. *et al. Brain Edema X: Proceedings of the Tenth International Symposium San Diego*. (Springer Science & Business Media, 1996).

153. Preuß, S. *et al.* Inositol-trisphosphate reduces alveolar apoptosis and pulmonary edema in neonatal lung injury. *Am. J. Respir. Cell Mol. Biol.* **47**, 158–169 (2012).

154. Vivekananda, J., Smith, D. & King, R. J. Sphingomyelin metabolites inhibit sphingomyelin synthase and CTP:phosphocholine cytidylyltransferase. *Am. J. Physiol. Cell. Mol. Physiol.* **281**, L98–L107 (2001).

155. Ryan, A. J., McCoy, D. M., McGowan, S. E., Salome, R. G. & Mallampalli, R. K. Alveolar sphingolipids generated in response to TNF-α modifies surfactant biophysical activity. *J. Appl. Physiol.* **94**, 253–258 (2003).

156. Kölzer, M. *et al.* Phosphatidylinositol-3,5-Bisphosphate Is a Potent and Selective Inhibitor of Acid Sphingomyelinase. *Biol. Chem.* **384**, (2003).

157. Spengler, D. *et al.* Novel therapeutic roles for surfactant-inositols and -phosphatidylglycerols in a neonatal piglet ARDS model: A translational study. *Am. J. Physiol. - Lung Cell. Mol. Physiol.* **314**, L32–L53 (2018).

158. Pfalzgraff, A. *et al.* LPS-neutralizing peptides reduce outer membrane vesicle-induced inflammatory responses. *Biochim. Biophys. Acta - Mol. Cell Biol. Lipids* **1864**, 1503–1513 (2019).

159. BLIGH, E. G. & DYER, W. J. A rapid method of total lipid extraction and purification. *Can. J. Biochem. Physiol.* **37**, 911–917 (1959).

160. Liebisch, G. *et al.* High throughput quantification of cholesterol and cholesteryl ester by electrospray ionization tandem mass spectrometry (ESI-MS/MS). *Biochim. Biophys. Acta - Mol. Cell Biol. Lipids* **1761**, 121–128 (2006).

161. Raghavendran, K., Willson, D. & Notter, R. Surfactant Therapy of ALI and ARDS. *Crit. Care Clin.* **27**, 525–559 (2012).

162. Nguyen, L. *et al.* Sex-differences in LPS-induced neonatal lung injury. *Sci. Rep.* **9**, 8514 (2019).

163. del Fresno, C. *et al.* Potent phagocytic activity with impaired antigen presentation identifying lipopolysaccharide-tolerant human monocytes: demonstration in isolated monocytes from cystic fibrosis patients. *J. Immunol.* **182**, 6494–507 (2009).

164. Pena, O. M., Pistolic, J., Raj, D., Fjell, C. D. & Hancock, R. E. W. Endotoxin Tolerance Represents a Distinctive State of Alternative Polarization (M2) in Human Mononuclear Cells. *J. Immunol.* **186**, 7243–7254 (2011).

165. Jablonski, K. A. *et al.* Novel Markers to Delineate Murine M1 and M2 Macrophages. *PLoS One* **10**, e0145342 (2015).

166. Cuschieri, J., Billigren, J. & Maier, R. V. Endotoxin tolerance attenuates LPS-induced TLR4 mobilization to lipid rafts: a condition reversed by PKC activation. *J. Leukoc. Biol.* **80**, 1289–1297 (2006).

167. Remmerie, A. & Scott, C. L. Macrophages and lipid metabolism. *Cell. Immunol.* **330**, 27–42 (2018).

168. Yin, K., Liao, D. fang & Tang, C. K. ATP-binding membrane cassette transporter A1 (ABCA1): A possible link between inflammation and reverse cholesterol transport. *Mol. Med.* **16**, 438–449 (2010).

169. ONY Biotech. Infasurf (Calfactant): Uses, Dosage, Side Effects, Interactions, Warning. Available at: https://www.rxlist.com/infasurf-drug.htm#indications. (Accessed: 9th October 2020)

170. Abate, W., Alghaithy, A. A., Parton, J., Jones, K. P. & Jackson, S. K. Surfactant lipids regulate LPS-induced interleukin-8 production in A549 lung epithelial cells by inhibiting translocation of TLR4 into lipid raft domains. *J. Lipid Res.* **51**, 334–344 (2010).

171. Chiesi Farmaceutici S.p.a. *Poractant Alfa Curpsurf product monograph*. (2008).

172. Wang, L. *et al.* Role of lung surfactant in phagocytic clearance of apoptotic cells by macrophages in rats. *Lab. Investig.* **86**, 458–466 (2006).

173. Mueller, M., Brandenburg, K., Dedrick, R., Schromm, A. B. & Seydel, U. Phospholipids Inhibit Lipopolysaccharide (LPS)-Induced Cell Activation: A Role for LPS-Binding Protein. *J. Immunol.* **174**, 1091–1096 (2005).

174. Wang, P. Y., Kitchens, R. L. & Munford, R. S. Phosphatidylinositides bind to plasma membrane CD14 and can prevent monocyte activation by bacterial lipopolysaccharide. *J. Biol. Chem.* **273**, 24309–24313 (1998).

175. Netea, M. G. *et al.* Differential requirement for the activation of the inflammasome for processing and release of IL-1β in monocytes and macrophages. *Blood* **113**, 2324 (2009).

176. Choudhary, V. *et al.* Phosphatidylglycerol Inhibits Toll-Like Receptor–Mediated Inflammation by Danger-Associated Molecular Patterns. *J. Invest. Dermatol.* **139**, 868–877 (2019).

177. Chiumello, D., Pristine, G. & Slutsky, A. S. Mechanical ventilation affects local and systemic cytokines in an animal model of acute respiratory distress syndrome. *Am. J. Respir. Crit. Care Med.* **160**, 109–116 (1999).

178. Backhaus, S. *et al.* Surfactant inhibits ATP-induced release of interleukin-1 via nicotinic acetylcholine receptors. *J. Lipid Res.* **58**, 1055–1066 (2017).

179. MacEyka, M. & Spiegel, S. Sphingolipid metabolites in inflammatory disease. *Nature* **510**, 58–67 (2014).

180. Li, J., Lee, D. S. W. & Madrenas, J. Evolving Bacterial Envelopes and Plasticity of TLR2-Dependent Responses: Basic Research and Translational Opportunities. *Front. Immunol.* **4**, 347 (2013).

181. Aksoy, E. *et al.* The p110δ isoform of the kinase PI(3)K controls the subcellular compartmentalization of TLR4 signaling and protects from endotoxic shock. *Nat. Immunol.* **13**, 1045–1054 (2012).

182. Staats, K. A. *et al.* Genetic ablation of IP3 receptor 2 increases cytokines and decreases survival of SOD1G93A mice. *Hum. Mol. Genet.* **25**, 3491–3499 (2016).

183. Santoni, G. *et al.* 'Immuno-transient receptor potential ion channels': The role in monocyte- and macrophage-mediated inflammatory responses. *Frontiers in Immunology* **9**, 1273 (2018).

184. Chiang, C. Y., Veckman, V., Limmer, K. & David, M. Phospholipase Cγ-2 and intracellular calcium are required for lipopolysaccharide-induced toll-like receptor 4 (TLR4) endocytosis and interferon regulatory factor 3 (IRF3) activation. *J. Biol. Chem.* **287**, 3704–3709 (2012).

185. Husebye, H. *et al.* Endocytic pathways regulate Toll-like receptor 4 signaling and link innate and adaptive immunity. *EMBO J.* **25**, 683–692 (2006).

186. Best, M. D., Zhang, H. & Prestwich, G. D. Inositol polyphosphates, diphosphoinositol polyphosphates and phosphatidylinositol polyphosphate lipids: Structure, synthesis, and development of probes for studying biological activity. *Natural Product Reports* **27**, 1403–1430 (2010).

187. Miakotina, O. L. & Snyder, J. M. TNF-α inhibits SP-A gene expression in lung epithelial cells via p38 MAPK. *Am. J. Physiol. Cell. Mol. Physiol.* **283**, L418–L427 (2002).

188. Hamacher, J. *et al.* Tumor necrosis factor-alpha and angiostatin are mediators of endothelial cytotoxicity in bronchoalveolar lavages of patients with acute respiratory distress syndrome. *Am. J. Respir. Crit. Care Med.* **166**, 651–656 (2002).

189. Mubarak, R. Al, Roberts, N., Mason, R. J., Alper, S. & Chu, H. W. Comparison of pro- and anti-inflammatory responses in paired human primary airway epithelial cells and alveolar macrophages. *Respir. Res.* **19**, 1–14 (2018).

190. Thorley, A. J. *et al.* Innate Immune Responses to Bacterial Ligands in the Peripheral Human Lung – Role of Alveolar Epithelial TLR Expression and Signalling. *PLoS One* **6**, e21827 (2011).

191. DeForge, L. E. & Remick, D. G. Kinetics of TNF, IL-6, and IL-8 gene expression in LPS-stimulated human whole blood. *Biochem. Biophys. Res. Commun.* **174**, 18–24 (1991).

192. Baer, M. *et al.* Tumor necrosis factor alpha transcription in macrophages is attenuated by an autocrine factor that preferentially induces NF-kappaB p50. *Mol. Cell. Biol.* **18**, 5678–5689 (1998).

193. Zhong, W. W. *et al.* Regulation of Cytokine mRNA Expression in Lipopolysaccharide-Stimulated Human Macrophages. *Arch. Surg.* **128**, 158–164 (1993).

194. Greene, K. E. *et al.* Serial changes in surfactant-associated proteins in lung and serum before and after onset of ARDS. *Am. J. Respir. Crit. Care Med.* **160**, 1843–1850 (1999).

195. Todd, D. A. *et al.* Surfactant phospholipids, surfactant proteins, and inflammatory markers during acute lung injury in children. *Pediatr. Crit. Care Med.* **11**, 82–91 (2010).

196. Schmidt, R. *et al.* Time-dependent changes in pulmonary surfactant function and composition in acute respiratory distress syndrome due to pneumonia or aspiration. *Respir. Res.* **8**, 55 (2007).

197. Del Riccio, V., Van Tuyl, M. & Post, M. Apoptosis in Lung Development and Neonatal Lung Injury. *Pediatric Research* **55**, 183–189 (2004).

198. Brass, D. M., Savov, J. D., Whitehead, G. S., Maxwell, A. B. & Schwartz, D. A. LPS binding protein

is important in the airway response to inhaled endotoxin. *J. Allergy Clin. Immunol.* **114**, 586–592 (2004).

199. Taddonio, M. A. *et al.* Influence of Lipopolysaccharide-Binding Protein on Pulmonary Inflammation in Gram-Negative Pneumonia. *Shock* **43**, 612–619 (2015).

200. Wurfel, M. M., Kunitake, S. T., Lichenstein, H., Kane, J. P. & Wright, S. D. Lipopolysaccharide (LPS)-binding protein is carried on lipoproteins and acts as a cofactor in the neutralization of LPS. *J. Exp. Med.* **180**, 1025–1035 (1994).

201. Martin, T. R. *et al.* Lipopolysaccharide Binding Protein Enhances the Responsiveness of Alveolar Macrophages to Bacterial Lipopolysaccharide. **90**, 2209–2219 (1992).

202. Casson, C. N. *et al.* Human caspase-4 mediates noncanonical inflammasome activation against gram-negative bacterial pathogens. *Proc. Natl. Acad. Sci.* **112**, 6688–6693 (2015).

203. Ratner, D., Orning, M. P. A. & Lien, E. Bacterial secretion systems and regulation of inflammasome activation. *J. Leukoc. Biol.* **101**, 165–181 (2017).

204. Zamyatina, A. & Heine, H. Lipopolysaccharide Recognition in the Crossroads of TLR4 and Caspase-4/11 Mediated Inflammatory Pathways. *Frontiers in Immunology* **11**, 1 (2020).

205. Veldhuizen, R., Nag, K., Orgeig, S. & Possmayer, F. The role of lipids in pulmonary surfactant. *Biochim. Biophys. Acta - Mol. Basis Dis.* **1408**, 90–108 (1998).

206. Liau, D. F., Barrett, C. R., Bell, A. L. & Ryan, S. F. Normal surface properties of phosphatidylglycerol-deficient surfactant from dog after acute lung injury. *J. Lipid Res.* **26**, 1338–44 (1985).

207. Hallman, M. & Gluck, L. Phosphatidylglycerol in lung surfactant. III. Possible modifier of surfactant function. *J. Lipid Res.* **17**, 257–262 (1976).

208. Martin, S. J. *et al.* Early redistribution of plasma membrane phosphatidylserine is a general feature of apoptosis regardless of the initiating stimulus: Inhibition by overexpression of BCL-2 and Abl. *J. Exp. Med.* **182**, 1545–1556 (1995).

209. Pereira, J. *et al.* Platelet aging in vivo is associated with loss of membrane phospholipid asymmetry. *Thromb. Haemost.* **82**, 1318–1321 (1999).

210. Rysavy, N. M. *et al.* Beyond apoptosis: the mechanism and function of phosphatidylserine asymmetry in the membrane of activating mast cells. *Bioarchitecture* **4**, 127–137 (2014).

211. Dae Kyong Kim *et al.* Bronchoalveolar lavage fluid phospholipase A2 activities are increased in

human adult respiratory distress syndrome. *Am. J. Physiol. - Lung Cell. Mol. Physiol.* **269**, (1995).

212. De Luca, D. *et al.* Clinical and biological role of secretory phospholipase A2 in acute respiratory distress syndrome infants. *Crit. Care* **17**, R163 (2013).

213. Colombo, S. *et al.* Phospholipidome of endothelial cells shows a different adaptation response upon oxidative, glycative and lipoxidative stress. *Sci. Rep.* **8**, 12365 (2018).

214. Yang, Y. & Uhlig, S. The role of sphingolipids in respiratory disease. *Ther. Adv. Respir. Dis.* **5**, 325–44 (2011).

215. CUROSURF® (poractant alfa) | Surfactant profile : Curosurf. Available at: https://curosurf.com/why-curosurf/surfactant-profiles/. (Accessed: 1st November 2020)

216. Fornasier, M. *et al.* Evaluation of potentially injurious effects of exogenous surfactant lysophospholipids on the alveolar epithelium and pulmonary mechanics. *Neonatology* **71**, 337–344 (1997).

217. Chavarha, M., Loney, R. W., Rananavare, S. B. & Hall, S. B. An anionic phospholipid enables the hydrophobic surfactant proteins to alter spontaneous curvature. *Biophys. J.* **104**, 594–603 (2013).

218. Corrêa, R. *et al.* Lysophosphatidylcholine Induces NLRP3 Inflammasome-Mediated Foam Cell Formation and Pyroptosis in Human Monocytes and Endothelial Cells. *Front. Immunol.* **10**, 2927 (2020).

219. Jenkins, B., West, J. A. & Koulman, A. A review of odd-chain fatty acid metabolism and the role of pentadecanoic acid (C15:0) and heptadecanoic acid (C17:0) in health and disease. *Molecules* **20**, 2425–2444 (2015).

220. Rüdiger, M. *et al. Plasmalogens effectively reduce the surface tension of surfactant-like phospholipid mixtures*. *American Journal of Physiology - Lung Cellular and Molecular Physiology* **274**, (1998).

221. Kapetanovic, R. *et al.* Pig Bone Marrow-Derived Macrophages Resemble Human Macrophages in Their Response to Bacterial Lipopolysaccharide. *J. Immunol.* **188**, 3382–3394 (2012).

222. Vaure, C. & Liu, Y. A comparative review of toll-like receptor 4 expression and functionality in different animal species. *Frontiers in Immunology* **5**, (2014).

223. Patel, P. H., Antoine, M. & Ullah, S. *Bronchoalveolar Lavage*. *StatPearls* (StatPearls Publishing, 2020).

224. Interim Guidelines for Clinical Specimens for COVID-19 | CDC. Available at: https://www.cdc.gov/coronavirus/2019-ncov/lab/guidelines-clinical-specimens.html. (Accessed: 16th June 2020)

225. Wood, R. E. & Boesch, P. R. Kendig & Chernick's Disorders of the Respiratory Tract in Children. in 131–144 (2012).

226. Schneberger, D., Aharonson-Raz, K. & Singh, B. Pulmonary intravascular macrophages and lung health: What are we missing? *Am. J. Physiol. Cell. Mol. Physiol.* **302**, L498–L503 (2012).

227. Bordet, E. *et al.* Porcine alveolar macrophage-like cells are pro-inflammatory pulmonary intravascular macrophages that produce large titers of porcine reproductive and respiratory syndrome virus. *Sci. Rep.* **8**, 10172 (2018).

228. Longworth, K. E. The comparative biology of pulmonary intravascular macrophages. *Frontiers in bioscience : a journal and virtual library* **2**, (1997).

229. Robertson, B. *et al.* A 2-year follow up of babies enrolled in a European multicentre trial of porcine surfactant replacement for severe neonatal respiratory distress syndrome. Collaborative European Multicentre Study Group. *Eur. J. Pediatr.* **151**, 372–6 (1992).

230. Walther, F. J., Gordon, L. M. & Waring, A. J. Advances in synthetic lung surfactant protein technology. *Expert Rev. Respir. Med.* **13**, 499–501 (2019).

231. Halliday, H. L. History of surfactant from 1980. *Biol. Neonate* **87**, 317–322 (2005).

232. Davis, A. J., Jobe, A. H., Häfner, D. & Ikegami, M. Lung Function in Premature Lambs and Rabbits Treated with a Recombinant SP-C Surfactant. *Am. J. Respir. Crit. Care Med.* **157**, 553–559 (1998).

233. Johansson, J. *et al.* A synthetic surfactant based on a poly-Leu SP-C analog and phospholipids: effects on tidal volumes and lung gas volumes in ventilated immature newborn rabbits. *J. Appl. Physiol.* **95**, 2055–2063 (2003).

234. van Rensburg, L., van Zyl, J. & Smith, J. Deposition and transport of linezolid mediated by a synthetic surfactant Synsurf® within a pressurized metered dose inhaler: a Calu-3 model. *Drug Des. Devel. Ther.* **Volume 12**, 1107–1118 (2018).

235. Sweet, D. G. *et al.* A first-in-human clinical study of a new SP-B and SP-C enriched synthetic surfactant (CHF5633) in preterm babies with respiratory distress syndrome. *Arch. Dis. Child. Fetal Neonatal Ed.* **102**, F497–F503 (2017).

236. Ricci, F., Murgia, X., Razzetti, R., Pelizzi, N. & Salomone, F. In vitro and in vivo comparison between poractant alfa and the new generation synthetic surfactant CHF5633. *Pediatr. Res.* **81**,

369–375 (2017).

237. Elifactant - Chiesi Farmaceutici - AdisInsight. Available at: https://adisinsight.springer.com/drugs/800014435. (Accessed: 10th June 2019)

238. Echaide, M., Autilio, C., López-Rodríguez, E., Cruz, A. & Pérez-Gil, J. In Vitro Functional and Structural Characterization of A Synthetic Clinical Pulmonary Surfactant with Enhanced Resistance to Inhibition. *Sci. Rep.* **10**, 1–10 (2020).

239. Bollag, W. B. & Gonzales, J. N. Phosphatidylglycerol and surfactant: A potential treatment for COVID-19? *Med. Hypotheses* **144**, 110277 (2020).

240. Mirastschijski, U., Dembinski, R. & Maedler, K. Lung Surfactant for Pulmonary Barrier Restoration in Patients With COVID-19 Pneumonia. *Front. Med.* **7**, 254 (2020).

A. Supplementary information

A.1. Calculations

1) Amount of Curosurf® per piglet

Curosurf® (80 mg/mL) was diluted 1:4 in 0,9% NaCl (C = 20 mg/mL; dCurosurf). Each piglet weighed approximately 2.5 kg and received 2.5 mL Curosurf® per kg bodyweight (according to initial dosing recommendation provided in user guide by manufacturer).

$$2.5\ ml\ dCurosurf * 2.5\ kg = \ 6.25\ mL\ dCurosurf\ per\ piglet$$

$6.25\ mL\ dCurosurf\ per\ piglet * 20\frac{mg}{mL} = 125\ mg\ Curosurf\ per\ piglet$ (= 50 mg/kg)

Exception: The piglets in the **S200 control group** received undiluted Curosurf® (80 mg/mL):

$$6.25\ mL\ Curosurf\ per\ piglet * 80\frac{mg}{mL} = 500\ mg\ Curosurf\ per\ S200\ piglet$$

2) Amount of anionic phospholipid substitution per piglet

DOPG/POPG and IP3/PIP2 were diluted to a stock concentration of 7.5 mg/mL and 2.5 mg/mL, respectively. The piglets received 1 mL of either DOPG, POPG, IP3 or PIP2 stock in total at each intervention point as described in chapter 2.2.1.

$$6.25\ mL\ dCurosurf + 1\ mL\ anionic\ lipid = 7.25\ mL\ per\ piglet$$

In total, the piglets received **125 mg Curosurf® + 7.5 mg DOPG or 7.5 mg POPG or 2.5 mg IP3 or 2.5 mg PIP2** per piglet.

3) Concentration of POPG

7.5 mg POPG total was given to the piglets in 1 mL PBS at each intervention point mixed with 6.25 mL dCurosurf®.

POPG MW = 770.989 g/mol

➔ Concentration of POPG stock solution

$$n = \frac{0.0075\ g}{770.989\ g/mol} = 0.000009727\ mol$$

$$C = \frac{0.000009727\ mol}{0.001\ L} = 0.009727\,\frac{mol}{L} = 9727\ \mu M$$

➔ Final concentration of 1 mL POPG in dCurosurf® (V_{Ges} = 7,25 mL)

$$C = \frac{0.000009727\ mol}{0.00725\ L} = 0.001342\,\frac{mol}{L} = 1342\ \mu M$$

4) Concentration of DOPG

7.5 mg DOPG total was given to the piglets in 1 mL PBS at each intervention point mixed with 6.25 mL dCurosurf®.

DOPG MW = 797.026 g/mol

➔ Concentration of DOPG stock solution

$$n = \frac{0.0075\ g}{797.026\ g/mol} = 0{,}000009409\ mol$$

$$C = \frac{0.000009409\ mol}{0.001\ L} = 0.009409\,\frac{mol}{L} = 9409\ \mu M$$

➔ Final concentration of 1 mL DOPG in dCurosurf® (V_{Ges} = 7.25 mL)

$$C = \frac{0.000009409\ mol}{0.00725\ L} = 0.001298\,\frac{mol}{L} = 1298\ \mu M$$

5) Concentration of IP3

2.5 mg IP3 total was given to the piglets in 1 mL water at each intervention point mixed with 6.25 mL dCurosurf®.

IP3 MW = 486.0 g/mol

➔ Concentration of IP3 stock solution

$$n = \frac{0.0025\ g}{486\ g/mol} = 0.000005144\ mol$$

$$C = \frac{0.000005411\ mol}{0.001\ L} = 0.005144 \frac{mol}{L} = 5144\ \mu M$$

➔ Final concentration of 1 mL IP3 in dCurosurf® (V_{Ges} = 7.25 mL)

$$C = \frac{0.000005144\ mol}{0.00725\ L} = 0.0007095 \frac{mol}{L} = 709.5\ \mu M$$

6) Concentration of PIP2

2.5 mg PIP2 total was given to the piglets in 1 mL PBS at each intervention point mixed with 6.25 mL dCurosurf®.

PIP2 MW = 1036.9 g/mol

➔ Concentration of PIP2 stock solution

$$n = \frac{0.0025\ g}{1036.9\ g/mol} = 0.000002411\ mol$$

$$C = \frac{0.000002411\ mol}{0.001\ L} = 0.002411 \frac{mol}{L} = 2411\ \mu M$$

➔ Final Concentration of 1 mL PIP2 in dCurosurf® (V_{Ges} = 7.25 mL)

$$C = \frac{0.000002411\ mol}{0.00725\ L} = 0.0003325 \frac{mol}{L} = 332.5\ \mu M$$

7) Comparison of lipid concentrations (µM) applied to the piglets *in vivo* and the IC50

IN µM	APPLIED IN VIVO	IC50 TNFA	IC50 IL-1B
PIP2	332.5	0.62	2.61
POPG	1342	1.96	23.78
DOPG	1298	1.01	11.53

8) Total lipid concentration in Curosurf® (MS-Data)

10 µL of undiluted Curosurf® were analysed via mass spectrometry in triplicate.

Curosurf® Sample	*pmol/10 µL*	*Mean*
30654	581087.5	**557210.6 pmol/10 µL (= 55.72 µmol/mL)**
30655	497876.4	
30656	592668.0	

$$55.72\,\frac{\mu mol}{mL} * 0.25 * \ 6.25\,mL = \mathbf{87.06}\ \boldsymbol{\mu mol\ per\ piglet}$$

➔ Lipid ratios given to piglets:

SPECIES	CURO	POPG	CURO	DOPG	CURO	IP3	CURO	PIP2
µMOL	87.06	9.72	87.06	9.41	87.06	5.14	87.06	2.41
RATIO	8.95	1	9.25	1	16.94	1	36.12	1

A.2. Supplemental Figures and Tables

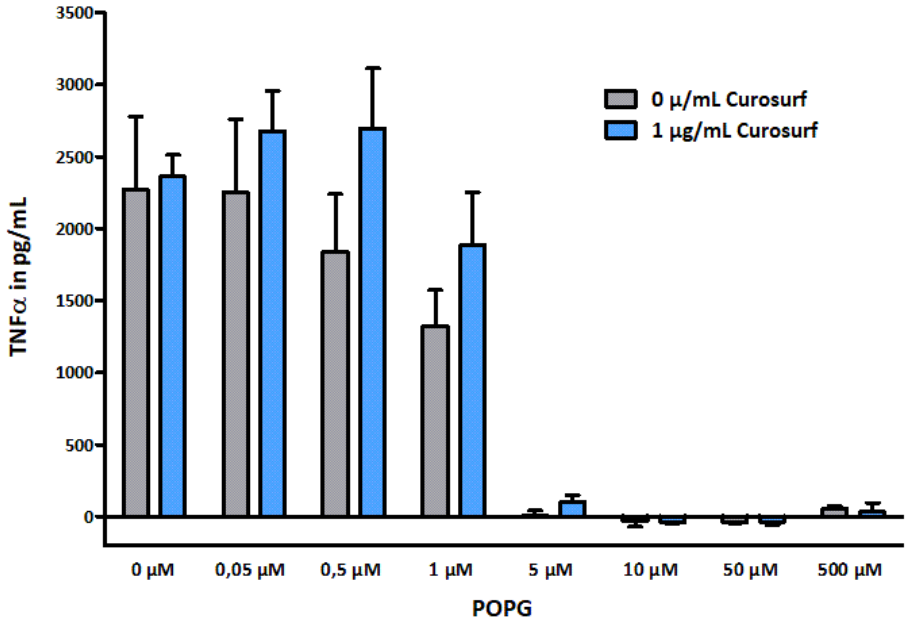

Figure A1: The inhibition of LPS-induced TNFα secretion by POPG is not dampened by pre-incubation with 1 µg/mL Curosurf®. Peripheral blood monocytes from human volunteers were differentiated into macrophages for 7 days, seeded at $1x10^5$ cells per well and incubated with Curosurf® at the indicated concentrations for 30 min at 37°C. Incubation with the indicated concentrations of POPG for 30 min at 37°C was followed by LPS addition to a final concentration of 10 ng/mL for 4 h. The TNFα concentration was subsequently measured in cell-free culture supernatant by ELISA. Data are expressed as mean±SD. N=3 (technical triplicates).

Table A1: Lipid species detected in the piglet surfactant samples and Curosurf. Lipid species was detected (X) or not detected (O) in at least one of the samples per group. Sample number per group (n). Grey shaded are the control groups.

SPECIES	0h (n=40)	Control (n=7)	S50 (n=8)	S200 (n=3)	IP3 (n=5)	PIP2 (n=6)	POPG (n=6)	DOPG (n=6)	Curosurf (n=3)
Cer [34:1;2]	X	X	X	X	X	X	X	X	X
Cer [36:1;2]	X	X	X	O	X	X	O	O	O
Cer [40:1;2]	X	O	X	O	X	X	X	X	O
Cer [42:1;2]	X	X	X	X	X	X	X	X	O
Cer [42:2;2]	X	X	X	X	X	X	X	X	X
CL [72:3]	X	X	O	X	O	X	O	O	O
CL [76:3]	X	X	X	X	X	X	X	X	X
CL [76:5]	X	X	X	X	O	X	X	O	O
Cholesterol	X	O	X	X	X	X	X	X	X
DAG [30:0]	X	X	O	O	O	X	X	O	O
DAG [32:0]	X	X	X	X	X	X	X	X	X
DAG [32:1]	X	X	X	X	X	X	X	X	X
DAG [34:1]	X	X	X	X	X	X	X	X	X
DAG [34:2]	X	X	X	X	X	X	X	X	X
DAG [36:1]	X	X	O	O	X	X	X	X	X
DAG [36:3]	X	X	X	X	X	X	X	X	X
HexCer [34:1;2]	X	X	X	X	X	X	X	X	O
HexCer [35:1;2]	X	X	X	X	X	X	X	X	X
HexCer [36:1;2]	X	X	X	X	X	X	X	X	X
HexCer [37:1;2]	X	X	X	X	X	X	X	X	X
HexCer [38:1;2]	X	X	X	X	X	X	X	X	X
LPC [16:0]	X	X	X	X	X	X	X	X	X
LPE [18:0]	X	X	X	X	X	X	X	X	X
LPE [20:4]	X	X	X	O	X	X	X	X	X
LPG [18:1]	X	O	O	X	X	X	X	X	X
PA [34:1]	X	X	X	O	X	X	X	O	X
PC [28:0]	X	X	X	X	X	X	X	X	X
PC [29:0]	X	X	X	X	O	X	X	O	X
PC [30:0]	X	X	X	X	X	X	X	X	X
PC [30:1]	X	X	X	X	X	X	X	X	X
PC [31:0]	X	X	X	X	X	X	X	X	X
PC [31:1]	X	X	X	X	X	X	X	X	X
PC [32:0]	X	X	X	X	X	X	X	X	X
PC [32:1]	X	X	X	X	X	X	X	X	X
PC [32:2]	X	X	X	X	X	X	X	X	X
PC [33:0]	X	X	X	X	X	X	X	X	X
PC [33:1]	X	X	X	X	X	X	X	X	X
PC [33:2]	X	X	X	X	X	X	X	X	X
PC [33:4]	X	X	O	X	X	X	X	O	O
PC [34:0]	X	X	X	X	X	X	X	X	X
PC [34:1]	X	X	X	X	X	X	X	X	X
PC [34:2]	X	X	X	X	X	X	X	X	X
PC [34:3]	X	X	X	X	X	X	X	X	X
PC [34:4]	X	X	X	X	X	X	X	X	O
PC [35:1]	X	X	X	X	X	X	X	X	X
PC [35:2]	X	X	X	X	X	X	X	X	X
PC [35:3]	X	X	O	X	X	O	X	X	O
PC [35:4]	X	O	X	X	X	X	X	X	O
PC [35:5]	X	X	X	X	X	X	X	X	O
PC [36:1]	X	X	X	X	X	X	X	X	X
PC [36:2]	X	X	X	X	X	X	X	X	X
PC [36:3]	X	X	X	X	X	X	X	X	X
PC [36:4]	X	X	X	X	X	X	X	X	X
PC [36:5]	X	X	X	X	X	X	X	X	X
PC [37:8]	X	X	O	X	X	O	X	X	O
PC [38:2]	X	O	X	X	X	X	X	X	X
PC [38:3]	X	X	X	X	X	X	X	X	X
PC [38:4]	X	X	X	X	X	X	X	X	X
PC [38:5]	X	X	X	X	X	X	X	X	X
PC [38:6]	X	X	X	X	X	X	X	X	O
PC [38:7]	X	X	X	X	X	X	X	X	O
PC [40:5]	X	X	X	X	X	X	X	X	O
PC [40:6]	X	X	X	X	X	X	X	X	O
PC [40:7]	X	X	X	X	X	X	X	X	O
PC [40:8]	X	X	X	X	X	X	X	O	O

SPECIES	0h (n=40)	Control (n=7)	S50 (n=8)	S200 (n=3)	IP3 (n=5)	PIP2 (n=6)	POPG (n=6)	DOPG (n=6)	Curosurf (n=3)
PC-O [30:0]	X	X	X	X	X	X	X	X	X
PC-O [31:0]	X	X	X	X	X	X	X	X	X
PC-O [32:0]	X	X	X	X	X	X	X	X	X
PC-O [32:1]	X	X	X	X	X	X	X	X	O
PC-O [34:1]	X	X	X	X	X	X	X	X	X
PC-O [34:2]	X	X	X	X	X	X	O	X	X
PC-O [36:4]	X	X	X	X	X	X	X	X	X
PC-O [38:5]	X	X	X	X	X	X	X	X	O
PC-O [39:1]	O	O	X	X	X	X	X	X	X
PE [32:0]	X	X	X	X	X	X	X	X	X
PE [32:1]	X	X	X	X	X	X	X	X	X
PE [33:0]	X	X	X	X	X	X	X	X	X
PE [33:1]	X	X	X	X	O	X	X	O	X
PE [34:0]	X	X	X	X	X	X	X	X	X
PE [34:1]	X	X	X	X	X	X	X	X	X
PE [34:2]	X	X	X	X	X	X	X	X	X
PE [35:0]	X	X	X	O	X	X	X	X	X
PE [35:1]	X	X	X	X	X	X	X	X	X
PE [36:0]	X	X	X	X	X	X	X	X	X
PE [36:1]	X	X	X	X	X	X	X	X	X
PE [36:2]	X	X	X	X	X	X	X	X	X
PE [36:3]	X	X	X	X	X	X	X	X	X
PE [36:4]	X	X	X	X	X	X	X	X	X
PE [36:5]	X	X	O	X	X	X	X	O	O
PE [38:1]	X	X	X	X	X	X	X	X	X
PE [38:2]	X	X	X	X	X	X	X	X	X
PE [38:4]	X	X	X	X	X	X	X	X	X
PE [38:5]	X	X	X	X	X	X	X	X	X
PE [38:6]	X	X	X	X	X	X	X	X	O
PE [40:5]	X	X	X	X	X	X	X	X	O
PE [40:6]	X	X	X	X	X	X	X	X	O
PE [40:7]	X	X	X	X	X	X	X	O	O
PE [48:6]	O	O	X	X	X	X	X	X	X
PE-O [34:0]	X	X	X	X	X	X	O	O	O
PE-O [34:2]	X	X	X	X	X	X	X	X	O
PE-O [34:3]	X	X	X	X	X	X	X	O	O
PE-O [36:3]	O	X	X	X	X	X	X	X	O
PE-O [36:4]	X	O	X	X	X	O	X	O	O
PE-O [36:5]	X	X	X	X	X	X	X	X	O
PE-O [36:6]	X	X	O	X	O	X	X	O	O
PE-O [38:5]	X	X	X	X	X	X	X	X	O
PE-O [38:6]	X	X	X	X	X	X	X	X	O
PE-O [38:7]	X	X	X	X	X	X	X	X	O
PG [30:0]	X	O	X	X	X	X	X	X	X
PG [32:0]	X	X	X	X	X	X	X	X	X
PG [32:1]	X	X	X	X	X	X	X	X	X
PG [34:0]	X	O	X	X	X	X	X	X	X
PG [34:1]	X	X	X	X	X	X	X	X	X
PG [34:2]	X	X	X	X	X	X	X	X	X
PG [34:3]	X	X	X	X	X	X	X	X	X
PG [36:1]	X	X	X	X	X	X	X	X	X
PG [36:2]	X	X	X	X	X	X	X	X	X
PG [36:3]	X	X	X	X	X	X	X	X	X
PG [36:4]	X	X	X	X	X	X	X	X	X
PG [36:5]	X	X	X	O	X	X	X	X	X
PG [38:4]	X	X	X	X	X	X	X	X	X
PG [38:5]	X	X	X	X	X	X	X	X	X
PG [38:6]	X	X	X	X	X	X	X	X	O
PG [40:5]	X	X	X	X	X	X	X	X	X
PG [40:6]	X	X	X	X	X	X	X	X	X
PG [40:7]	X	X	X	X	X	X	X	X	X
PG [40:8]	X	X	X	X	X	X	X	X	O
PG [42:8]	X	O	X	X	O	X	X	O	X
PG [47:6]	X	X	X	X	X	X	O	X	O

SPECIES	0h (n=40)	Control (n=7)	S50 (n=8)	S200 (n=3)	IP3 (n=5)	PIP2 (n=6)	POPG (n=6)	DOPG (n=6)	Curosurf (n=3)
PI [32:0]	X	X	X	X	X	X	X	X	X
PI [32:1]	X	X	X	X	X	X	X	X	X
PI [33:1]	X	X	X	X	X	X	X	X	X
PI [34:0]	X	X	X	X	X	X	X	X	X
PI [34:1]	X	X	X	X	X	X	X	X	X
PI [34:2]	X	X	X	X	X	X	X	X	X
PI [34:3]	X	X	X	X	X	X	X	X	X
PI [35:1]	X	X	X	X	X	X	X	X	X
PI [35:2]	X	X	X	X	X	X	X	X	X
PI [35:3]	X	X	X	O	X	X	X	O	X
PI [36:1]	X	X	X	X	X	X	X	X	X
PI [36:2]	X	X	X	X	X	X	X	X	X
PI [36:3]	X	X	X	X	X	X	X	X	X
PI [36:4]	X	X	X	X	X	X	X	X	X
PI [36:8]	X	X	X	X	O	X	O	X	O
PI [37:3]	X	X	X	X	X	X	X	X	X
PI [37:4]	X	X	X	X	X	X	X	X	X
PI [38:2]	X	X	O	X	X	X	X	X	O
PI [38:3]	X	X	X	X	X	X	X	X	X
PI [38:4]	X	X	X	X	X	X	X	X	X
PI [38:5]	X	X	X	X	X	X	X	X	X
PI [38:6]	X	X	X	X	X	X	X	X	X
PI [38:8]	X	X	X	X	O	X	X	O	O
PI [39:0]	X	X	X	X	X	X	X	X	X
PI [40:0]	X	X	O	X	O	X	O	O	O
PI [40:5]	X	X	X	X	X	X	X	X	X
PI [40:6]	X	X	X	X	X	X	X	X	O
PI [40:7]	X	X	X	X	X	X	X	X	O
PI [41:0]	X	X	X	X	X	X	X	X	X
PI [41:1]	X	X	X	X	X	X	X	X	O
PI [43:0]	X	X	X	O	X	X	X	X	O
PI [43:2]	X	X	X	X	X	X	X	X	O
PI [44:6]	X	X	X	X	X	X	X	X	O
PI [44:7]	X	O	X	O	X	O	X	O	O
PI [45:3]	X	X	X	X	X	X	X	X	O
PI [45:4]	X	X	X	X	X	X	X	X	O
PI [46:7]	X	X	X	X	X	X	X	O	O
PS [36:0]	X	X	X	X	O	X	O	X	X
PS [36:8]	X	X	X	X	X	X	X	X	X
PS [37:2]	X	X	X	X	X	X	X	X	X
PS [38:8]	X	X	X	X	X	X	X	X	X
PS [39:2]	X	X	X	X	X	X	X	X	O
PS [39:3]	X	X	X	X	X	X	X	X	X
PS [40:8]	X	X	X	X	X	X	O	X	X
PS [40:9]	X	X	X	X	X	X	X	X	X
PS [41:4]	X	X	X	X	O	X	X	O	O
SM [34:0;1]	O	X	X	X	X	X	X	X	X
SM [34:1;1]	X	X	X	X	X	X	X	X	X
SM [36:1;1]	X	X	X	X	X	X	X	X	X
SM [38:1;1]	O	O	X	X	X	X	X	X	X
SM [40:1;1]	X	O	X	X	X	X	X	X	X
SM [42:1;1]	X	O	X	X	X	X	X	X	X

X detected
O not detect

Table A2: Piglet surfactant samples excluded from lipidome statistical analysis.

Sample ID	Piglet ID	Group	Total pmol	# lipid species	Cutoff
30637	F65	POPG	38583.65411	35	Low 4
30643	F68	S50	27986.97435	38	
30574	F29	DOPG	17713.37531	41	
30600	F43	Control	1490.381456	42	
30613	F50	PIP2	47622.58348	156	High 4
30565	F22	0h	840484.349	163	
30638	F66	0h	160724.0768	164	
30645	F69	PIP2	138643.8185	166	

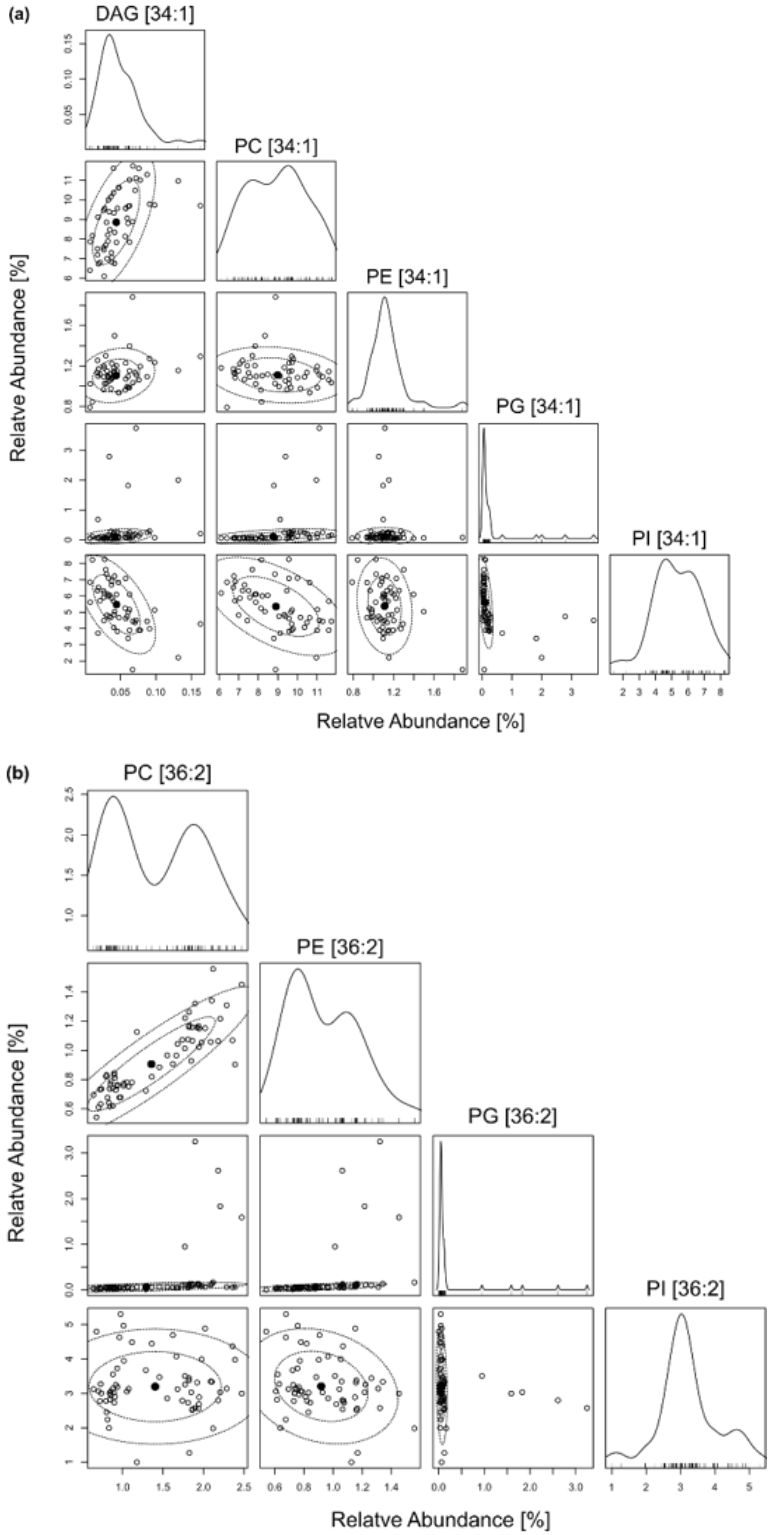

Figure A2: No lipid headgroup exchange was observed in lipids from piglet pulmonary surfactant. Correlation analysis of relative abundances of different lipid species with acyl chains [34:1] and [36:2] did not give a strong indication of a possible head group exchange, for example between PG 34:1 (POPG) and PC 34:1 (POPC), or between PG 36:2 (DOPG) and PC 36:2 (DOPC).

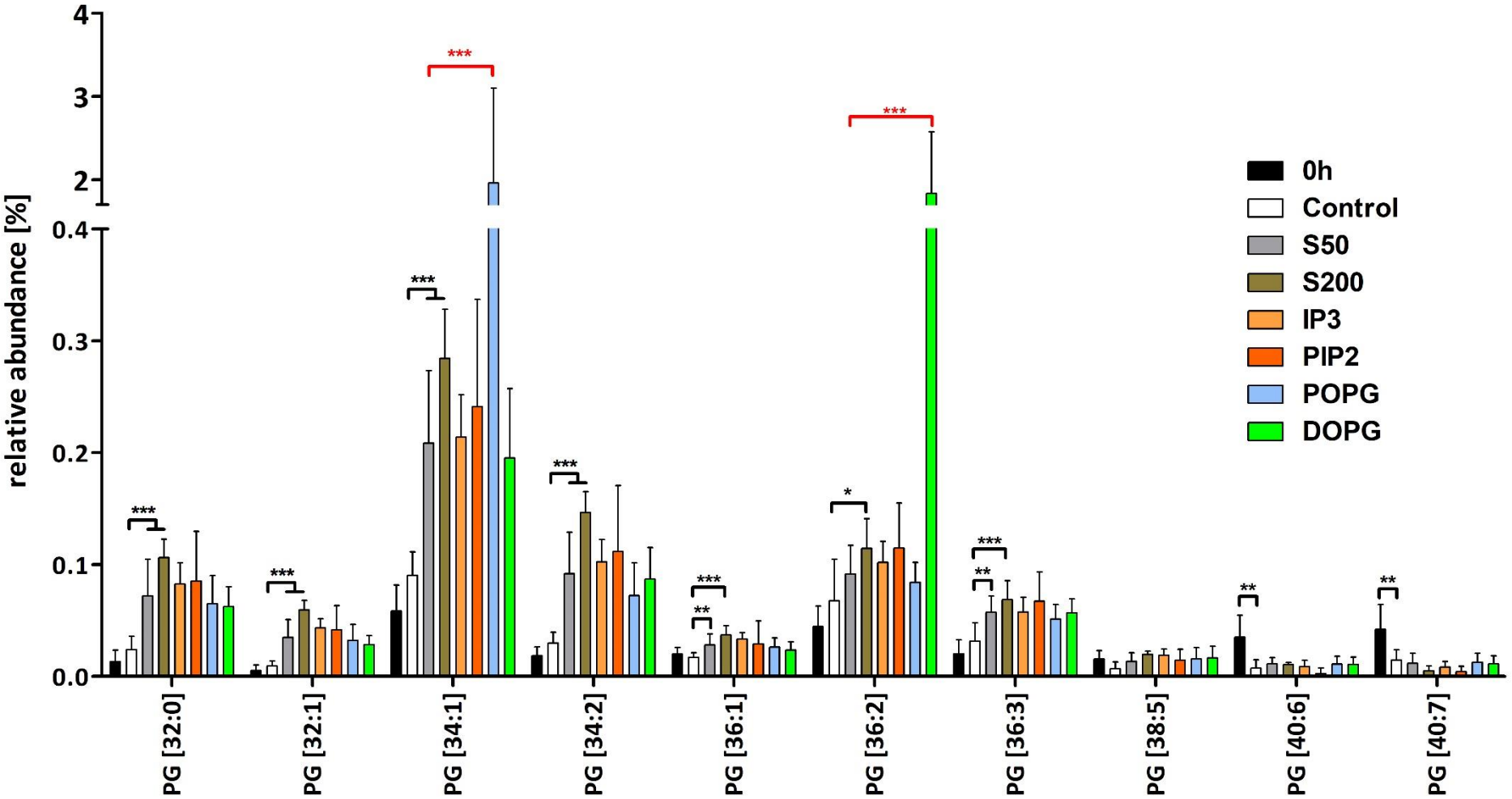

Figure A3: Enlarged version of Figure 4.19b, page 88.

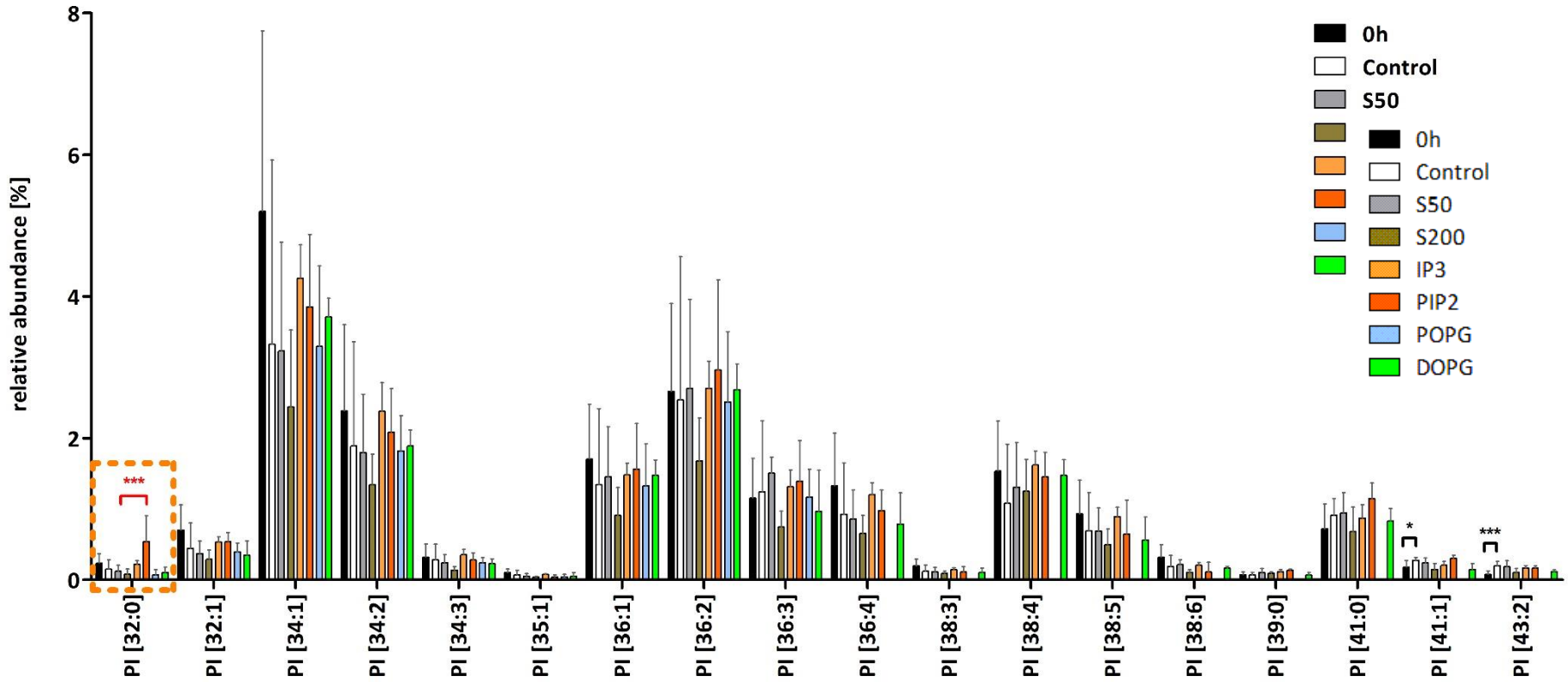

Figure A4: Enlarged version of Figure 4.19c, page 88.

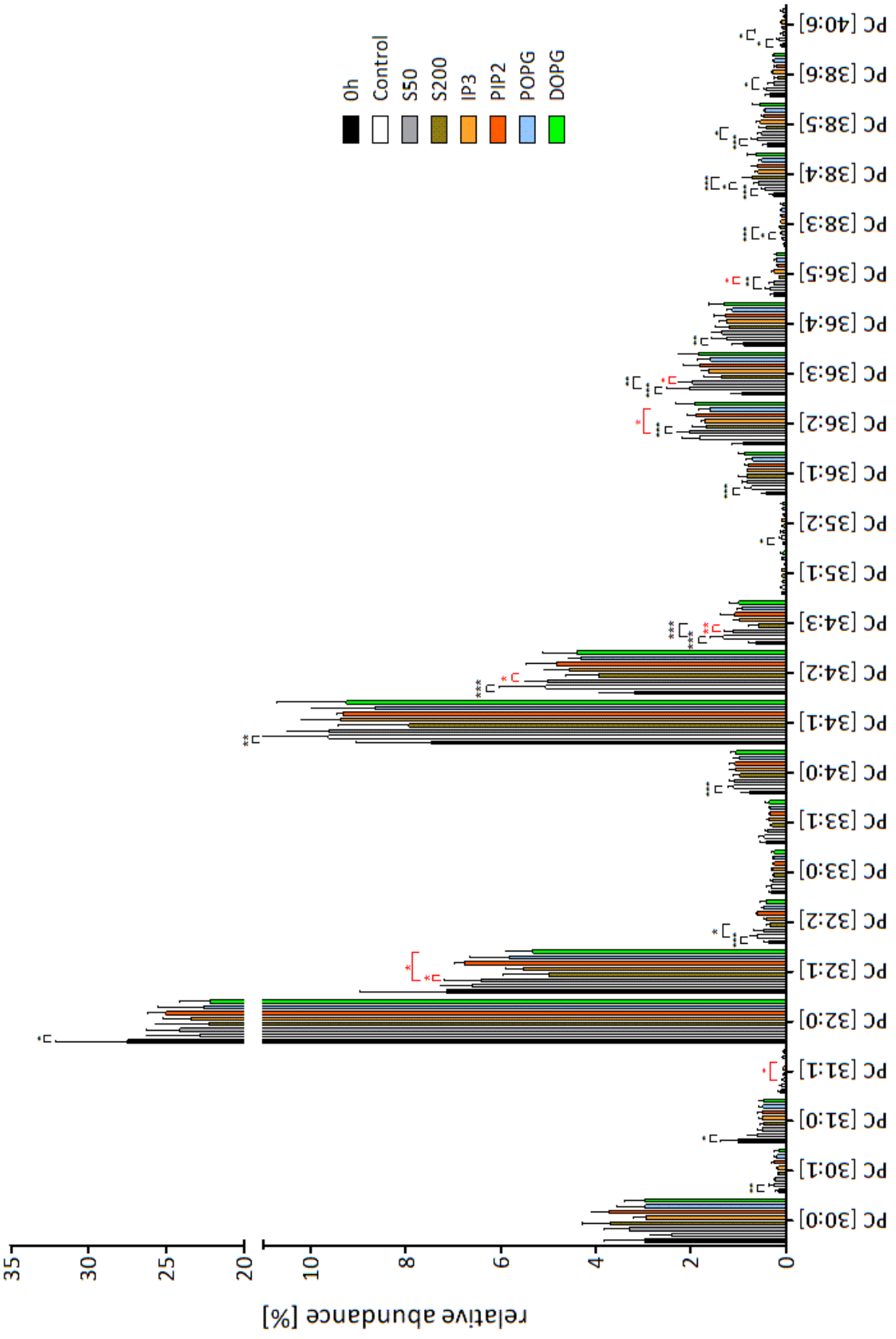

Figure A5: Enlarged version of Figure 4.20a, page 90.

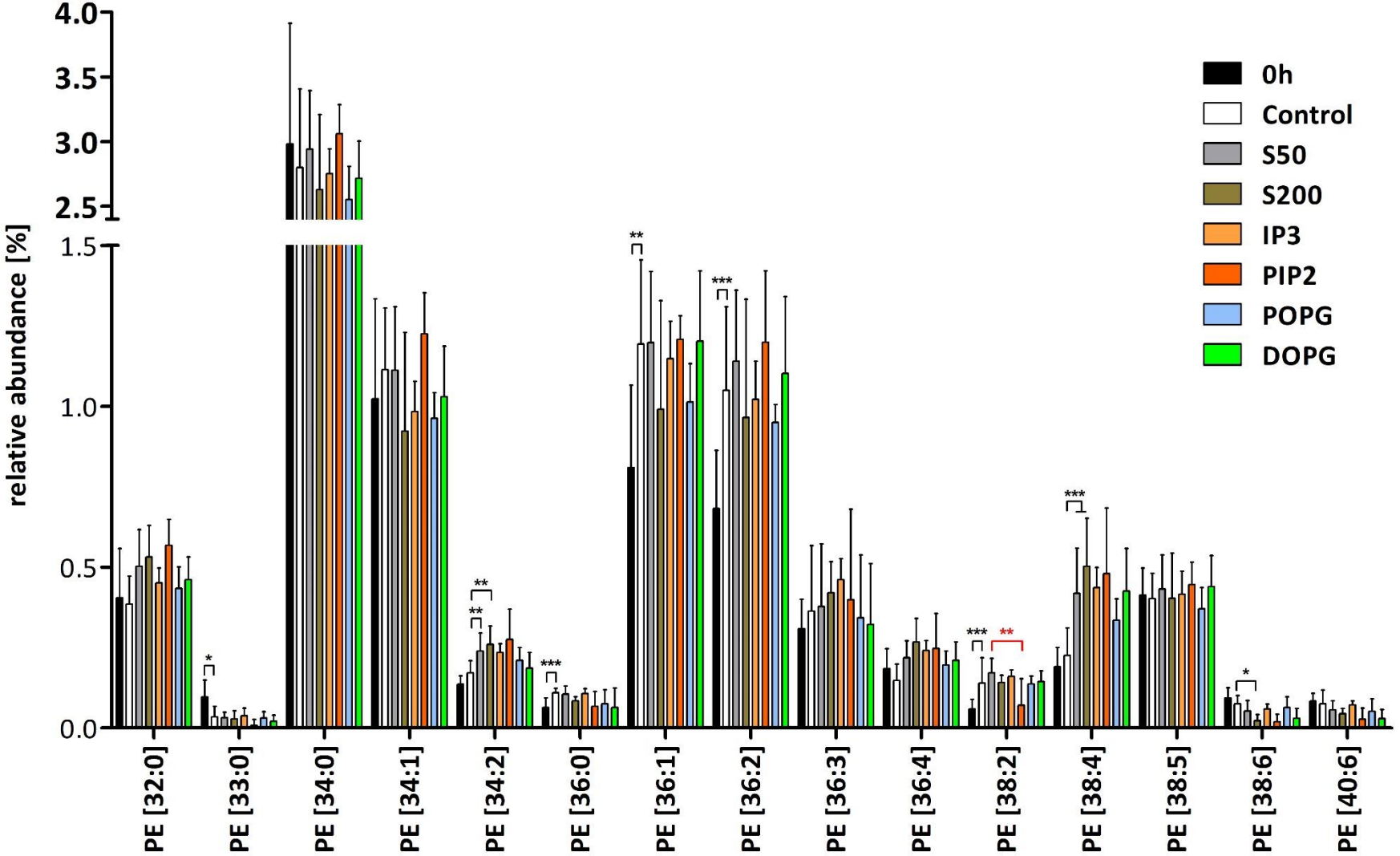

Figure A6: Enlarged version of Figure 4.21a, page 91.

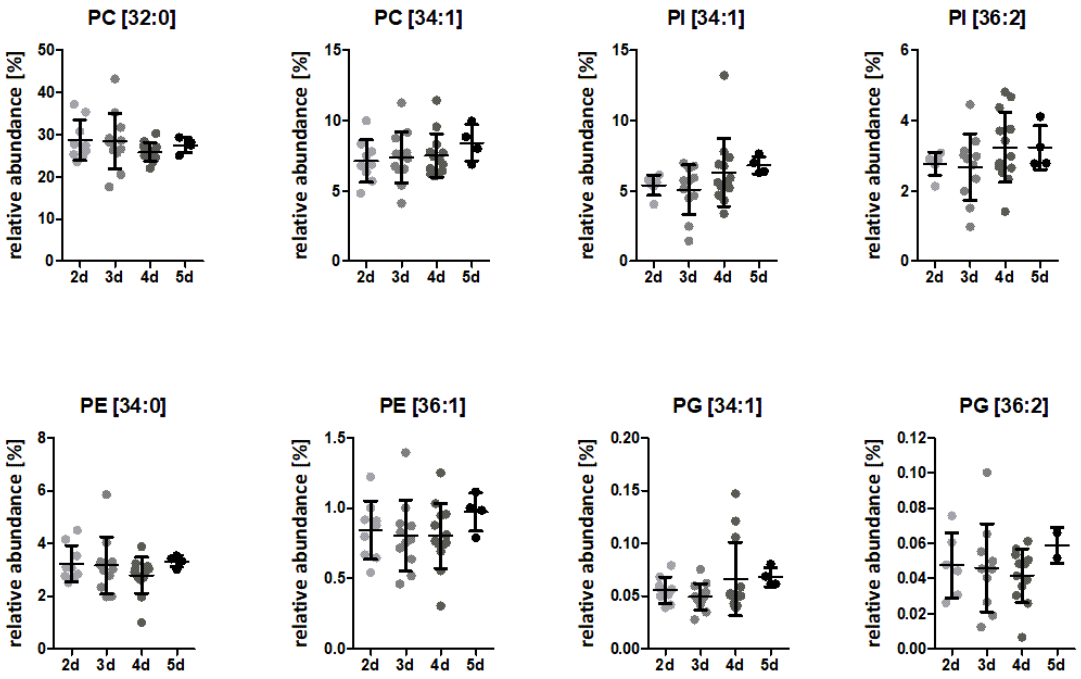

Figure A7: Distribution of the most abundant PC, PI, PE and PG lipid species in healthy piglet surfactant by age. No significant change in relative abundance of the lipid species PC [32:0], PC [34:1], PI [34:1], PI [36:2], PE [34:0], PE [36:1], PG [34:1] and PG [36:2] in the piglet surfactant lipid*ome* was detected with increased age of the piglet. 2d n=9; 3d n=12; 4d n=13; 5d n=4.

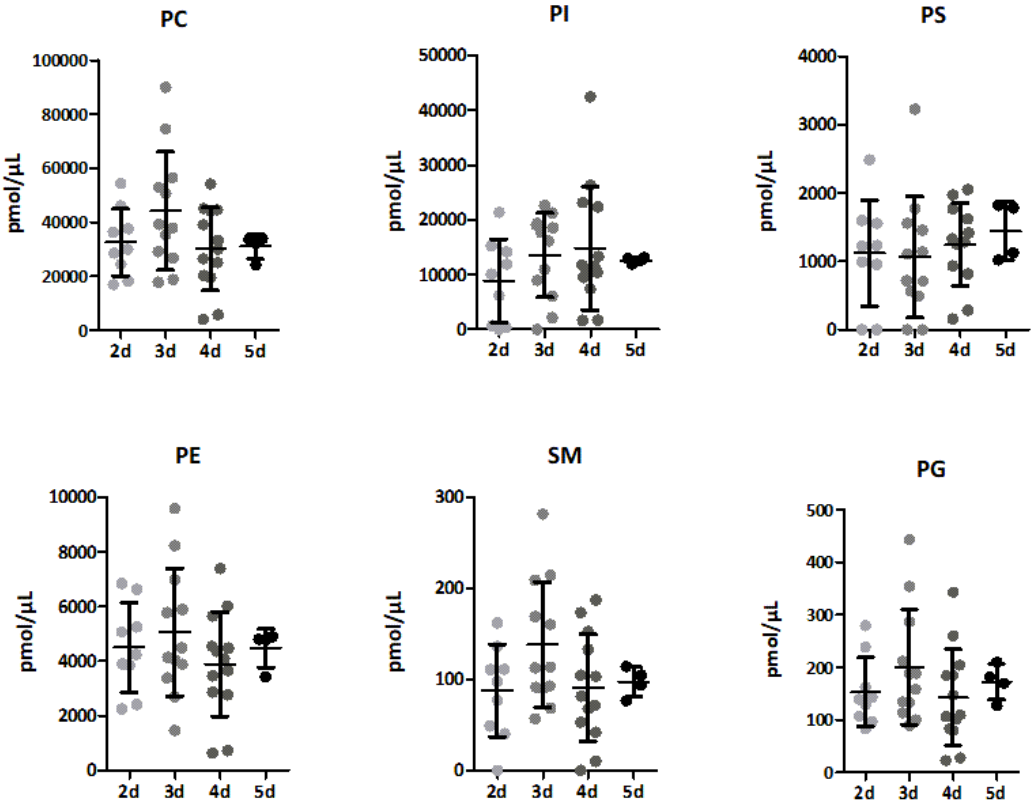

Figure A8: Absolute abundance of the main lipid species in healthy piglet surfactant by age. No significant change in absolute abundance of the main lipid groups in the piglet surfactant lipid*ome* was detected with increased age of the piglet. Data taken from healthy piglets at 0h without cutoff. 2d n=9; 3d n=12; 4d n=13; 5d n=4.

B. Grants and Gifts

This project was funded by the Cluster of Excellence “Inflammation at Interfaces” projects Exc306OTP1 to Martin F. Krause and EXC306OTP4 to Andra B.Schromm.

Curosurf® was kindly provided by Chiesi (Parma, Italy).

C. Acknowledgements

First and foremost, I would like to express my gratitude to my supervisor Prof. Dr. Andra Schromm, for her seemingly endless patience and kindness, for research guidance, for accepting me into her scientific family and for her awesome Halloween party!

My thanks goes out to Prof. Dr. Ulrich Schaible for being my Co-Supervisor and for many helpful discussions on the state of this research project.

It was a most wonderful experience to work closely with Prof. Dr. Martin Krause und Dr. Dietmar Spengler on this collaborative research project. In the same context, I would like to thank Dr. Supandi-Winoto-Morbach, Prof. Dr. Sabine Fuchs, Prof. Dr. Heinz Fehrenbach and Prof. Dr. Stefan Schütze.

I would like to sincerely thank Verena Scholz for helping me to extract countless surfactant samples and Dr. Lars-Florian Eggers and PD Dr. Dominik Schwudke for the mass spectrometric analysis of said samples, introduction to data analysis and the discussion of the results.

The days spent in the lab would have been long and cold without the excellent company and technical assistance of Irina von Cube, and our discussions about postcards, paintings and crafts.

I am grateful for the many colleagues that have contributed to create a colorful and 'musical' work life in Borstel. Cordula Stamme, who shared her knowledge in the immunology repetitorium. The Biophysics labgroup, especially Prof. Dr. Thomas Gutsmann, Dr. Christian Nehls and Dr. Wilmar-Alexander Correa-Vargas who were always open for helpful discussions and provided a kind word where needed. Prof. Dr. Torsten Goldmann and Prof. Dr. Otto Holst who supported any musical adventures with their guitars.

A big thank you to my wonderful friends, especially Jule, Enrico and Jana, for the great moral support, help with proof reading and your valued friendship over so many years.
And to my lovely family, that always, always believes in me, no matter where I go next.

It would not have been possible to put this work down in writing had it not been for my Sebastiano whose confidence in me was the biggest support of all!

Thank you!